J. Fluid Mech. (1992), *vol.* 237, *pp.* 101–187
Printed in Great Britain

On the evolution of a turbulent boundary layer induced by a three-dimensional roughness element

By P. S. KLEBANOFF, W. G. CLEVELAND AND K. D. TIDSTROM

National Institute of Standards and Technology, Gaithersburg, MD 20899, USA

(Received 6 July 1990 and in revised form 19 July 1991)

An experimental investigation is described which has as its objectives the extension of the technical data base pertaining to roughness-induced transition and the advancement of the understanding of the physical processes by which three-dimensional roughness elements induce transition from laminar to turbulent flow in boundary layers. The investigation was carried out primarily with single hemispherical roughness elements surface mounted in a well-characterized zero-pressure-gradient laminar boundary layer on a flat plate. The critical roughness Reynolds number at which turbulence is regarded as originating at the roughness was determined for the roughness elements herein considered and evaluated in the context of data existing in the literature. The effect of a steady and oscillatory free-stream velocity on eddy shedding was also investigated. The Strouhal behaviour of the 'hairpin' eddies shed by the roughness and role they play in the evolution of a fully developed turbulent boundary layer, as well as whether their generation is governed by an inflexional instability, are examined. Distributions of mean velocity and intensity of the u-fluctuation demonstrating the evolution toward such distributions for a fully developed turbulent boundary layer were measured on the centreline at Reynolds numbers below and above the critical Reynolds number of transition. A two-region model is postulated for the evolutionary change toward a fully developed turbulent boundary layer: an inner region where the turbulence is generated by the complex interaction of the hairpin eddies with the pre-existing stationary vortices that lie near the surface and are inherent to a flow about a three-dimensional obstacle in a laminar boundary layer; and an outer region where the hairpin eddies deform and generate turbulent vortex rings. The structure of the resulting fully developed turbulent boundary layer is discussed in the light of the proposed model for the evolutionary process.

CONTENTS

1. Introduction

The transition from laminar to turbulent flow in boundary layers has been a subject of active research for many years. The intense interest in this subject stems not only from its intrinsic importance for an understanding of boundary-layer behaviour but also from important technological considerations associated with many aerodynamic and hydrodynamic flows, and the need to predict essential design criteria and to exert some measure of control over the state of the boundary layer. Considerable progress has been made in revealing the fundamentals and evolutionary nature of the instability and transition processes that are involved. Excellent summaries of the progress made to date can be found in Betchov & Criminale (1967), Tani (1969), Morkovin (1969), Stuart (1971) and Reshotko (1976). However, despite the progress that has been made, the inherent complexities of the problem have prevented the prediction of transitional behaviour with the degree of accuracy required for practical applications. Such complexities affect the transition process, and much more needs to be known about the nature of the interaction of such factors as free-stream turbulence, surface roughness, surface curvature, surface temperature, pressure gradients, Mach number, sound, and vibration on the transition process, either singly or in combination. All of the aforementioned factors have been investigated to some degree with surface roughness receiving the most attention. This emphasis on surface roughness stems not only from the obvious interest in maximizing the extent of laminar flow, but also from the converse, in that it is often desirable, for example, in wind tunnel tests to artificially 'trip' the boundary layer into turbulence. It is important to trip the boundary layer as efficiently as possible, i.e. with as small a roughness as possible. This not only avoids contributing to the form drag but also avoids 'distortion' of the resulting turbulent boundary layer (Klebanoff & Diehl 1951), and the effect on test data resulting from such distortion. Although much work has been carried out on roughness-induced transition, too little attention has been given to characterizing the state of the resulting boundary layer.

The experimental activity dealing with the effect of roughness on boundary-layer transition at both incompressible and compressible flow speeds spans a period of approximately forty years, and may be considered to consist of two approaches: one concerned with the location of transition and its dependence on parameters characterizing the boundary layer and roughness, and the other with details of the flow behaviour and its relation to instability processes and the mechanism of transition. Using the former approach, considerable data were obtained for both two-dimensional and three-dimensional roughness elements in which correlations of Reynolds numbers of transition with roughness size and position and boundary-layer thickness were obtained. Excellent accounts of this method with appropriate bibliographies have been given by Smith & Clutter (1959) and Tani (1961). Although the parametric approach has provided the basic data base which is used for present-day criteria involving the effect of roughness, it has not clarified the basic processes.

In general, the effect of roughness is to induce earlier transition. However, it has been demonstrated that the behaviour of a three-dimensional roughness element

(Klebanoff, Schubauer & Tidstrom 1955; Tani 1961) is markedly different than that for two-dimensional roughness elements. It is not as effective as a two-dimensional roughness in inducing transition, and its behaviour is much more critical. Transition moves forward gradually with increasing velocity for two-dimensional roughness, whereas for a three-dimensional roughness transition moves rapidly toward the roughness with a relatively small increase in velocity after a critical velocity has been reached. It is generally recognized that in order to materially advance our understanding of the basic mechanisms involved, a detailed investigation of the steady and fluctuating flow fields is required. This more basic approach has been used with some success in connection with two-dimensional roughness elements, and it has been shown (Klebanoff & Tidstrom 1972) that the basic mechanism by which a two-dimensional roughness element induces earlier transition to turbulent flow is by the destabilizing influence of the flow in the immediate downstream vicinity of the roughness. The flow downstream of isolated three-dimensional roughness elements has received considerable attention (Gregory & Walker 1950; Weske 1957; Mochizuki 1961*a*, *b*; Tani *et al.* 1962; Matsui 1962; Hall 1967; Furuya & Miyata 1972; Norman 1972; Gupta 1980; Acarlar & Smith 1984, 1987). However, much of this work utilized flow-visualization techniques and the resulting insight into the flow processes is primarily qualitative in nature. Detailed measurements of the flow downstream of a three-dimensional roughness are limited and as yet no clear explanation of its behaviour in inducing transition, similar to that for two-dimensional roughness, exists. Nevertheless, it is felt that the behaviour should in some manner be stability governed. Thus, an objective of the present investigation is to evaluate the role stability may play in the interaction of a three-dimensional roughness element with a laminar boundary layer, and the resulting transition to turbulent flow.

Another objective is to characterize in considerable detail the mean and fluctuating flow fields associated with the interaction of a three-dimensional roughness with a laminar layer, even if only for a single roughness element of a given size and shape. Such data can provide insight into the evolutionary process involved in the development of a turbulent boundary layer, and contribute to an understanding of its structure. Measurements of the mean and fluctuating flow fields can also be useful in clarifying the nonlinear process involved in the evolution from a regular periodic type of velocity fluctuation to the randomization of fully turbulent flow. In this connection, it should be noted that Klebanoff, Tidstrom & Sargent (1962) made an explicit analogy between the behaviour of a three-dimensional roughness element and the secondary instability in a transitional boundary layer. In addition, Frenkiel & Klebanoff (1973) proposed that the 'hairpin' vortices associated with the secondary instability are structures consistent with the kinematic behaviour of the turbulent boundary layer. It is therefore a natural consequence that the present study of the behaviour of a three-dimensional roughness element investigates whether these two views can be reconciled. This aspect received added impetus from the work of Head & Bandyopadhyay (1981) who by their flow visualization and hot-wire study of the turbulent boundary layer have demonstrated the presence of hairpin structures. Apart from its intrinsic importance a complementary aspect of detailed measurements of the mean and fluctuating flow fields is that they provide an appropriate perspective, as well as an extended data base, to aid in the development of computational models for roughness behaviour. Their development at some future date may well be deemed essential for the practical evaluation of the parametric behaviour of roughness elements. In this regard, a concomitant objective is to summarize, within the context of the present investigation, the pertinent

features of the behaviour of three-dimensional roughness elements that have been reported in the literature to date. In addition, an attempt has been made to provide insight into the physical processes involved in the evolution of a turbulent boundary layer induced by a three-dimensional roughness element that goes beyond the more qualitative nature of the behaviour deduced from flow-visualization studies. Regrettably, circumstances prevented some aspects of the behaviour from being studied to the extent they merited and as a result some of the conclusions drawn may be regarded, as noted in the text, as remaining in the realm of speculation. However, it is hoped that they are sufficiently rational in the context of the data presented to stimulate interest toward a more definitive resolution.

2. Experimental arrangement and procedure

The investigation was conducted in an unsteady flow facility of the closed-return type with a square test section 1.37 m in cross-section and 4.88 m in length. The tunnel can be operated either in a steady mode as a conventional wind tunnel, or in an unsteady mode for generating oscillatory flows with varying frequency and amplitude. Both modes of operation were used in the present investigation. The maximum velocity that can be obtained in the test section when operating in a conventional steady mode is 27 m/s. The centreline turbulence intensity, i.e. the ratio of the r.m.s. value of the axial component of the velocity fluctuations, u'_0, to U_0, a reference mean velocity and its variation with U_0 at 0.5 m upstream from the boundary-layer plate is shown in figure 1. The turbulence intensity above 12 m/s is about 0.06% and is characteristic of turbulence levels of conventional low-turbulence wind tunnels. Below 12 m/s and over the speed range covered in the present study, the turbulence intensity increases with decreasing velocity to about 0.15% at 5 m/s. A more detailed description of the flow facility is given in Klebanoff, Cleveland & Tidstrom (1987).†

A flat plate was used to establish an appropriate boundary layer. It was an aluminium plate, 3.66 m long, 1.22 m wide, and 9.5 mm thick which had a leading edge in the form of a half-wedge with a 5° angle on the non-working side of the plate. The leading edge itself is rounded with a radius of approximately 0.4 mm. The plate is mounted vertically and centrally with the leading edge at a distance 1.0 m downstream of the entrance to the test section. A false wall made of Plexiglas mounted on the tunnel wall opposite the working side of the plate permitted the adjustment of the pressure gradient within moderate limits and was used to compensate for the boundary-layer growth and establish a zero pressure gradient along the plate. A positive angle of attack was obtained by some blocking of the air passage on the working side of the plate with screens of 16-mesh and wire diameter 0.28 mm. Since the blocking screens had to be placed farther downstream than any usable portion of the plate, the passage was extended 0.86 m by joining the trailing edge of the plate with a section of plywood. This extension also prevented the sharp change in pressure along the plate that would otherwise occur once the carriage for the traversing equipment passed the downstream end of the plate. The positive angle of attack, with the stagnation point on the working side of the plate, provided a smooth flow condition at the leading edge, with a resulting favourable pressure gradient over the first 2 ft. of surface. The distribution of mean velocity, U_1, in the free stream outside the boundary layer, with distance from the leading edge, x,

† The flow facility is no longer at the National Institute of Standards and Technology, having been moved to Arizona State University.

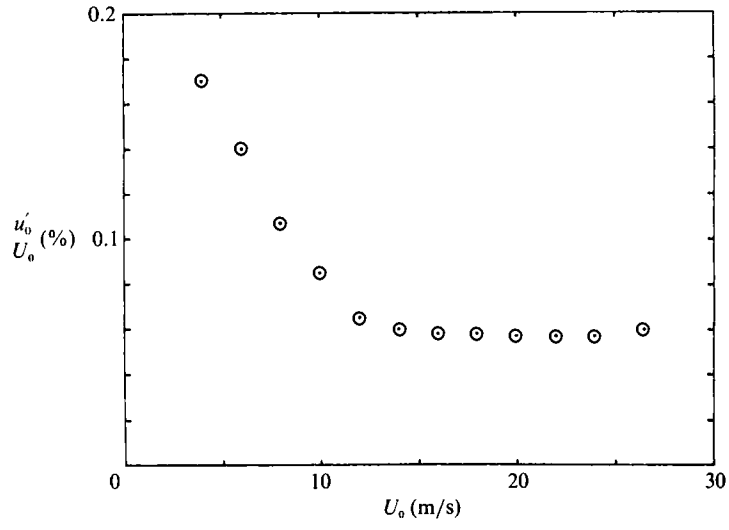

FIGURE 1. Turbulence intensity upstream of the plate.

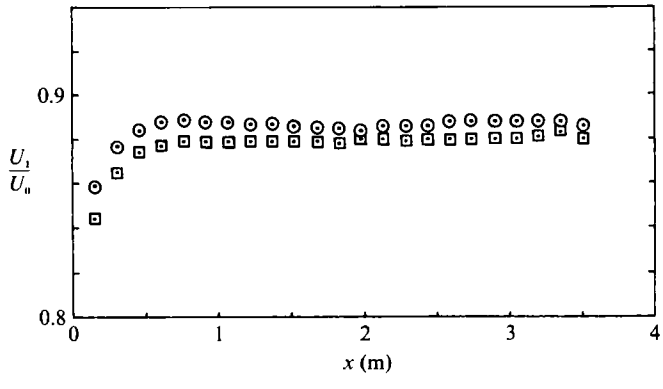

FIGURE 2. Distribution of free-stream velocity along the flat plate: ⊙, $U_0 = 13.5$ m/s; ⊡, 7.4 m/s.

obtained by adjusting the false wall, is shown in figure 2. It is seen that beyond the first 2 ft. of surface a reasonable zero-pressure-gradient condition has been obtained.

Most of the roughness elements were hemispherical with nominal diameters, d, of 3.18 and 6.36 mm. They were individually studied and were attached, using rubber cement, to the surface on the centreline ($z = 0$) at varying distances from the leading edge, x_k, which were well within the laminar boundary-layer 'window'. The actual roughness height, k, owing to the method of attachment and tolerance in the nominal values, could differ from the nominal value and was measured in each case with a dial indicator. A cylindrical element with $d = 3.18$ mm, $k/d = 1.0$, and positioned at $x_k = 91.4$ cm, with its axis in the y-direction was also used.

In documenting the behaviour of a single roughness element a number of different aspects required attention. One was the variation of the Reynolds number of transition, Re_t, with roughness Reynolds number, Re_k, defined by $U_1 x_t/\nu$ and $U_k k/\nu$, respectively, where x_t is the distance from the leading edge of the plate to the beginning of transition to turbulent flow in the boundary layer, and U_k is the mean velocity that would exist in the boundary layer at the height of the roughness

without the roughness present. Another aspect is the parametric behaviour of the frequency, f, of eddies generated by the roughness. Attention was also given to the nature of the boundary-layer distributions of mean velocity and intensity of disturbances at various distances downstream from the roughness, $\bar{x}$, as well as to the effect of an oscillatory flow on eddy shedding and roughness-induced transition. In regard to the latter two aspects, the behaviour of only one size of roughness at one position was investigated, i.e. $d = 3.18$ mm, $k = 1.7$ mm, and $x_k = 91.4$ cm.

The distributions of U and u', at $\bar{x}$ ranging from 1.27 to 91.4 cm, were measured on the centreline and in the spanwise direction for various unit Reynolds numbers, U_1/ν, using conventional constant-temperature hot-wire anemometry. The distributions are presented on a dimensional rather than a non-dimensional basis. The measurements were made for only one size of roughness and the non-dimensional values can be readily obtained. In addition, the appropriateness of scaling in terms of k and d has not been established, and it was felt that the data on a dimensional basis would be a more useful form. During the boundary-layer surveys, a given unit Reynolds number was constant to within $\pm 2\%$ and measurements of fluctuations in velocity were limited to the u-fluctuation. Platinum wires 1.27 μm in diameter and 0.25 mm in length were used, and no correction for wire length, nor for the nonlinear response of the hot wire was deemed necessary. This length of wire was selected as being adequate for the size of the roughness under study from comparative measurements of the mean velocity immediately downstream of the roughness with different wire lengths. Equipment customarily used in association with hot-wire anemometry for processing data, such as a real-time spectral analyser with an on-line x-y plotter, film recordings from an oscilloscope, and strip-chart recordings also proved useful.

3. Laminar boundary layer

It was necessary before proceeding with the study of the behaviour of a roughness element to determine the extent and character of the laminar boundary layer that was established on the plate. The extent of the laminar boundary-layer 'window' is shown in figure 3. The figure shows the well-known phenomenon of transverse contamination of turbulent flow originating at the top and bottom corners of the plate at the leading edge. The transverse contamination angle, as measured from the rail support for the strut is about 10°, in good agreement with existing similar data. Figure 4 shows the mean velocity distributions across the boundary layer at the centreline of the plate at two free-stream speeds, and for two downstream positions. The two downstream positions were chosen so as to cover a considerable extent of the laminar boundary-layer window. The distributions are plotted non-dimensionally for comparison with the Blasius distribution for a zero-pressure-gradient boundary layer, where U is the x-component of the local mean velocity in the boundary layer, y is the distance from the surface, and ν is the kinematic viscosity. It may be that the tendency of the velocity profiles to be slightly steeper in shape than the Blasius reflects the effect of the favourable pressure gradient over the forward part of the plate, and/or a virtual origin other than at the leading edge. However, the effect, if any, is sufficiently small, and within the experimental uncertainty the boundary layer may be considered to be of the Blasius type. Consequently, in characterizing the flow or flow parameters at the roughness element, with the roughness element present, the Blasius distribution is used. Although this assumption neglects the distortion immediately upstream of the roughness, and at the roughness, the Blasius

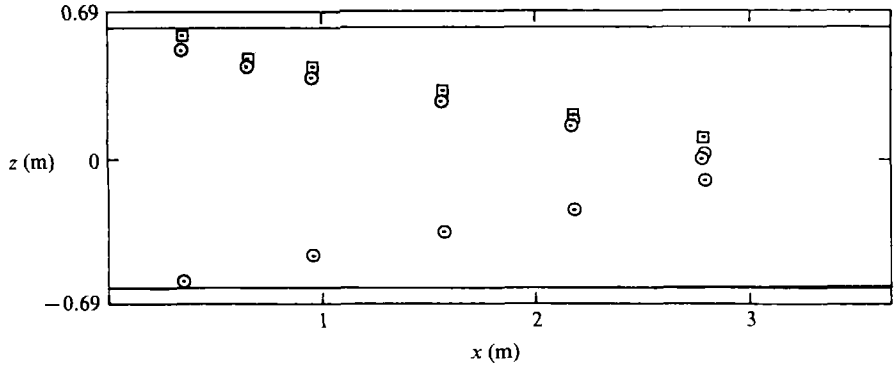

FIGURE 3. Transverse contamination along the flat plate: ⊙, $U_0 = 16.4$ m/s; ⊡, 8.5 m/s.

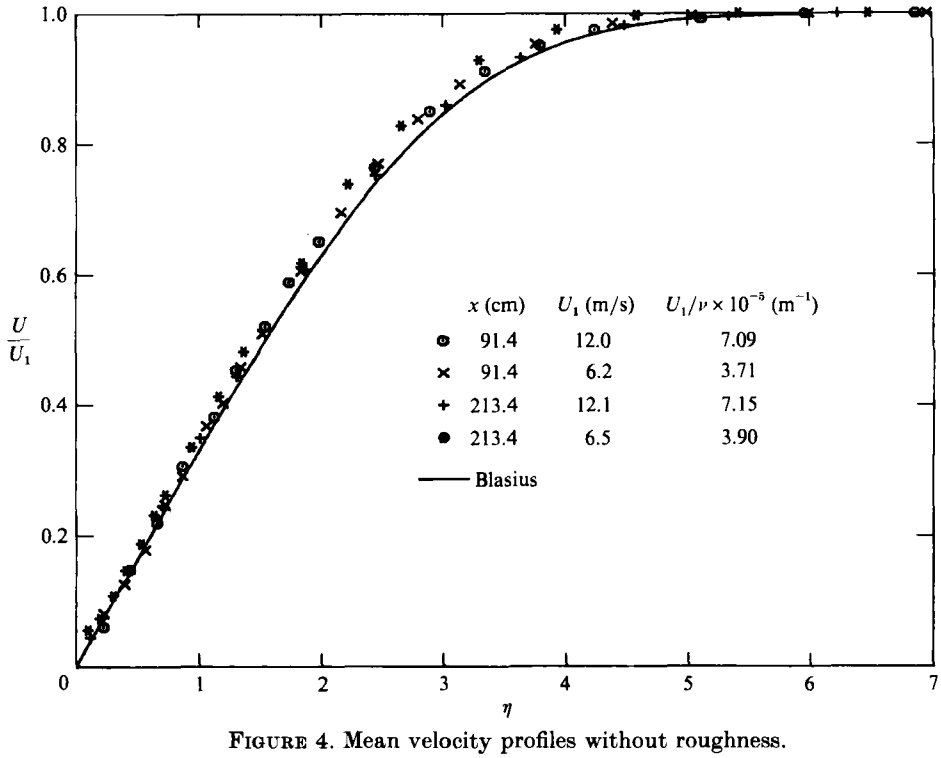

FIGURE 4. Mean velocity profiles without roughness.

lengthscale, $\eta = (\nu x/U_1)^{\frac{1}{2}}$, is a realizable lengthscale, and provides consistency with other investigations. Measurements of the disturbance level in the boundary layer without roughness within the laminar boundary-layer window are shown in figure 5.

Distributions across the boundary layer of the r.m.s. value of the longitudinal component of the velocity fluctuation, u', are shown relative to its value in the free stream, u'_1, for the same x-positions and for about the same free-stream velocities as for figure 4. The nature of the distributions is such that one can infer that, to a considerable degree, the disturbance level is a consequence of variations of boundary-layer thickness in space and time associated with free-stream turbulence effects as proposed in Klebanoff (1971) and not as a result of a Tollmien–Schlichting type of instability. The maximum in the disturbance level, at about 0.5 of the boundary-

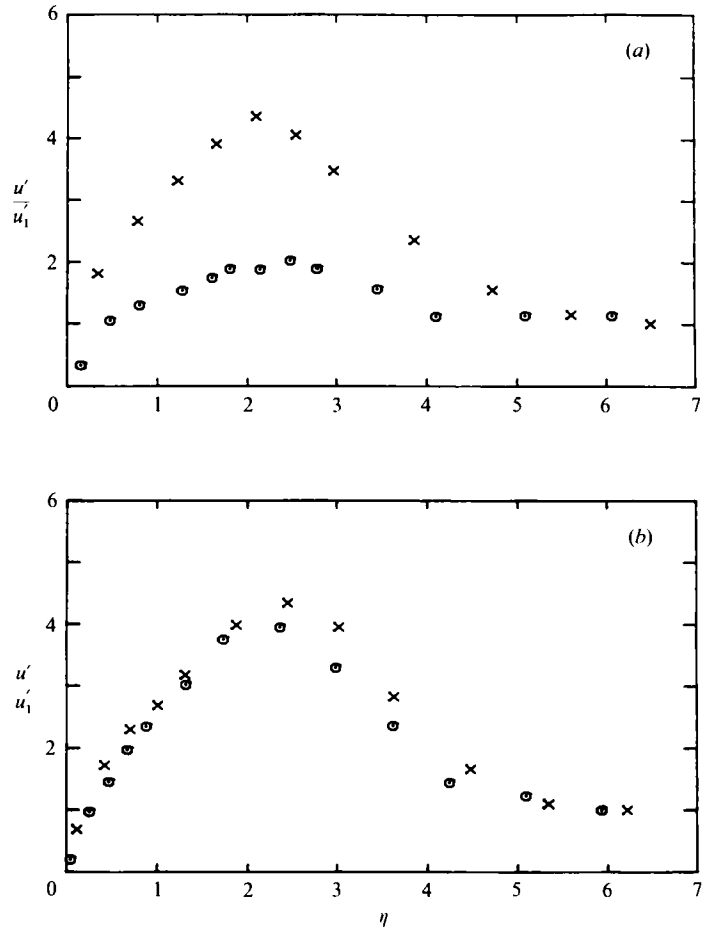

FIGURE 5. Intensity of u-fluctuation without roughness: (a) $x = 91.4$ cm: ×, $U_1 = 12.0$ m/s; ⊙, 6.7 m/s. (b) $\bar{x} = 213.4$ cm: ×, $U_1 = 12.1$ m/s; ⊙, 6.4 m/s.

layer thickness, which in Blasius coordinates is at 2.5, and the relatively large low-frequency content of the disturbance, i.e. below the Tollmien–Schlichting range of instability, are consistent with this conclusion. This behaviour is illustrated in figure 6, which shows the spectral content relative to the range of Tollmien–Schlichting frequencies for the highest boundary-layer Reynolds number of figure 5, i.e. at $U_1 = 12.1$ m/s and $x = 213.4$ cm, for which the boundary-layer Reynolds number based on displacement thickness, R_{δ^*}, was 2070. The spectral distribution was obtained in the region of the maximum in u'/u_1' at $\eta = 2.45$, and the Roman numerals I and II noted on the figure indicate the frequencies corresponding to Branches I and II of the stability diagram for a Blasius flow. The nominal r.m.s. bandwidth of the spectral analyser is proportional to the bandpass, and for the 100 Hz bandpass it is 0.3 Hz. In addition, the nominal low-frequency cutoff of the analyser is 0.4 Hz. Consequently, no particular significance should be attached to the fall-off in spectral intensity that is shown in the range from 0 to 1.0 Hz. The peak in the spectral intensity at 20 Hz, in the view of its proximity to Branch I, should not be interpreted as being due to a Tollmien–Schlichting instability. It is a consequence of vibration induced by the fan motor and is accentuated by the velocity gradient in the

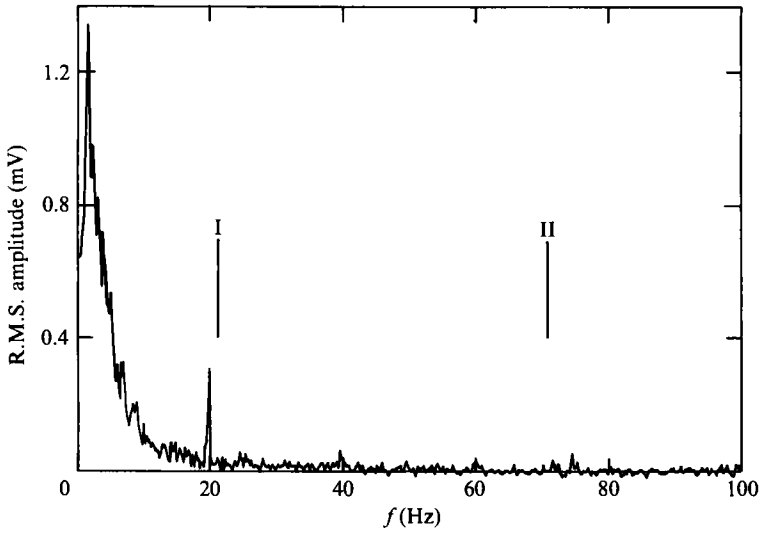

FIGURE 6. Spectrum of u-fluctuation in a boundary-layer without roughness.

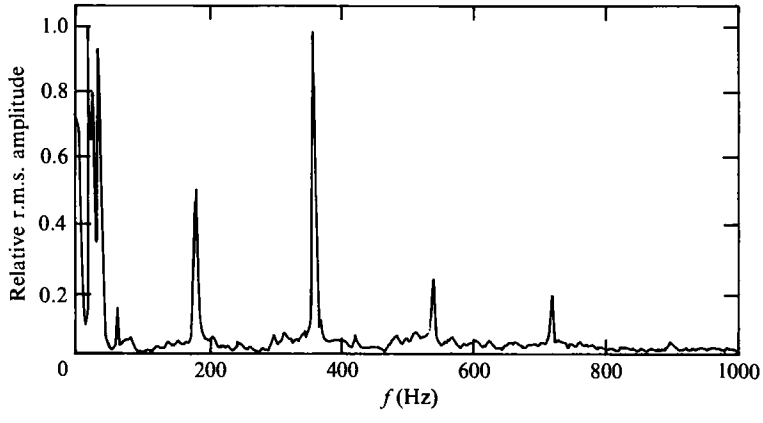

FIGURE 7. Spectrum of u-fluctuation in the free stream.

boundary layer. Attempts to eliminate the 20 Hz vibration by soft-mounting, damping, etc., were not successful. Although it was minimized to the extent shown, it was not possible to eliminate it inasmuch as this vibration from the fan motor was transmitted to the flat plate and wind tunnel walls as evidenced by accelerometer measurements. The free-stream disturbance level, u_1'/U_1, along the plate is a factor of about $1.9 \pm 10\%$ larger than the corresponding disturbance level, u_0'/U_0, upstream of the plate. This increase in disturbance level along the plate, although it has never been thoroughly evaluated, has been observed in previous investigations. However, it is not unexpected and may be attributed to potential fluctuations arising from the turbulent boundary layers on the walls of the tunnel. The magnitude of the effect may therefore differ from one flow configuration to another. In addition there may be very low-frequency potential fluctuations, i.e. below 2 Hz, in the free stream arising from an intermittent separation in the wind tunnel circuit. It is believed that this may be responsible for much of the increase in disturbance intensity at the lower velocities shown in figure 1. Another contributing component to the free-stream

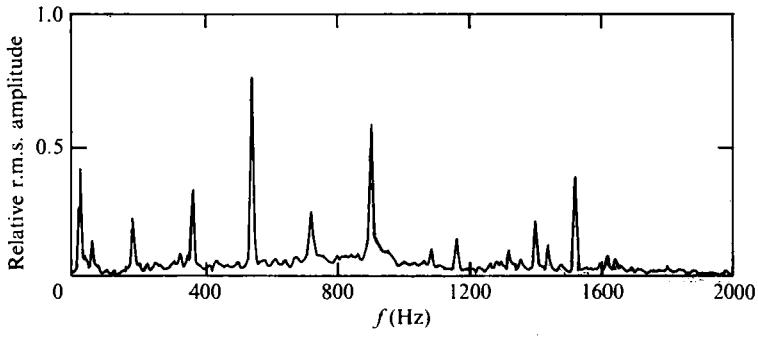

FIGURE 8. Spectrum of the output of an accelerometer attached to the fan housing.

disturbance level is the free-stream turbulence, i.e. turbulent vorticity fluctuations, which were the type of disturbances considered in Klebanoff (1971).

It is evident that sound and vibration are factors that may affect the state of the boundary layer and are important considerations particularly in investigations pertaining to flow instability. In order to assess this aspect the spectrum of the u-fluctuation was measured in the free stream at $x = 221$ cm, $y = 3.49$ cm, and $U_1 = 8.1$ m/s. The spectrum in terms of the relative r.m.s. amplitude is shown in figure 7. No particular significance should be attached to the relative amplitudes. The position at which the spectrum was measured was arbitrarily selected, and the amplitude of the various frequencies may vary with position in the test section. The purpose is to illustrate the spectral peaks present in the free-stream turbulence that may serve as a source of input disturbances for any flow instability. The source of the spectral peaks is attributed to the wind tunnel fan. The peak at 20 Hz, as alluded to previously, corresponds to the fan motor r.p.m. The peaks at 180 Hz and the higher harmonics of 180 Hz are a consequence of the passage frequency of a 9-bladed fan. A more direct evaluation is given by figure 8 which shows the spectrum of the output of an accelerometer attached to the fan housing. It is seen that the peaks correlate well with the peaks observed in the spectrum of the free-stream turbulence. Microphone spectra taken in the room near the test section also corroborated that the spectral peaks were a consequence of sound and vibration.

It is noted, as is reflected in figure 5, that there is an anomaly in the increase in u'/u'_1 from $x = 91.4$ to 213.4 cm for the lower free-stream velocity as compared to that at the higher free-stream velocity. There is no ready explanation for this. One may speculate that in addition to the complex interactions referred to above, the situation is further complicated by the transverse contamination, and that the effect of free-stream turbulence on the boundary layer may also depend on the thickness of the layer relative to the scale of the turbulence. Be that as it may, the state of the layer is such as to not prevent, nor unduly complicate, an adequate study of the effect of roughness.

4. Critical Reynolds number

The existence of a critical roughness Reynolds number for correlating the Reynolds number of transition for three-dimensional roughness elements was first proposed by Schiller (1932). It was predicated on the analogy to the critical Reynolds number for an obstacle in uniform flow at which the downstream flow becomes altered by vortex shedding. Although considerable data on the critical roughness

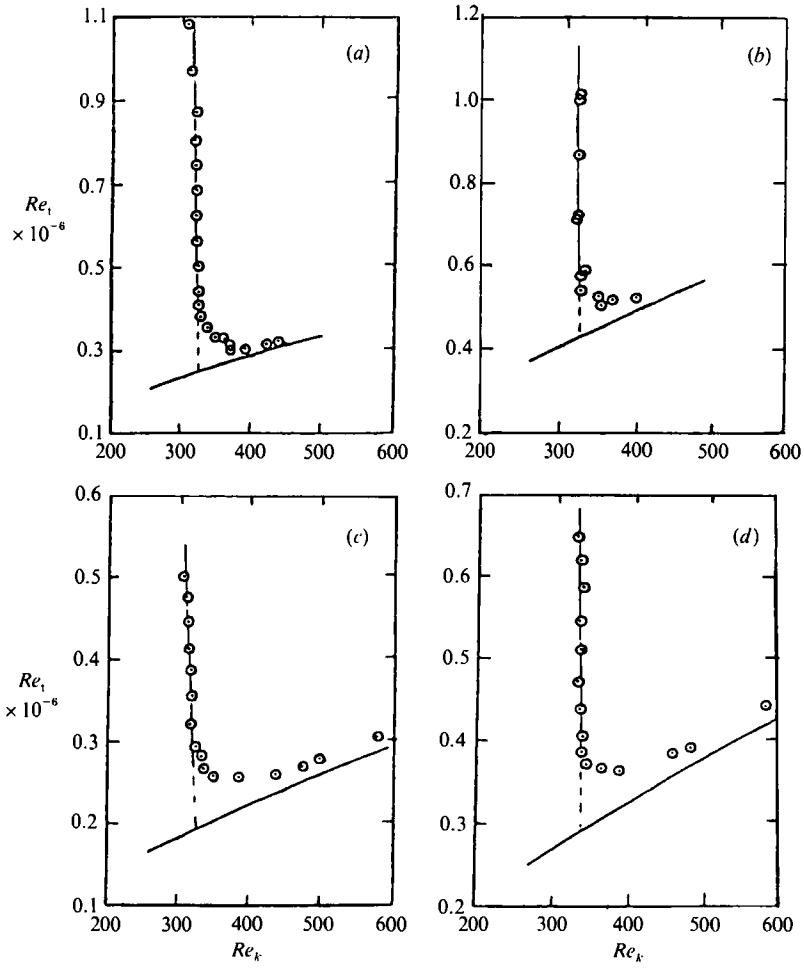

FIGURE 9. Variation of Reynolds number of transition with roughness Reynolds number for hemispherical roughness elements: (*a*) $k = 0.17$ cm, $x_k = 61.0$ cm; (*b*) $k = 0.17$ cm, $x_k = 91.4$ cm; (*c*) $k = 0.31$ cm, $x_k = 91.4$ cm; (*d*) $k = 0.31$ cm; $x_k = 121.9$ cm.

Reynolds number for three-dimensional elements exists in the literature for a variety of geometrical shapes such as spheres, cones, and cylinders (Loftin 1946; Klebanoff *et al.* 1955; Gregory & Walker 1950; Smith & Clutter 1959; Tani *et al.* 1962), no comparable data exist for hemispherical roughness elements.

The critical behaviour of three-dimensional hemispherical roughness elements in inducing earlier transition to turbulent flow, as observed in the present study, is illustrated in figure 9. The measurements shown were made for two different sizes of roughness elements mounted at different positions from the leading edge. The position, x_t, was determined by placing a hot-wire probe close to the surface along the centreline at different locations, $\bar{x}$, and slowly increasing U_1 until turbulent bursts first occurred. The results clearly demonstrate the critical behaviour of the transition process induced by the roughness, in that transition moves rapidly upstream toward the roughness element with a relatively small increase in velocity after a critical velocity has been reached. The limiting case of $x_t = x_k$ is shown by the solid line, and the critical Re_k is determined, as in Tani *et al.* (1962), by the extrapolated intersection

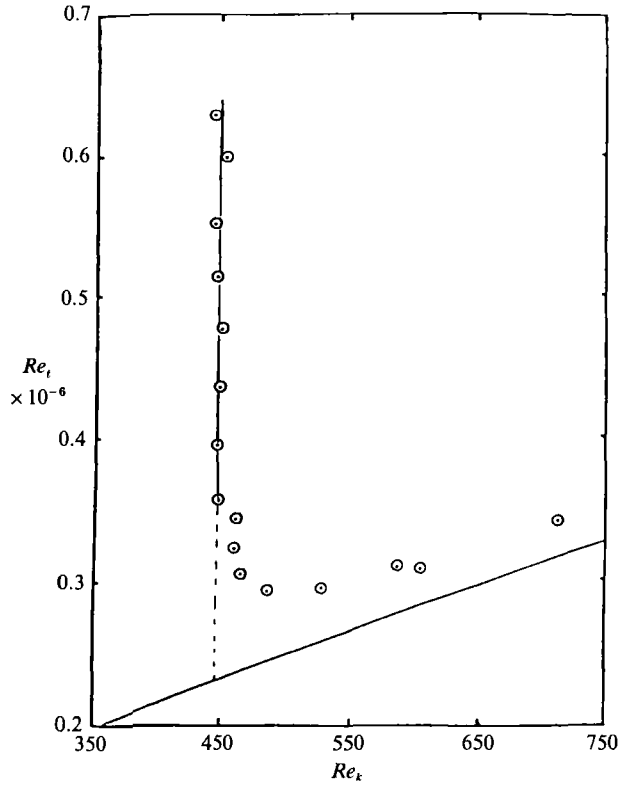

FIGURE 10. Variation of Reynolds number of transition with roughness Reynolds number for a cylindrical roughness element; $k = 0.32$ cm; $x_k = 91.4$ cm.

with the limiting curve indicated by the dashed line. The increase in Re_t with increasing Re_k at the larger values of Re_k, indicating that the transition is not moving forward as rapidly, is generally observed to be the case when x_t is less than 30.5 cm from the roughness element. This is apparently a consequence of the finite distance required for the transition to turbulence associated with the stability of the flow. It illustrates that considerable care should be given to the state of the tripped boundary layer, particularly when using trips in wind tunnel testing, in order to ascertain the degree to which the boundary layer is free of distortion. This question is addressed further for a given size of roughness in §§7 and 8.

It should be noted that Re_k is constant with a value of about 325 for the various conditions shown in figure 9. This is at variance with the results of Tani *et al.* (1962) for cylindrical roughness elements for which the critical value of Re_k was found to vary from 600 to 1000 and to increase with decreasing Re_t. However, in Tani *et al.* (1962), x_t was defined as the position where the turbulent 'bursts' had an intermittency factor of 50%, and the aspect ratio, k/d, of the cylindrical elements was 1.0 compared to a value of 0.5 for hemispherical elements. Smith & Clutter (1959), using the data of Loftin (1946), Klebanoff *et al.* (1955), and Gregory & Walker (1950), coupled to their own data for cylindrical elements with ratios of k/d which ranged from 0.046 to 0.48, concluded that the critical Re_k increased with k/d. However, the scatter in the data exceeded 100%. In view of the differences among the various experiments, not only in regard to the type of roughness but to such

factors as the nature of the free-stream turbulence, pressure gradient, and as to how the critical roughness Reynolds number was determined, it was deemed advisable to assess the effect of k/d, if only in a limited way, in the present investigation in which the same experimental 'environment' is provided. The result obtained for a cylindrical element with a k/d of 1.0, and $k = 3.18$ mm at an $x_k = 91.4$ cm is shown in figure 10. The critical Re_k has a value of 450 and is higher than that obtained with a hemispherical element of comparable k. However, the values of 325 and 450 are on the extreme low side of the range of data for the same k/d examined by Smith & Clutter (1959). In addition to the effect of k/d it is reasonable to expect from a stability point of view that roughness shape may play a role but the data in the literature are rather limited and inconclusive on this point. Klanfer & Owen (1953) reanalysed the data of Gregory & Walker (1950) for conical elements with a k/d of 0.87 and suggested a critical value of 440 for Re_k. Klebanoff *et al.* (1955) for spherical elements in a lateral row with various spacings obtained an average value for the critical Re_k of 577, whereas Hall (1967) for isolated spherical elements, obtained critical values of Re_k ranging from 585 to 655. Smith & Clutter (1959) on the other hand, for a spanwise row of circular discs with k/d ranging from 0.046 to 0.48 obtained values ranging from 100 to 500. In the latter case, the critical Re_k was that for which the Reynolds number of transition had decreased to 95% of the value without roughness. The average of the critical Re_k they obtained when transition was considered as having moved to the roughness was 600. The lowest value of the critical Re_k for a three-dimensional type of roughness was a value of 45 obtained by Hama (1957), who used a spanwise row of flat equilateral triangular patches, 1 mm thick, with their vertex pointing upstream and touching at their base. It is evident that there is a need for more controlled and well-defined experiments in order to satisfactorily resolve the variation of the critical roughness Reynolds number with roughness size and shape for single roughness elements. Improved insight into this may well provide the basis for an improved experimental approach to the study and interpretation of the behaviour of distributed roughness.

5. Eddy shedding – steady flow

It has been known for some time (Gregory & Walker 1950; Weske 1957; Kovasznay 1960; Mochizuki 1961*a*, *b*; Klebanoff *et al.* 1962; Matsui 1962; Hall 1967; Furuya & Miyata 1972; Norman 1972; Gupta 1980; Acarlar & Smith 1984, 1987) that associated with the behaviour of three-dimensional roughness elements there are periodic disturbances in the immediate downstream vicinity of the roughness. The view stemming primarily from the flow-visualization studies is that these periodic disturbances reflect the presence of an eddy-shedding mechanism that involves the generation of three-dimensional vortices having a hairpin or 'arch' shape.

The presence of periodic disturbances was readily detected by hot-wire anemometry in the present investigation. They are illustrated by oscillograms of the u-fluctuation shown in figure 11. The oscillograms were obtained downstream of a hemispherical element for the conditions, $k = 1.7$ mm, $\bar{x} = 2.54$ cm, and $\bar{z} = 0$ cm, where $\bar{z} = z - z_k$, and z_k is the spanwise position of the roughness. It is seen from figure 11 that the frequency increases with U_1. The distance from the surface at which the oscillograms were obtained was, in general, increased with increasingly U_1, reflecting the tendency of the region of periodicity to extend further from the surface with increasing U_1 and $\bar{x}$. This is consistent with the flow-visualization studies in

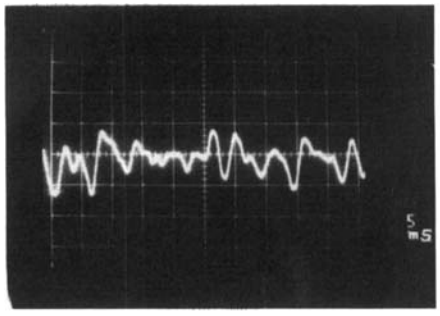

$U_1 = 6.6$ m/s
$y = 2.16$ mm

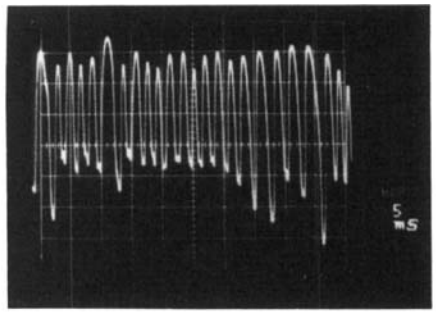

8.2 m/s
2.77 mm

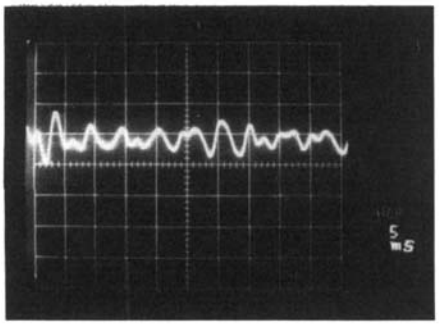

7.0 m/s
2.04 mm

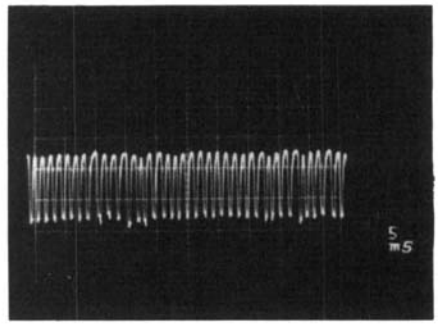

10.1 m/s
3.31 mm

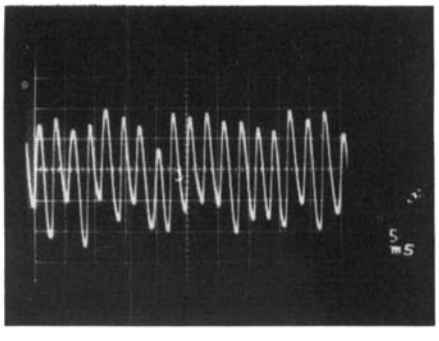

7.7 m/s
2.16 mm

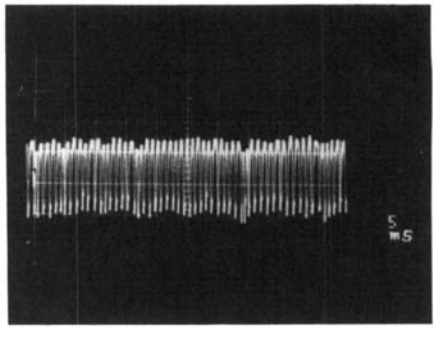

11.8 m/s
3.47 mm

FIGURE 11. Oscillograms of u-fluctuation illustrating variation in frequency with free-stream velocity. $k = 1.7$ mm, $x_k = 91.4$ cm, $\bar{x} = 2.54$ cm, $\bar{z} = 0$ cm. Time increasing from left to right, decreasing velocity in downward direction, sweep speed = 5 ms/cm.

which the increasing extent of the hairpin eddies was observed with their heads' moving out from the surface with increasing U_1 and $\bar{x}$.

Wygnanski & Petersen (1985) showed that the presence of vortical structures and their behaviour inferred from flow-visualization studies may not always be of

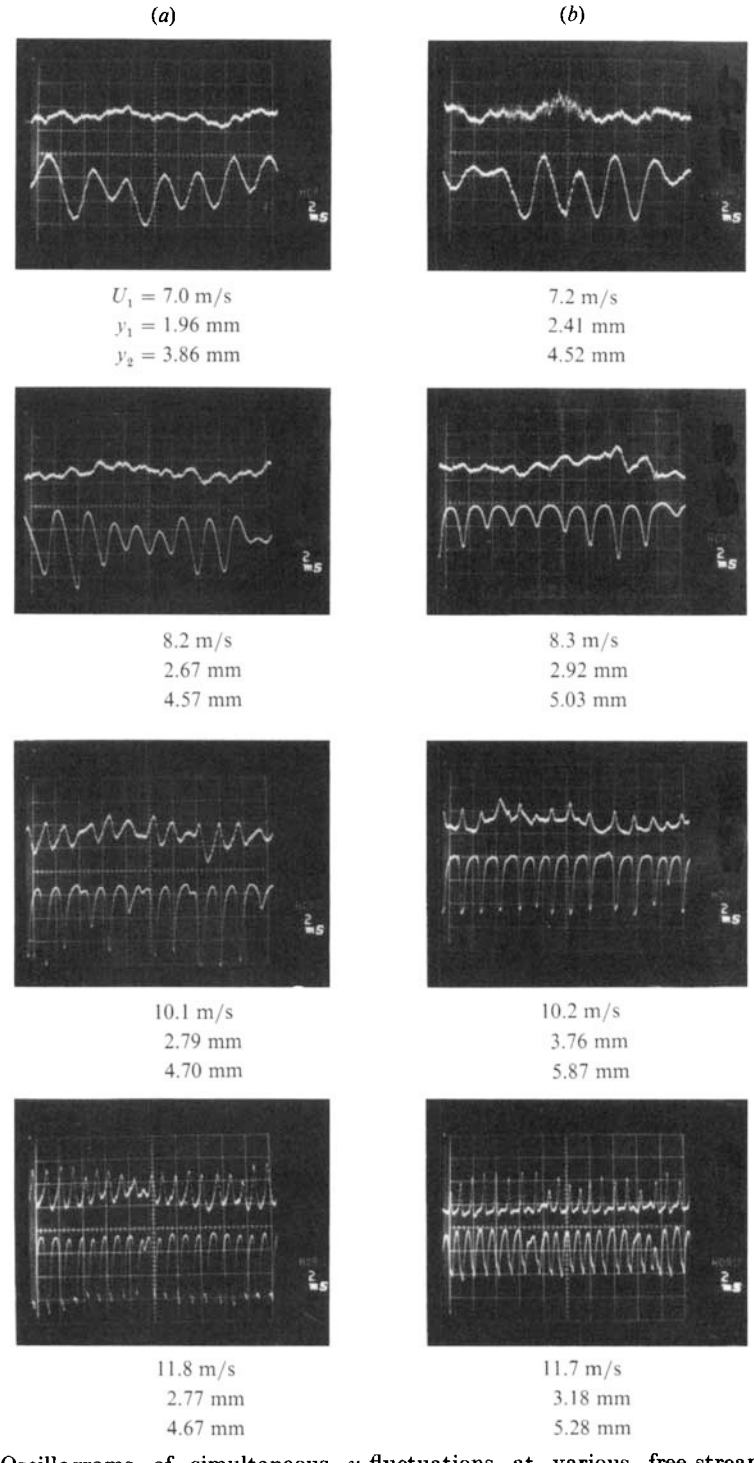

FIGURE 12. Oscillograms of simultaneous u-fluctuations at various free-stream velocities illustrating phase reversal in the y-direction. $k = 1.7$ mm, $x_k = 91.4$ cm, $\bar{z} = 0$ cm. Time increasing from left to right, decreasing velocity in downward direction, sweep speed = 2 ms/cm. (*a*) $\bar{x} = 1.27$ cm; (*b*) 2.54 cm.

dynamical significance. Such structures in free-shear flows could be viewed as a manifestation of Rayleigh instability, and an amalgamation of 'tagged' particles evidenced by streaklines does not necessarily coincide with a redistribution of vorticity. In an earlier paper Hama (1962*a*) had obtained a similar result. He showed that the 'rolling-up' of a streakline in a mixing layer which had one fluid at rest could result from a superposed neutral wave, and therefore could not necessarily be viewed as a positive indication of the presence of vortices. The question of wave or vortex may be viewed as alternative approaches to the same phenomenon. Nevertheless, it is desirable to identify the physical entity actually involved since each view can provide a different mechanism for the final onset of turbulence.

The oscillograms of figure 11 do not necessarily distinguish between wave and vortex. In order to make this distinction, the oscillograms shown in figures 12 and 13 were obtained for the same roughness element and roughness position as for figure 11. The oscillograms of figure 12 are of simultaneous signals from two hot wires separated in the y-direction at $\bar{x} = 1.27$ and 2.54 cm. The top trace in each oscillogram is the signal from the hot wire that is furthest from the surface. The important features are the phase reversal with distance from the surface which is clearly evident with increasing U_1 and the characteristic 'spike' appearance of the fluctuation. The latter, by analogy to the spike appearance of the fluctuations associated with the observation of hairpin vortices by Klebanoff *et al.* (1962), implied that the hot wire could be used for detecting the existence of a phase reversal with varying $\bar{z}$. The resulting oscillograms obtained with $U_1 = 11.8$ m/s, $\bar{x} = 1.27$ cm, and $y = 3.18$ mm are shown in figure 13. It is seen that phase reversals occur at $+\bar{z}$ and $-\bar{z}$ with a spacing which is less than the diameter of the roughness. Although not shown in the figure, fluctuations associated with eddy shedding were observed to still be present at $\bar{z} = \pm 3.0$ mm. It is unlikely that the continuity condition between the boundary layer and the free stream associated with a wave motion in a wall-bounded flow would yield the observed asymmetries in phase with y and $\bar{z}$. Such phase changes are consistent with the configuration of a hairpin vortex, and yield the conclusion that the observed periodicity is indicative of an eddy-shedding frequency. Further support for this conclusion is presented in §7. In figure 12, with $U_1 = 7.0$ and 7.2 m/s at $\bar{x} = 1.27$ and 2.54 cm, respectively, it is seen that there is no discernible phase reversal, although there is clear evidence of a periodic fluctuation at the inner y-position. At $U_1 = 8.2$ and 8.3 m/s and $\bar{x} = 1.27$ and 2.54 cm, respectively, the phase reversal is barely discernible indicating a less intense vortex than at the higher velocities. The critical velocity, U_c, corresponding to the critical roughness Reynolds number of 325 is 8.1 m/s. The oscillograms in figure 11 also demonstrate the existence of periodicity at $U_1 < U_c$. It would thus appear that there is a rapid change from wave to vortex with increasing U_1, and that at $U_1 < U_c$ the discernible amplitude of any wave motion is limited in y-extent to a relatively narrow region within the boundary layer. This aspect is also addressed further in §7. It can also be inferred that there is a change from wave to vortex with $\bar{x}$ at a given $U_1 \geqslant U_c$. This implies an initial wave motion of relatively short wavelength with the change from wave to vortex occurring within a distance less than $7.5k$.

The dependence of the frequency on U_1 was determined for the hemispherical elements, and the cylindrical element under essentially the same conditions, i.e. roughness size and position, as for the determination of the critical roughness Reynolds number. The results obtained with the hemispherical elements are shown in figure 14. The data for $x_k/k = 359$ and 393 were, within the experimental accuracy, considered to be at the same x_k/k. The straight lines are a least-squares fit

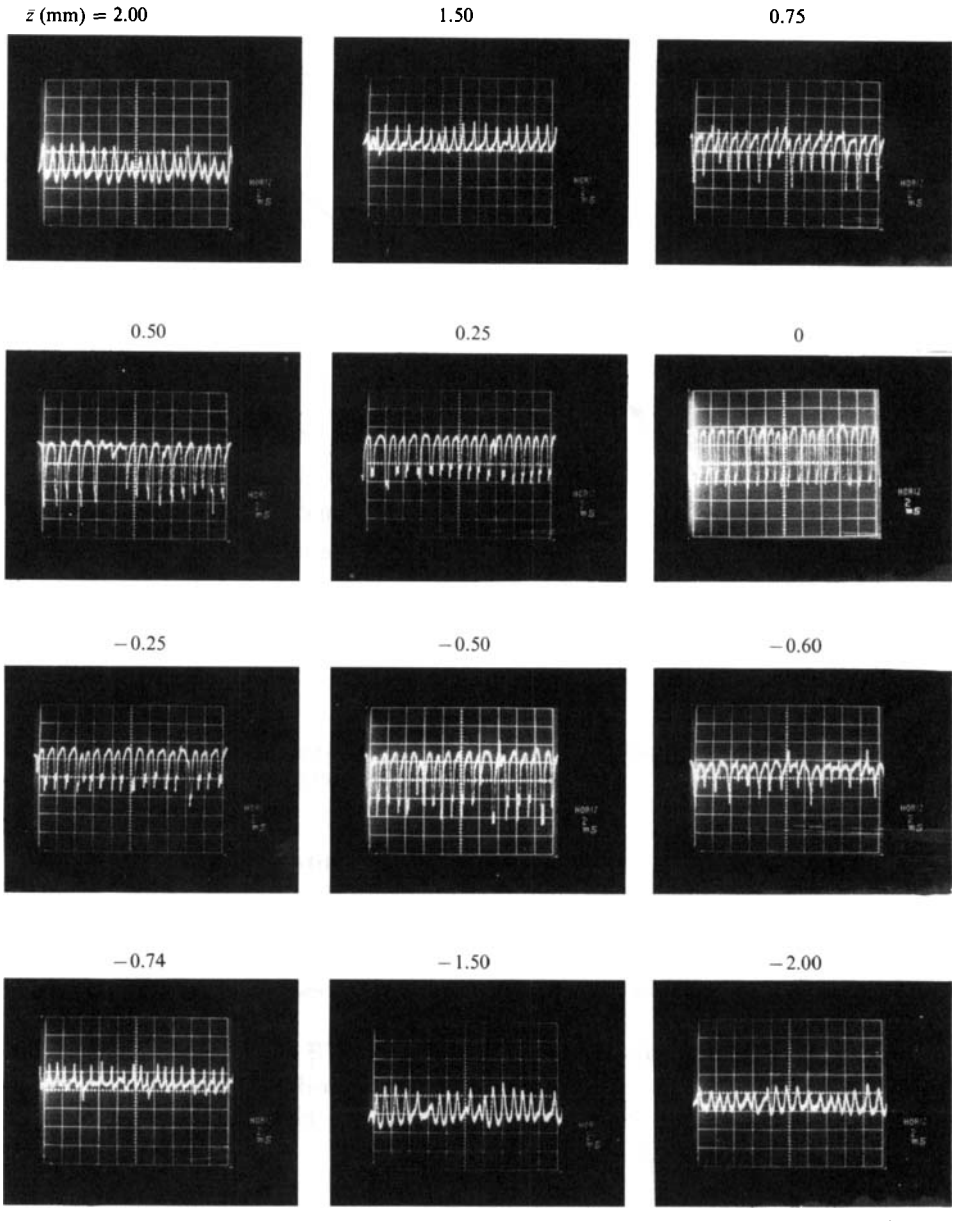

FIGURE 13. Oscillograms of u-fluctuation illustrating phase reversal in the $\bar{z}$-direction. $U_1 = 11.8$ m/s, $\bar{x} = 1.27$ cm, $y = 3.18$ mm, $k = 1.7$ mm, $x_k = 91.4$ cm, Time increasing from left to right, decreasing velocity in downward direction, sweep speed = 2 ms/cm.

to the data. The maximum and minimum deviations about an average value of 940 Hz shown for $x_k/k = 538$ were obtained from the twelve oscillograms of figure 13. Their magnitude should not be regarded as being applicable to any of the other measurements which were made at $\bar{x} = 2.54$ cm, $\bar{z} = 0$ cm, and were obtained at each U_1 from only one or two oscillograms of the type shown in figure 11. The deviations shown, however, do illustrate the variability of the eddy-shedding process and the lack of control over the frequency, in contrast to the control over the frequency when

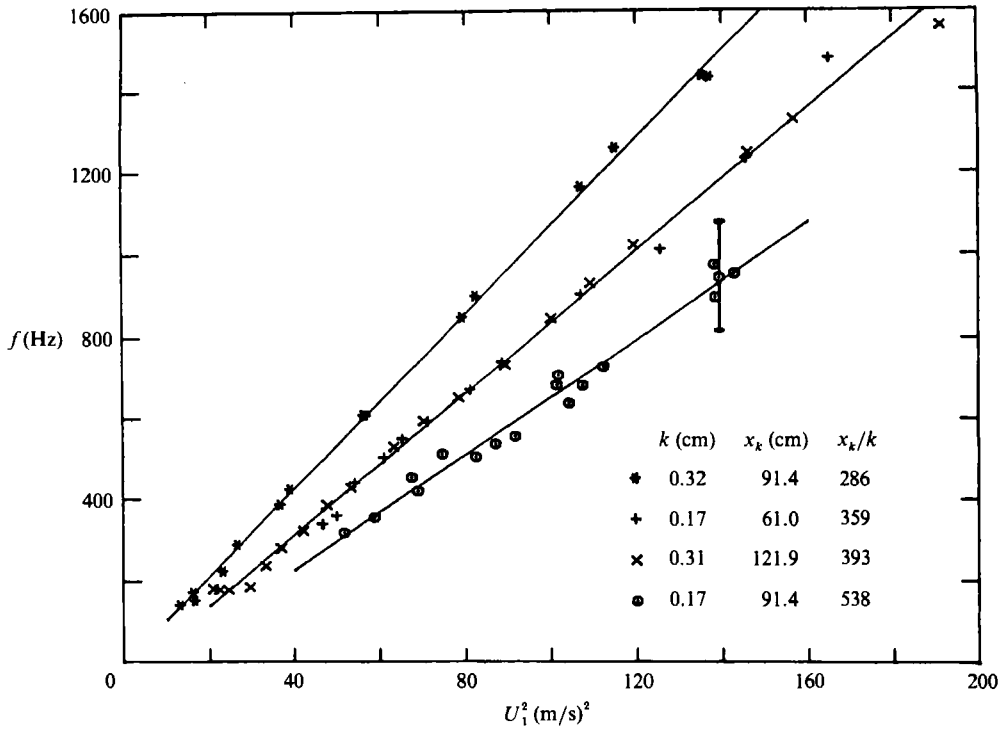

FIGURE 14. Variation of eddy-shedding frequency with free-stream velocity for hemispherical roughness elements of different size and position.

using a vibrating ribbon. In this connection, it is of interest to note that the more appreciable scatter occurs at frequencies which reflect the effect of the free-stream disturbances shown in figure 7, i.e. 180 Hz and its harmonics. The effects of free-stream disturbances in biasing the maximum amplified frequency is not unexpected under appropriate conditions of instability, and stresses the importance of the experimental environment.

The dependence of the eddy-shedding frequency on U_1^2 and x_k/k, as shown in figure 14, suggests that the Strouhal behaviour can be non-dimensionally characterized with U_k as the characteristic velocity and δ_k^* as the characteristic length with a resulting linear relation for f, such that

$$f \propto C \frac{U_1^2}{\nu} \frac{k}{x_k} \tag{1}$$

and

$$\frac{f\delta_k^*}{U_k} = 5.2C. \tag{2}$$

The frequency measurements are shown in figures 15 and 16 as suggested by (1) and (2). The Strouhal number obtained from the least-squares fit to the data in figure 15, in accordance with (2), is 0.29, and is compared in figure 16 with the actual values of $f\delta_k^*/U_k$. Implicit in (2) is the assumption that U_k varies linearly with U_1, which for a Blasius flow is reasonably valid for values of $k/\delta_k^* \leqslant 1.0$. The range of k/δ_k^* covered in the measurements is shown in figure 17 and it is seen that for Re_k greater than 700, the use of (2) would tend to underestimate the Strouhal number. However, the effect

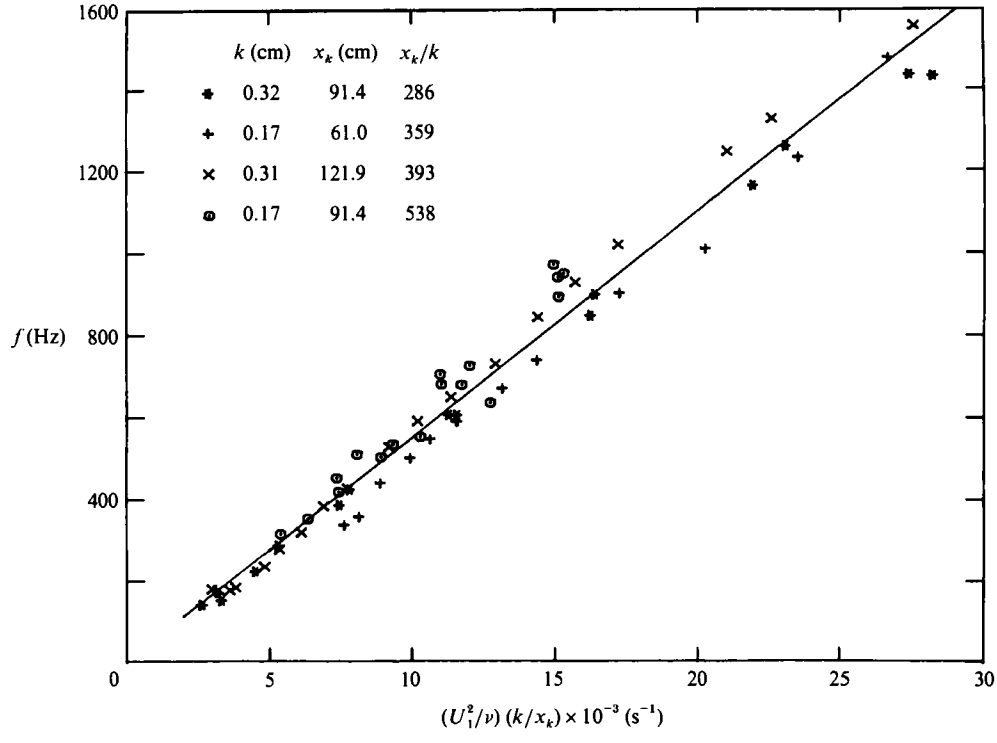

FIGURE 15. Scaling of data of figure 14 with k/x_k and ν.

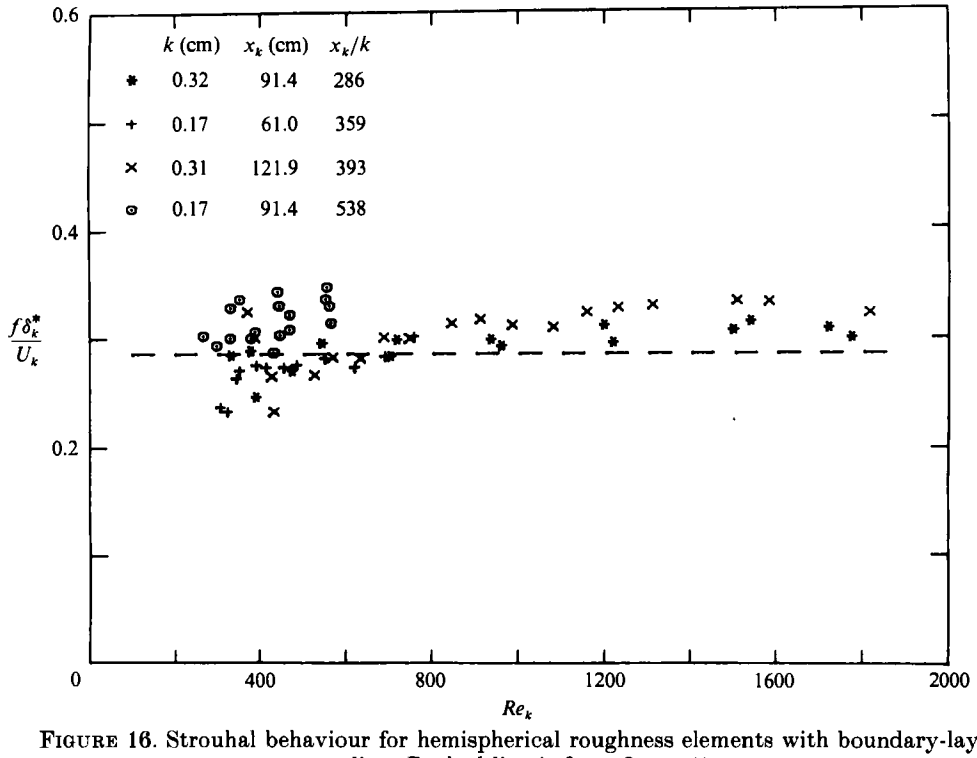

FIGURE 16. Strouhal behaviour for hemispherical roughness elements with boundary-layer scaling. Dashed line is from figure 15.

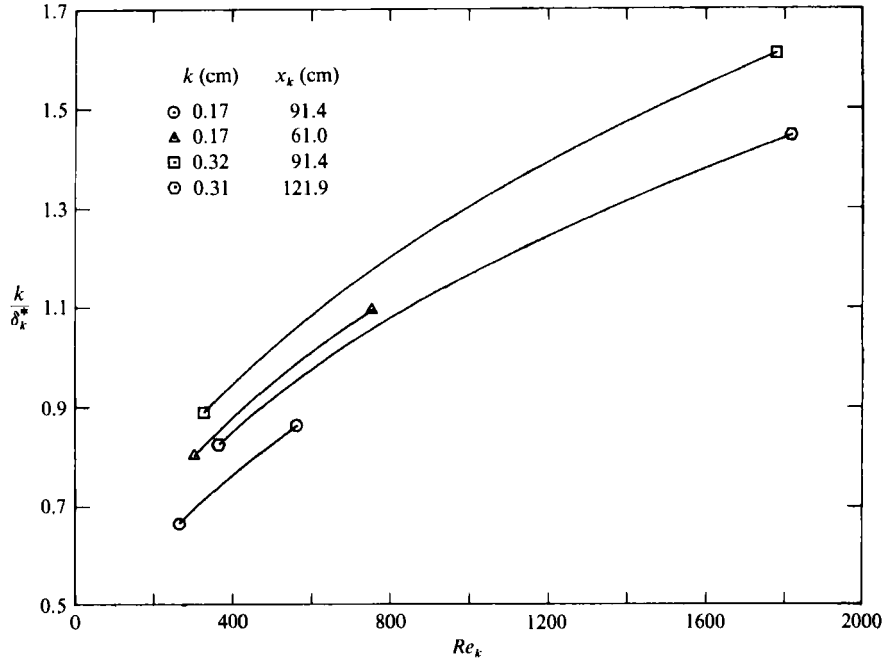

FIGURE 17. Variation of k/δ_k^* with roughness Reynolds number for hemispherical roughness elements of different size and position.

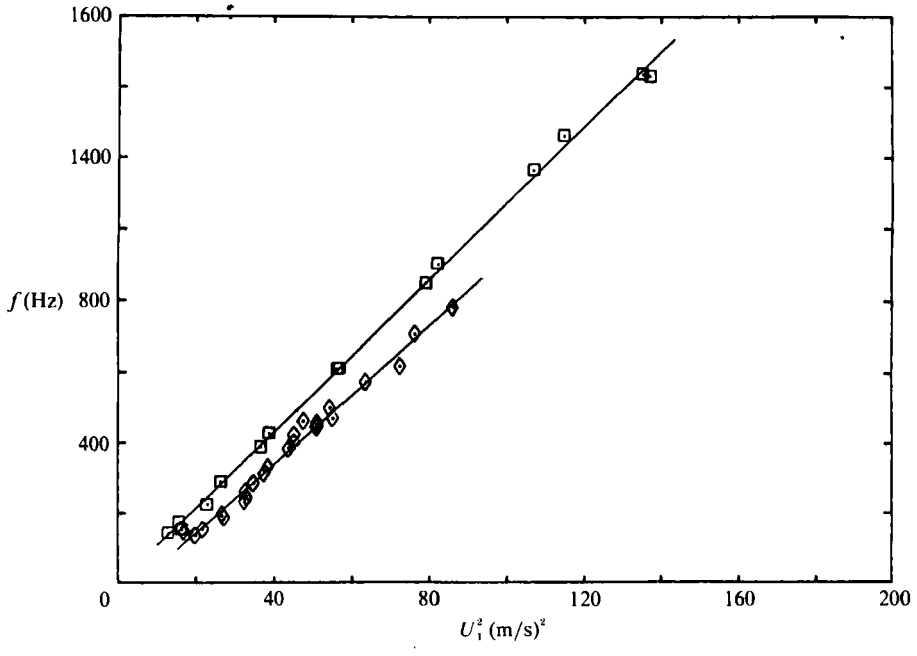

FIGURE 18. Comparison of eddy-shedding frequency with free-stream velocity for a hemispherical (⊡) and a cylindrical (◇) roughness element: $k = 0.32$ cm, $x_k = 91.4$ cm.

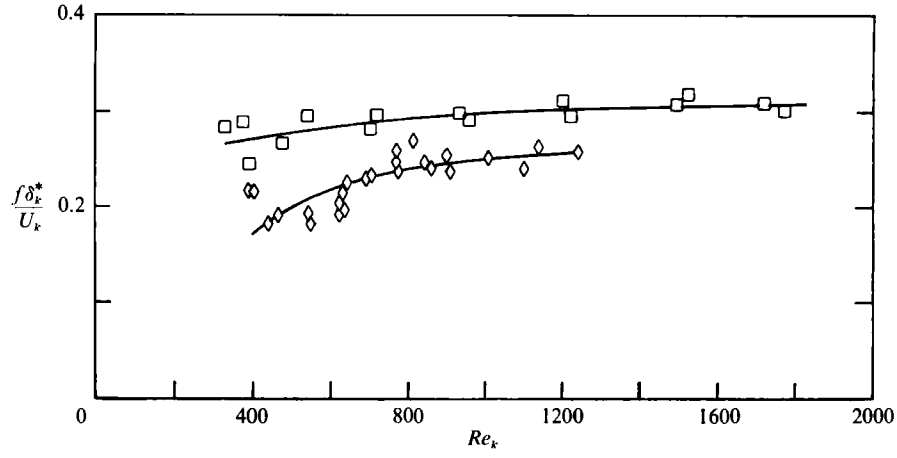

FIGURE 19. Comparison of Strouhal behaviour for a hemispherical (□) and a cylindrical (◇) roughness element: $k = 0.32$ cm; $x_k = 91.4$ cm.

of k/δ_k^* is not large, being on the order of 10% for its largest value. Although (2) appears to mask, particularly at the lower Reynolds numbers, a small dependence on Reynolds number, it is within the experimental uncertainty a reasonable representation of the Strouhal behaviour of hemispherical elements.

The shedding frequencies and the resulting Strouhal number obtained with a cylindrical element, albeit for only one size and position, are compared with the results obtained for a corresponding hemispherical element, i.e. the same k and x_k, in figures 18 and 19, respectively. Both sets of measurements were made at $\bar{x} = 2.54$ cm. It is seen that the shedding frequency for the cylindrical element is also linearly dependent on U_1^2. However, the frequency is lower than that for a hemispherical element at the same Re_k and k/δ_k^*. The Strouhal number is correspondingly lower, and exhibits a greater dependence on Re_k at the lower Reynolds numbers, i.e. for $Re_k < 800$. This difference in shedding frequency of the hemispherical and cylindrical elements is consistent with the greater stability of the cylindrical roughness. It is reasonable to infer that it is due to the difference in stability of the mean velocity profiles established immediately downstream by the elements. This behaviour of the profiles may be reflected not only in the greater variation of $f\delta_k^*/U_k$ with Re_k for the cylindrical element, but also in the variation of the critical Re_k referred to previously in §4.

It appears that δ_k^* is a more appropriate characteristic length for the Strouhal number for single roughness elements in a laminar boundary layer than the length k which has generally been used in characterizing Strouhal behaviour. The latter, in contrast, exhibits a very strong dependence on Reynolds number. Data in the literature pertaining to the parametric behaviour of the eddy-shedding frequencies is minimal and limited to Furuya & Miyata (1972) and Acarlar & Smith (1984, 1987). Furuya & Miyata (1972) provide data on the Strouhal behaviour for spherical and cylindrical elements with the latter having their axis in the spanwise direction rather than in the y-direction as in the present study. Acarlar & Smith (1984, 1987), however, did study the Strouhal behaviour of hemispherical elements. Both of these investigations, in contrast to the present study, were conducted in free-surface water channels, and in neither investigation are the results presented in a form sufficiently explicit to permit comparison with the present study on a basis other than with k as

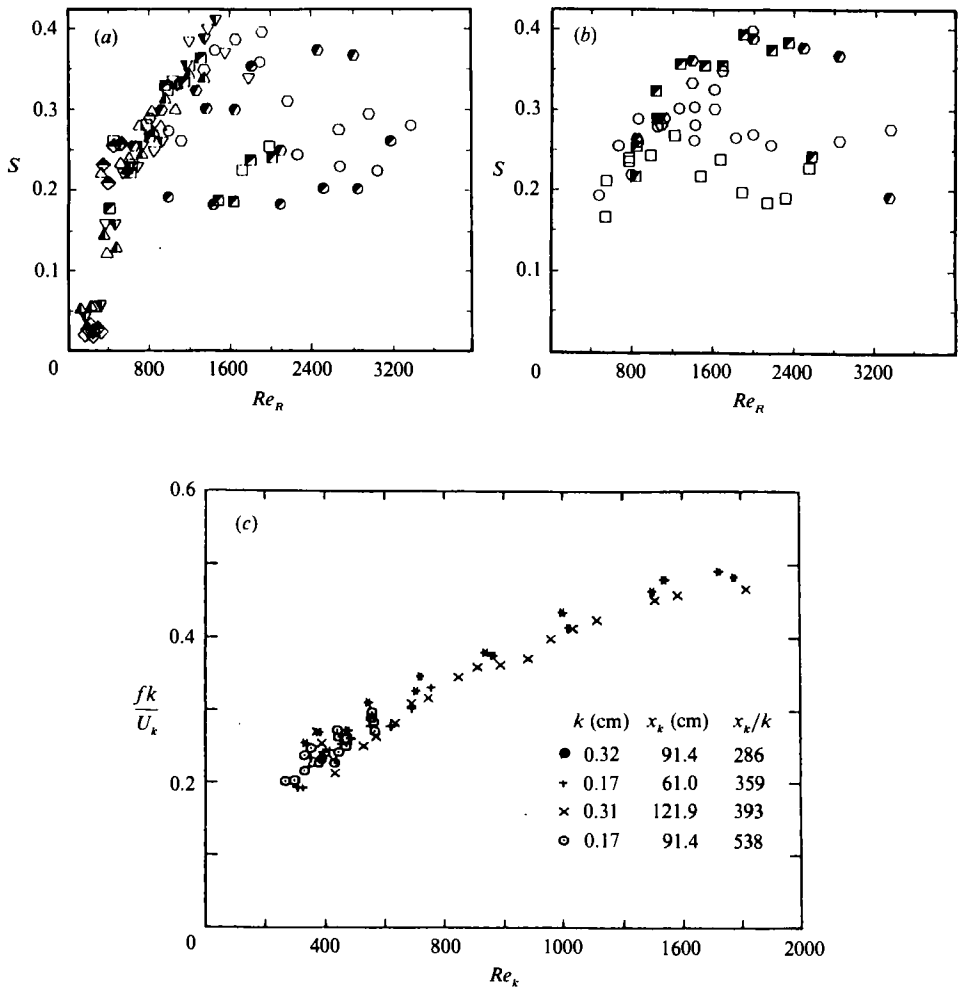

FIGURE 20. Comparison of Strouhal behaviour for hemispherical elements observed in the present study (*c*) with Acarlar & Smith (1984, 1987) (*a*, *b*). (*a*) Open symbols $x_R = 140$ cm, half-filled symbols $x_R = 35$ cm: ○, $R = 18$ mm; ○, 12 mm; □, 8 mm; ▽, 7 mm; ▽, 6 mm; ◇, 3 mm. (*b*) Open symbols $x_R = 67$ cm, half-filled symbols $x_R = 43$ cm: ○, $R = 8$ mm; □, 9 mm; ○, 12 mm.

the characteristic length. Be that as it may, the Strouhal behaviour for hemispherical elements on this basis is compared in figure 20 with that presented in Acarlar & Smith (1984, 1987). In their nomenclature S, R, x_R, and Re_R correspond to our fk/U_k, k, x_k, and Re_k, respectively. The present measurements are significantly higher with a steeper gradient than those of Acarlar & Smith (1984, 1987) over the range of Re_k. They observe that the large scatter in their results for $Re_k > 1000$ is not due to experimental uncertainties, but infer from the occurrence of multiple peak power spectra that there is an actual instability in the eddy-shedding behaviour. Apart from the deviations in shedding frequency previously mentioned, this unstable behaviour was not observed in the present study. The reason for the differences between the present study and that of Acarlar & Smith (1984, 1987) is not readily apparent; however, in their experiment the size of the roughness element relative to the boundary-layer thickness was much larger. This aspect is referred to further in

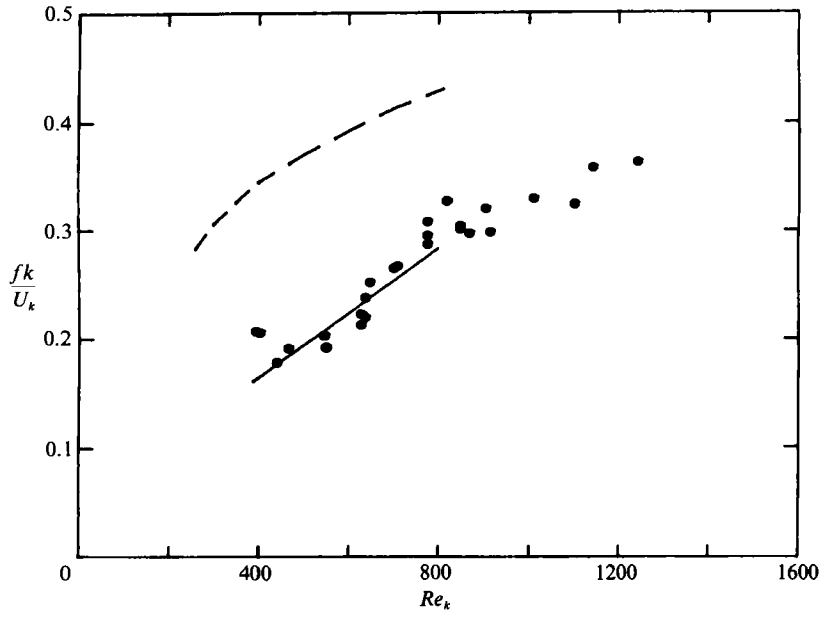

FIGURE 21. Comparison of Strouhal behaviour for a cylindrical roughness element observed in the present study (●) with Furuya & Miyata (1972) (– – –, cylindrical; ——, spherical).

§8. In addition, in the present study the frequencies were obtained from oscillograms, whereas in Acarlar & Smith (1984, 1987) the shedding frequency was determined from power spectra. It is perhaps worth commenting that the occurrence of multiple-peak power spectra is not a sufficient condition for unstable eddy-shedding behaviour. It is not surprising that power spectra of asymmetric and modulated signals, for example, as shown in figures 11, 12, and 13 would exhibit multiple peaks that vary not only with U_1 but with y and $\bar{x}$.

The variation of the Strouhal number, fk/U_k, with Re_k for the cylindrical element with $k/d = 1.0$ is compared in figure 21 with data faired from Furuya & Miyata (1972). The data selected are for a spherical element, and a cylindrical element with an aspect ratio of 1.0. The cylindrical element of the present study exhibits, within the experimental uncertainty, about the same Strouhal numbers for a comparable range of Reynolds number as does the spherical element. However, both have values that are almost half of those for the cylinder of Furuya & Miyata (1972). Inasmuch as a two-dimensional roughness element has been found to be more effective than a three-dimensional one in inducing transition, it is perhaps not surprising that the cylinder with its axis in the spanwise direction would exhibit greater instability, if such is to be inferred from the greater Strouhal number, than one with its axis normal to the surface. The inference drawn herein that the Strouhal number may reflect the degree of instability for a roughness element stems conceptually from the stability calculations for two-dimensional wall-bounded flows in an adverse pressure gradient, i.e. the instability extends to higher and higher frequencies with increasingly inflexional velocity profiles (Pretsch 1941, 1942; Schlichting & Ulrich 1942; Wazzan, Okamura & Smith 1968). The effect of aspect ratio on the Reynolds number of transition for cylindrical elements mounted on the surface with their axis in the spanwise direction was examined by Norman (1972). The Reynolds number of transition, as observed at a fixed distance downstream from the element, was found

to decrease with increasing aspect ratio, over a range of aspect ratios from 1 to 8, and at an aspect ratio of 8 the Reynolds number of transition was actually lower than for a two-dimensional element. Furuya & Miyata (1972) also investigated the effect of aspect ratio on Strouhal numbers for cylindrical elements with their axis in the spanwise direction. They found, over a range of aspect ratios from 1 to 6 that the Strouhal numbers decreased with increasing aspect ratio. These results lead to the inference of decreasing Strouhal numbers with decreasing critical roughness Reynolds numbers for cylindrical elements with their axis in the spanwise direction. This trend of Strouhal number with critical roughness Reynolds number is opposite in direction from that observed in the comparison of the behaviour of hemispherical elements and a cylindrical element in the present study. The issue is complicated by the evidence (Klebanoff & Tidstrom 1972) that two-dimensional roughness elements, in inducing earlier transition, do not exhibit the critical behaviour involving the shedding of discrete vortices. Roughness shape, as well as aspect ratio, appear to play a role, and it may well be that the Strouhal number is not a sufficient criterion for indicating the degree of instability. It is apparent that these aspects warrant further study. Their resolution is amenable to experiment, and would go a long way toward providing a better understanding of the mechanism by which discrete roughness elements induce earlier transition to turbulent flow.

6. Eddy shedding – unsteady flow

One would readily infer from the discussion in §5 that the hairpin eddies are intrinsic to the transition process induced by a three-dimensional roughness element. However, the view existing in the literature (Mochizuki 1961*a*; Norman 1972; Gupta 1980; Norman & Morkovin 1972; Tani 1981) is that such eddies are not related, or at best are only indirectly related, to the transition process. It was therefore deemed desirable to attempt to clarify the role they do play. To this end, the effect of an oscillatory free-stream velocity was investigated. The free-stream velocity, U_1, was oscillated sinusoidally with a small amplitude, ΔU_1, about some mean value, $\bar{U}_1$, and at a sufficiently low frequency, n, for a quasi-steady assumption to be valid. That is,

$$U_1(t) = \bar{U}_1(1 + A \sin \omega t), \tag{3}$$

where $A = \Delta U_1/\bar{U}_1$, and $\omega = 2\pi n$. Of particular interest is the effect of the variation of $\bar{U}_1$ relative to U_c.

The response of the laminar boundary layer without roughness to the free-stream oscillation is illustrated in figure 22. The dashed lines in the figure were drawn as a best fit to the data points. Figure 22 shows the distributions across the boundary layer of the oscillating velocity component, ΔU, and the phase of the oscillation, ϕ. A positive angle represents an advance in phase relative to the free-stream oscillation. The measurements were made at $x = 94$ cm with $\bar{U}_1 = 6.8$ m/s and $n = 1.0$ Hz. The resulting frequency parameter, $x\omega/\bar{U}_1$, was 0.87, and A was 0.12. The trends exhibited by the distributions are similar to previous results (Hill & Stenning 1960). The mean velocity distribution for the unsteady boundary layer without roughness is compared with its steady-flow counterpart in figure 23. Also shown in figure 23 is a comparison of the mean velocity profiles for steady and unsteady flow downstream of a hemispherical roughness element. In the latter case, the measurements were made on the centreline at 2.54 cm downstream of a hemispherical element which had a nominal diameter of 3.18 mm, an effective height of 1.7 mm and was positioned at $x_k = 91.4$ cm. The free-stream velocities were slightly above

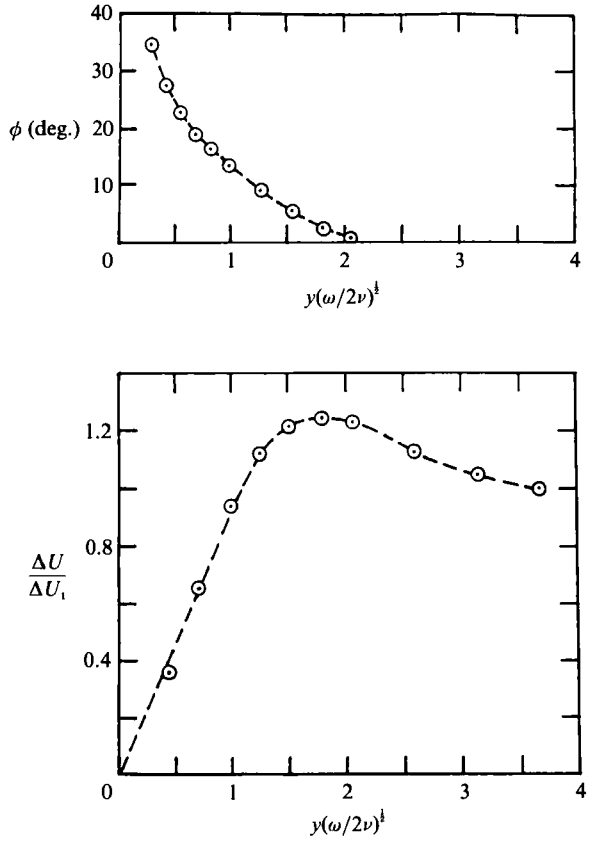

FIGURE 22. Phase and amplitude response of the laminar boundary layer without roughness to a free-stream oscillation. $U_1 = 6.8$ m/s, $x = 94$ cm, $n = 1.0$ Hz.

critical, being 8.3 and 8.2 m/s for the steady and unsteady flow, respectively. The oscillating frequency was 1 Hz with $A = 0.13$. It can be concluded from the agreement of the disturbances for steady and unsteady flow that the oscillation behaves linearly. In addition, it is of interest to note that the mean velocity distribution at $\bar{x} = 14.9k$ at about the critical speed is insensitive to the time dependence of the eddy-generating process associated with the unsteady flow.

The effect of an oscillating free stream on the eddy-shedding process was studied with the hemispherical element positioned at $x_k = 91.4$ cm with $k = 1.7$ mm. Simultaneous signals of u in the boundary layer and of U_1 in the free stream with free-stream oscillation frequencies of 1 and 2 Hz, at various $\bar{U}_1$ and associated ΔU_1, were monitored by strip-chart recording at $\bar{z} = 0$ cm and $\bar{x} = 2.54$, 30.5, and 61.0 cm. The upper trace in each recording is the free-stream oscillating velocity, and the lower trace is the u-fluctuation in the boundary layer. Time increases from left to right, and a decreasing velocity is in a downward direction. Figures 24 and 25 show the recordings at $\bar{x} = 2.54$ cm for oscillation frequencies of 1 and 2 Hz, respectively. The position in the boundary layer was at $y = 3.18$ mm. The eddy shedding is characterized by intense fluctuations in the direction of lower velocity superposed on the primary oscillation. This type of signal is consistent with the passage of hairpin eddies with legs that are rotating as indicated in §5. It should be noted that the asymmetry of the beginning and end of the eddy shedding relative to the free-stream

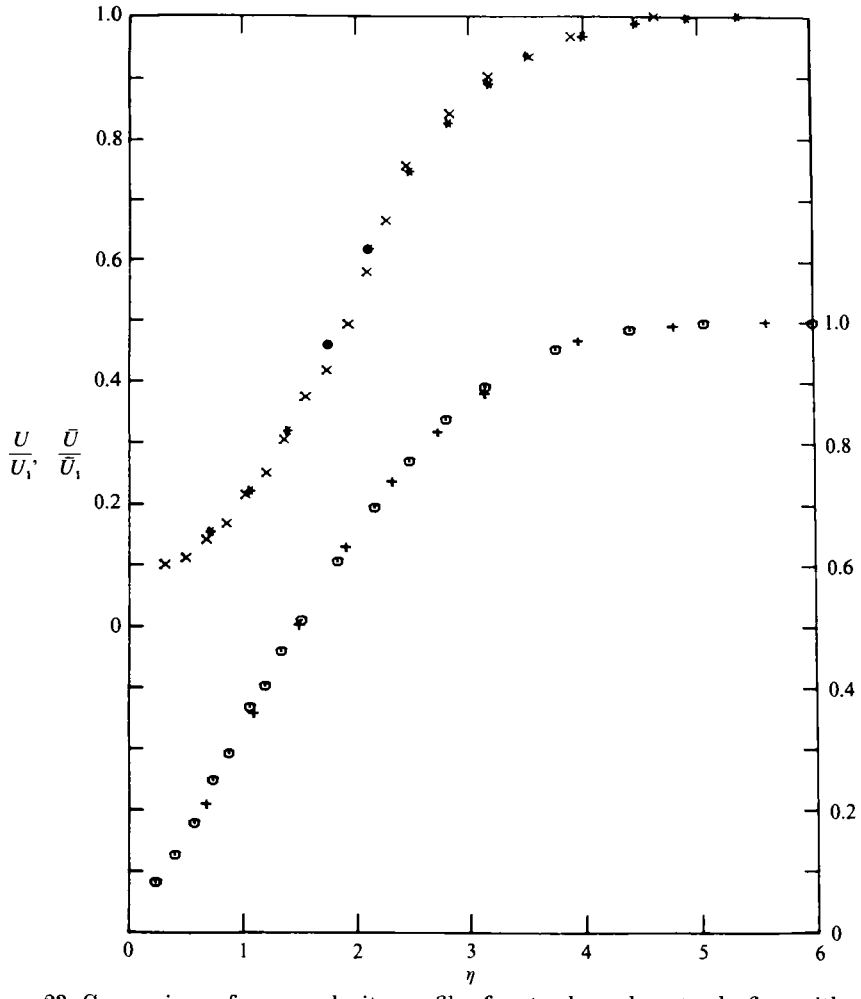

FIGURE 23. Comparison of mean velocity profiles for steady and unsteady flow with and without a roughness element: ⊙, without roughness, steady; +, without roughness, unsteady; ×, with roughness, steady; *, with roughness, unsteady.

oscillation as shown in figures 24 and 25 is not a real effect. It should not be interpreted, for example, as arising from a difference in the stability of an accelerating flow *vis à vis* a decelerating flow. It arises from an inadvertent low-frequency cutoff of 2 Hz in the hot-wire electronics for both probes, which introduced a 60° and a 40° phase advance relative to the phase of the eddies for oscillation frequencies of 1 and 2 Hz, respectively. In addition, the low-amplitude ripple of 20 Hz in the boundary-layer signal is a consequence of the vibration induced by the fan motor which was previously referred to in §3 and which manifests itself because of the velocity gradient in the boundary layer. In any event, these extraneous effects do not mitigate the essential features of the effect of unsteady flow on the behaviour of the roughness.

It is seen from figure 24 that for a steady flow at $U_1 = 8.5$ m/s ($Re_k = 337$) eddies are shed continuously. When the flow is oscillated at a value of $\bar{U}_1$ which coupled to the associated ΔU_1 is below some value of U_1 then no eddies are observed, as in the recording for $\bar{U}_1 = 5.8$ m/s with $\Delta U_1 = 0.64$ m/s. However, eddies, although of

relatively lower intensity, are observed over part of the cycle in the recording for $\bar{U}_1 = 6.9$ m/s and $\Delta U_1 = 0.84$ m/s. As $\bar{U}_1$ is further increased, the duration, ΔT, of the eddies increases, and at $\bar{U}_1 = 9.7$ m/s with $\Delta U_1 = 1.38$ m/s eddies are shed continuously over the cycle. A recording with a much faster chart speed, for the latter condition, is also shown in order to more clearly illustrate the nature of the fluctuations in the recording and their similarity to the fluctuations for the steady flow condition. If an appropriate allowance is made for the aforementioned phase advance, the variation of the amplitude and frequency of the fluctuation with U_1 is consistent with quasi-steady behaviour. The recordings in figure 25 show results similar to figure 24. The smaller amplitude at the various $\bar{U}_1$ with $n = 2$ Hz, as compared to $n = 1$ Hz, is a consequence of the time constant of the unsteady wind tunnel. However, it is evident that except for the effect the amplitude may have on ΔT the behaviour scales with the frequency n, and may be regarded as quasi-steady.

It appears from the recordings in figures 24 and 25 that the onset of the hairpin eddies is associated with a critical value, U_{1c}, of the oscillatory free stream. It can be readily shown from (3) that

$$\Delta T = \frac{1}{\omega}\left[\pi - 2\sin^{-1}\left(\frac{U_{1c} - \bar{U}_1}{\Delta U_1}\right)\right] \tag{4}$$

and

$$U_{1c} = \Delta U_1 \sin\left[\tfrac{1}{2}\omega\left(\frac{\pi}{\omega} - \Delta T\right)\right] + \bar{U}_1. \tag{5}$$

It is seen from (4) that the scaling of ΔT with frequency n is to be expected and that the effect of amplitude is to change the slope of the variations of ΔT with $\bar{U}_1$ about $\Delta T = 0.5$. It is of interest to compare the values of U_{1c} with the critical velocity, U_c, corresponding to the critical roughness Reynolds number of transition observed in §4. The values of U_{1c} obtained from (5) for the various recordings in figures 24 and 25, using the measured values of ΔT, averaged over a number of cycles, are summarized in Table 1. No attempt was made to establish with specificity the conditions for $\Delta T = 1$, and consequently the associated value of U_{1c} is not included in the table. The consideration of a critical value of velocity, U_{1c}, from the recordings in figures 24 and 25 is not inconsistent with the discussion in §5, i.e. the presence of periodic disturbances at values of $U_1 < U_c$ and the continuous transition from wave to vortex with increasing U_1. It is not inconsistent because of the inference from figures 24 and 25 that disturbances which may exist for $U_1 < U_{1c}$ are restricted in their extent from the surface to $y < 3.18$ mm. Concomitantly, at a given $\bar{U}_1$ and ΔU_1, U_{1c} is not a uniquely critical velocity. It may vary with $\bar{x}$ and y, depending on the 'topology' of the vortical structures. This is discussed further in §7. Nevertheless, the correspondence of the values of U_{1c} and $U_c = 8.3$ m/s ($Re_k = 325$) is consistent with the conclusion that the eddy generation is a necessary condition for the induced transition. The difference in the value of $U_c = 8.3$ m/s from the previously stated value of 8.1 m/s used in connection with the discussion of figures 11 and 12 arises from the variation in ν.

The question as to the intrinsic importance of the eddies to the transition process and the turbulence structure is addressed further by the strip-chart recordings shown in figures 26–29 for $n = 1$. These were obtained over a range of $\bar{U}_1$ and ΔU_1 comparable to those in figures 24 and 25. The various positions in the boundary layer for which the recordings shown in figures 26–29 were obtained are summarized in table 2. Similar strip-chart recordings were made at the same $\bar{x}$- and y-positions as shown in table 2 for $n = 2$. These are not shown because of their similarity to those for $n = 1$;

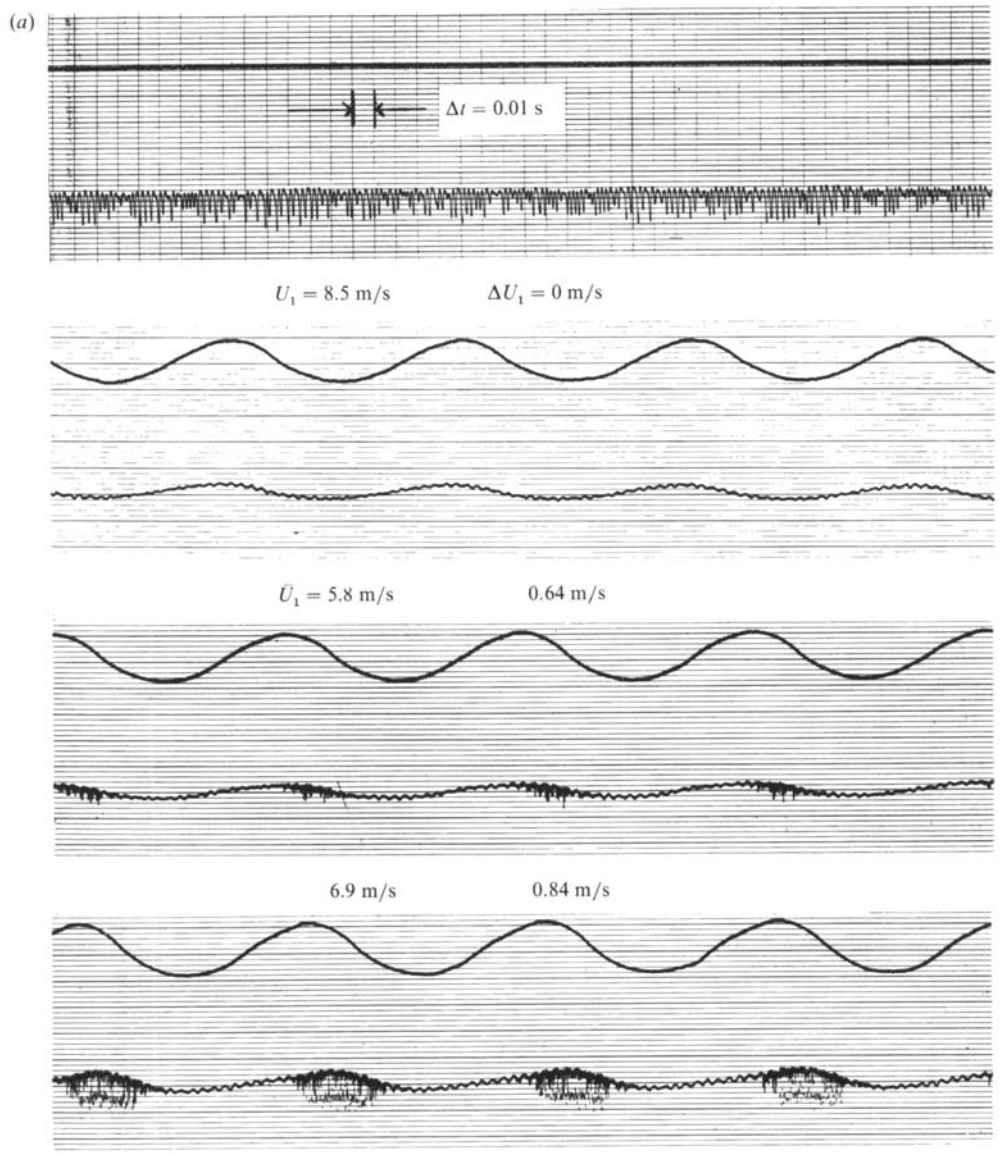

FIGURE 24 (a). For caption see facing page.

however, the results obtained therefrom are included in figure 30 below. As for figures 24 and 25, time increases from left to right, and a decreasing velocity is in a downward direction. The recordings reveal a number of interesting features. It is seen that the eddies which are clearly observable at $\bar{x} = 2.54$ cm have, by $\bar{x} = 30.5$ cm, induced or evolved into a turbulent spot. In this connection, it should be noted that the inadvertent low-frequency cutoff of 2 Hz, referred to previously, has distorted the signal associated with the spot in the recordings with an oscillating free stream. More specifically, it is responsible for the decreasing velocity associated with the spot passage and the minimum and rapid rise following the passage of the spot as seen, for example, in the recording for $\bar{U}_1 = 8.2$ m/s in figure 26. Apart from this

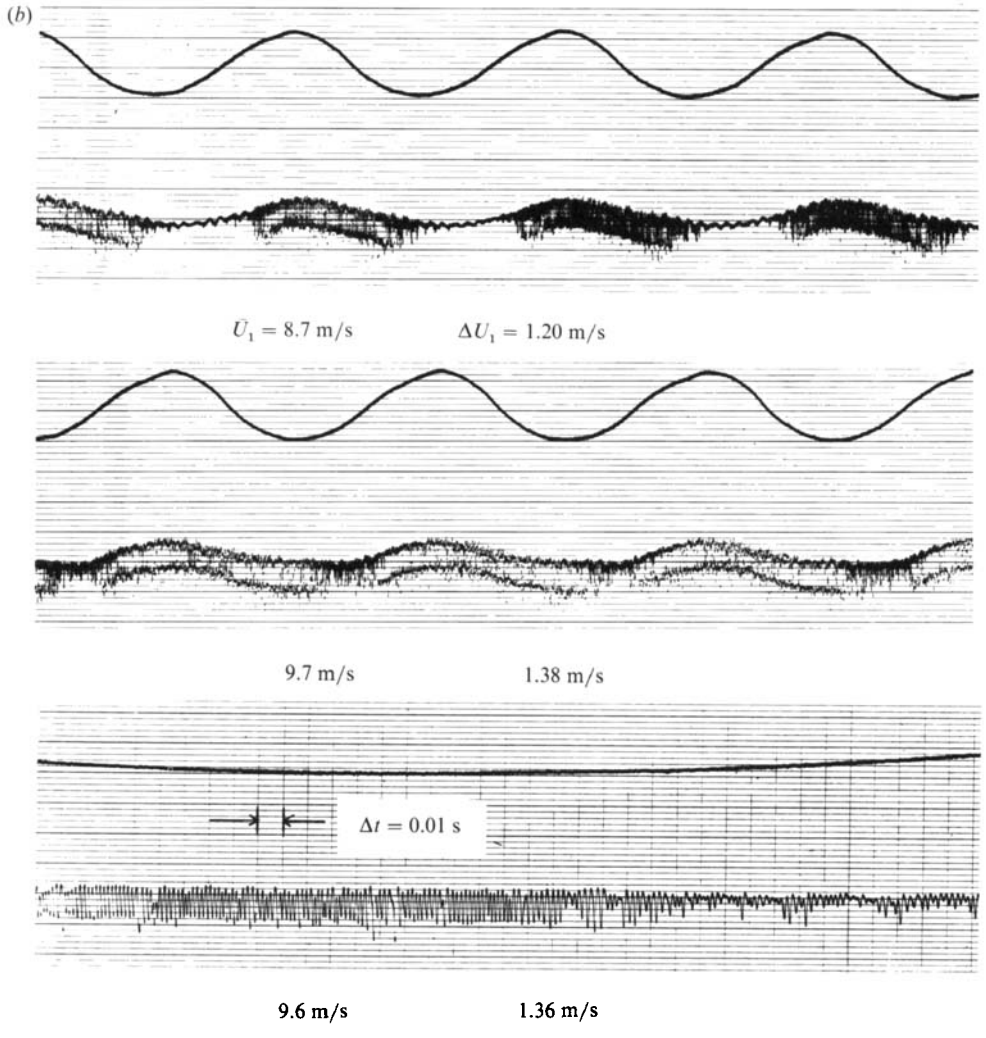

FIGURE 24. Strip-chart recordings of the simultaneous U_1-fluctuation in an oscillatory free stream, and the u-fluctuation in the boundary layer downstream of a hemispherical roughness element. $k = 1.7$ mm, $x_k = 91.4$ cm, $\bar{x} = 2.54$ cm, $y = 3.18$ mm, $z = 0$ cm, $n = 1.0$ Hz (top trace: $n = 0$).

extraneous effect the spots as shown in the various recordings of figures 26–29 exhibit the characteristic features generally associated with the passage of a turbulent spot (Schubauer & Klebanoff 1955; Wygnanski, Sokolov & Friedman 1976; Cantwell, Coles & Dimotakis 1978). These are an abrupt step-up in velocity near the surface, an abrupt step-down in velocity in the outer region of the boundary layer, and an increase in spot duration with $\bar{x}$ resulting from the difference in velocity at the leading and trailing interfaces of the spot. The changes in velocity associated with the spot passage reflect the difference between the turbulent velocity profile within the spot and the laminar velocity profile in the flow surrounding the spot.

For a steady velocity which is near the critical speed, U_c, random turbulent spots form downstream of the roughness element. This is evident from each of the recordings in figures 26–29 for which $U_1 = 8.2$ or 8.3 m/s, and $n = 0$ Hz. The corresponding values of Re_k are 312 and 319 for $U_1 = 8.2$ and 8.3 m/s, respectively.

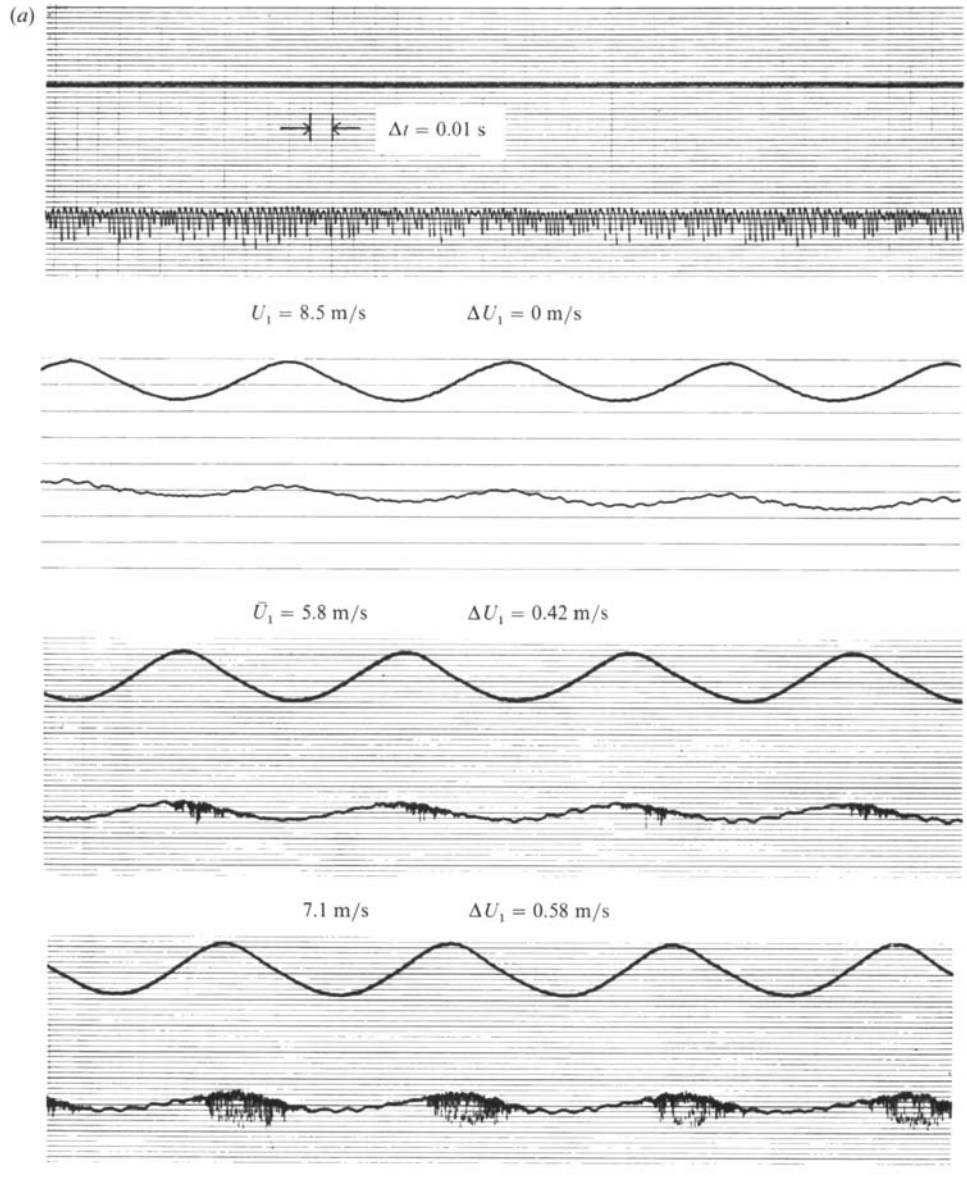

FIGURE 25 (*a*). For caption see facing page.

It appears that for the steady flow condition at $\bar{x} = 61.0$ cm the spots are not only much more developed in their turbulence structure as compared to $\bar{x} = 30.5$ cm but also may have increased in number. It is not unexpected that the spots will grow in size as they proceed downstream; however, it is not clear whether the aforementioned differences between the spots at $\bar{x} = 61.0$ cm and 30.5 cm are real or apparent. This aspect was not investigated further; however, the spot formation is extremely sensitive to U_1, and it may be that the differences reflect the imprecision in the measurement of U_1.

It is seen from the steady flow condition in figures 24 and 25 at $U_1 = 8.5$ m/s

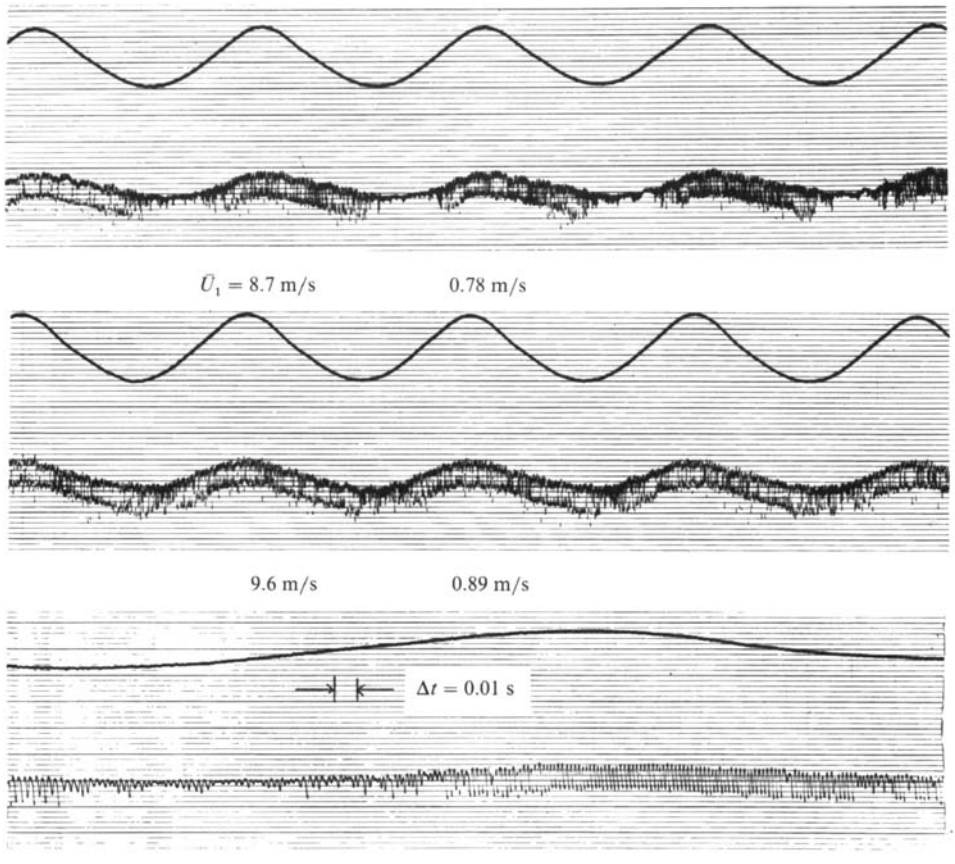

FIGURE 25. As figure 24 but for $n = 2.0$ Hz (top trace: $n = 0$).

$\bar{U}$(m/s)	ΔU_1(m/s)	n(Hz)	ΔT(s)	U_{1c}(m/s)
6.9	0.84	1.0	0.19	7.6
7.6	0.98	1.0	0.36	8.0
8.7	1.20	1.0	0.68	8.1
7.1	0.58	2.0	0.09	7.6
7.6	0.64	2.0	0.19	7.9
8.7	0.78	2.0	0.39	8.1

TABLE 1

Figure no.	$\bar{x}$(cm)	y(mm)
26	30.5	0.61
27	30.5	6.35
28	61.0	0.61
29	61.0	6.35

TABLE 2. Positions of recordings in the boundary layer

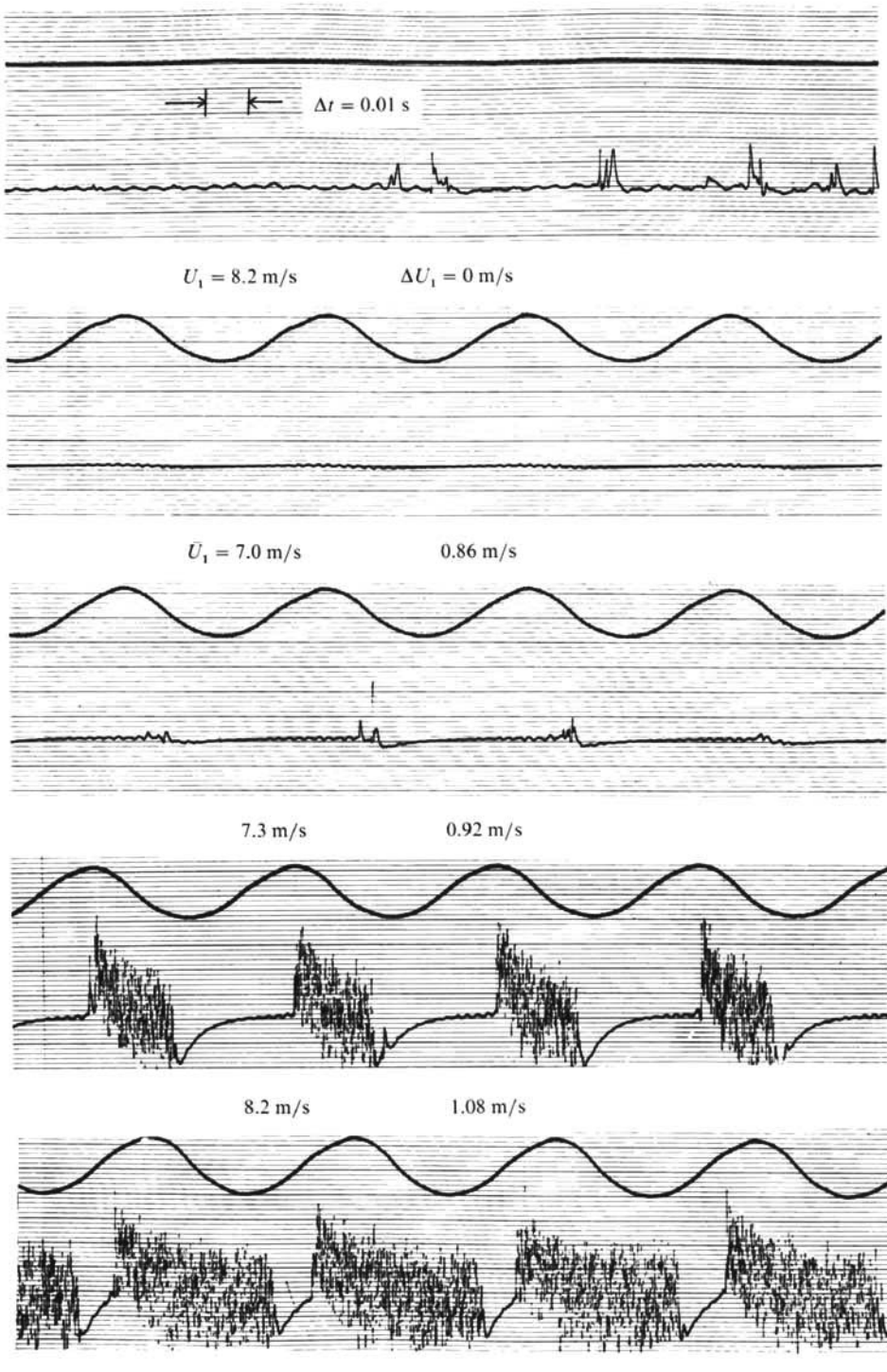

FIGURE 26. As figure 24 but at $\bar{x} = 30.5$ cm, $y = 0.61$ mm.

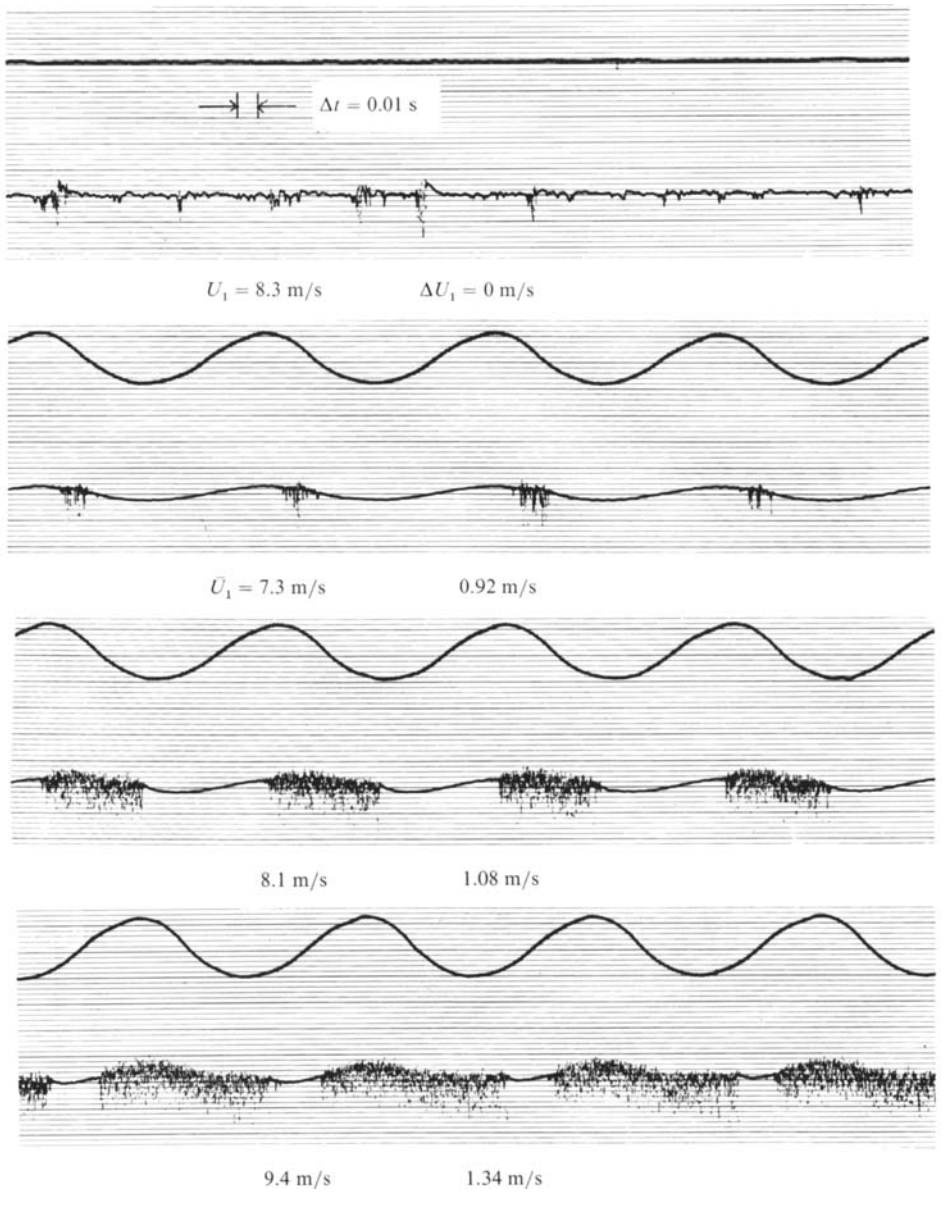

FIGURE 27. As figure 24 but at $\bar{x} = 30.5$ cm, $y = 6.35$ mm.

($Re_k = 337$) that the intensity of the eddies is highly modulated. This provides an explanation for the random occurrence of turbulent spots downstream of the roughness element, although there is a continuous generation of eddies by the roughness element. It is that since the eddy-shedding process is not well controlled and is highly modulated, eddies of relatively weak intensity may be damped, and not all eddies participate in the evolution of the turbulent spot. This point of view is supported by the behaviour with an oscillating free stream at the lower values of $U_1(m)$, where $U_1(m) = \bar{U}_1 + \Delta U_1$. In the recordings for $U_1(m) = 7.86$ and 7.74 m/s in figures 26 and 28, respectively, no turbulent spots are observed, although eddy shedding is observed in the recordings for $U_1(m) = 7.74$ and 7.68 m/s in figures 24 and

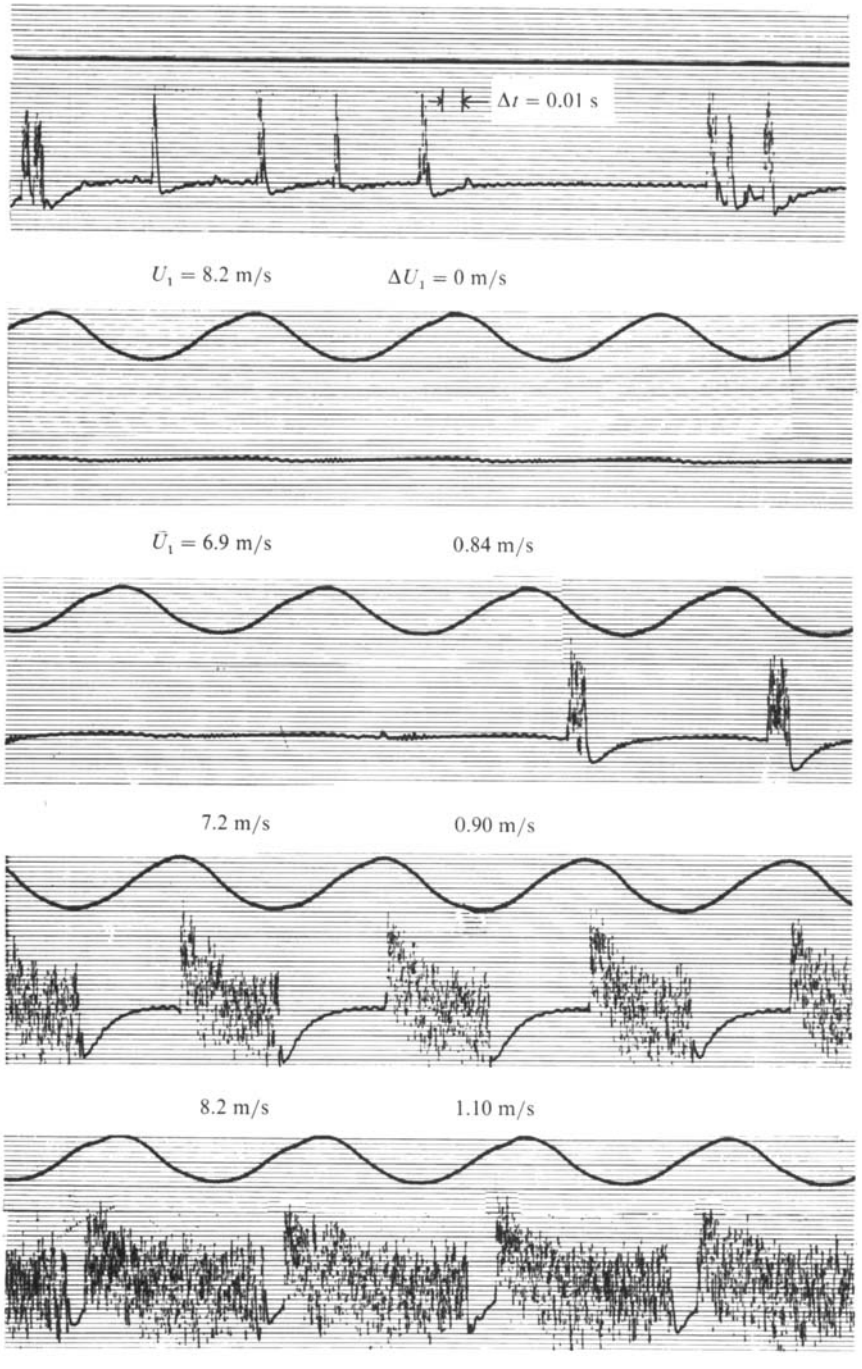

FIGURE 28. As figure 24 but at $\bar{x} = 61.0$ cm, $y = 0.61$ mm.

25. In addition the recordings at $U_1(m) = 8.22$, 8.10, and 7.98 m/s in figures 26, 28, and 29, respectively, show evidence of intermittency, i.e. spots do not necessarily occur during every cycle. It should be noted that the abovementioned conclusion that the recordings in figure 24 and 25 at $U_1(m) = 7.74$ and 7.68 m/s illustrate eddy

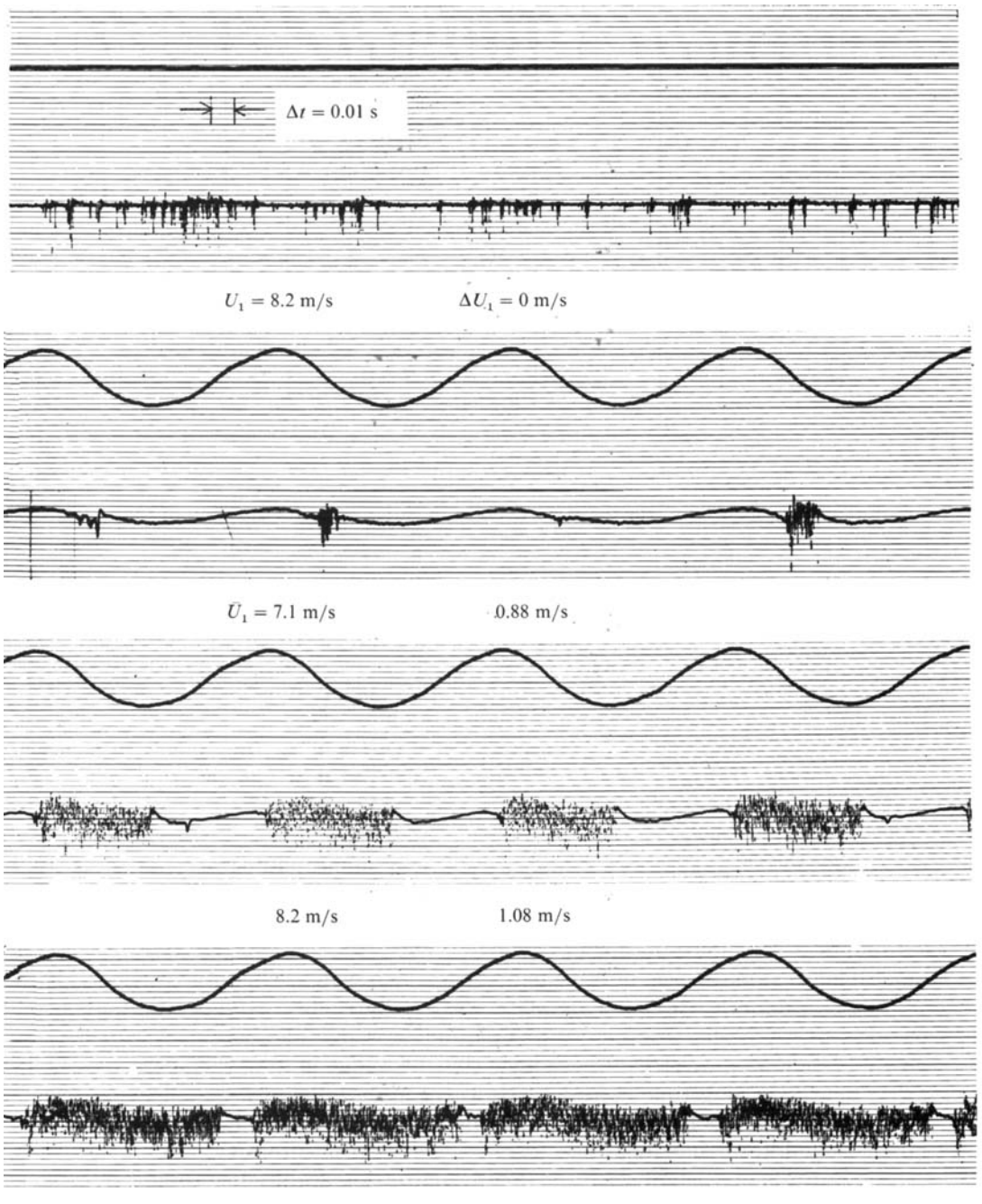

FIGURE 29. As figure 24 but at $\bar{x} = 61.0$ cm, $y = 6.35$ mm.

shedding is inferred from the decreasing velocity fluctuation associated with the disturbance, and that no attempt was made to specifically identify the vortical nature of the disturbance. In this connection, Hall (1967) in his smoke-visualization study of the flow behind a sphere observed that although strong periodic laminar

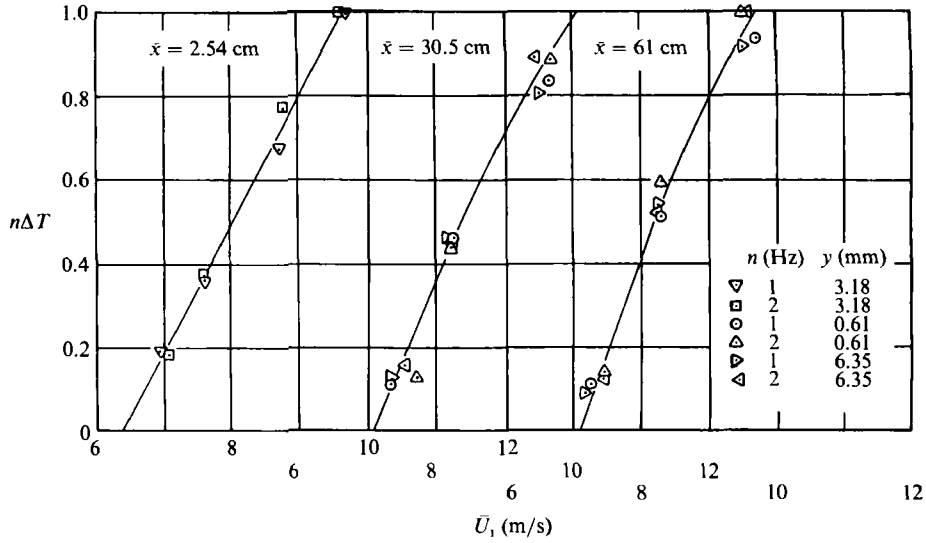

FIGURE 30. Comparison of the duration of eddy shedding with the duration of the resulting turbulent spot.

vortices were formed at subcritical Reynolds numbers, no turbulence occurred downstream, and the vortices decayed as they propagated downstream. Although Norman (1972) did not explicitly address this question, Morkovin (1984) has commented that Norman did observe similar behaviour behind a fence-type roughness element with an intensity level as high as 4%.

The presence of random turbulent spots downstream of the roughness at about the critical velocity provides a view different from the flow-visualization studies in regard to the detailed behaviour of the transitional region where transition moves rapidly upstream as shown in figure 9. The china-clay studies of Gregory & Walker (1950) and Matsui (1962) and the long-exposure smoke photographs of Mochizuki (1961*a*) have led to the view that the rapid upstream movement of transition is due to the vertex of a turbulent wedge that moves rapidly forward with a slight increase in roughness Reynolds number. The view from the present study is that this transitional region consists of turbulent spots which increase in number with a slight increase in roughness Reynolds number. As they move downstream, the spots grow laterally, overtake one another, and sweep out a wedge-like boundary which gives the impression of an upstream-moving turbulent wedge in flow-visualization studies with a relatively long-time exposure. However, at a value of Re_k sufficiently above the critical roughness Reynolds number, the spots may have so increased in number, and/or the eddies being shed may have so increased in intensity, that a turbulent wedge condition consistent with the flow-visualization studies has been established.

It is shown in figures 24–29 that as $\bar{U}_1$ increases, the duration of the turbulent spots as well as the duration of eddy shedding increases. It was of particular interest to examine how the duration of spots and eddies compared. For this purpose, the variation of $n\Delta T$ with $\bar{U}_1$ at $\bar{x} = 2.54$, 30.5, and 61.0 cm is shown in figure 30. Within the experimental accuracy, the small differences between the duration of eddy shedding at 1 Hz and 2 Hz at $\bar{x} = 2.54$ cm may be real and reflect the effect of amplitude as given by equation (4). This effect may also influence the scatter in the data at $\bar{x} = 30.5$ cm. However, faired curves are drawn through the data in order to

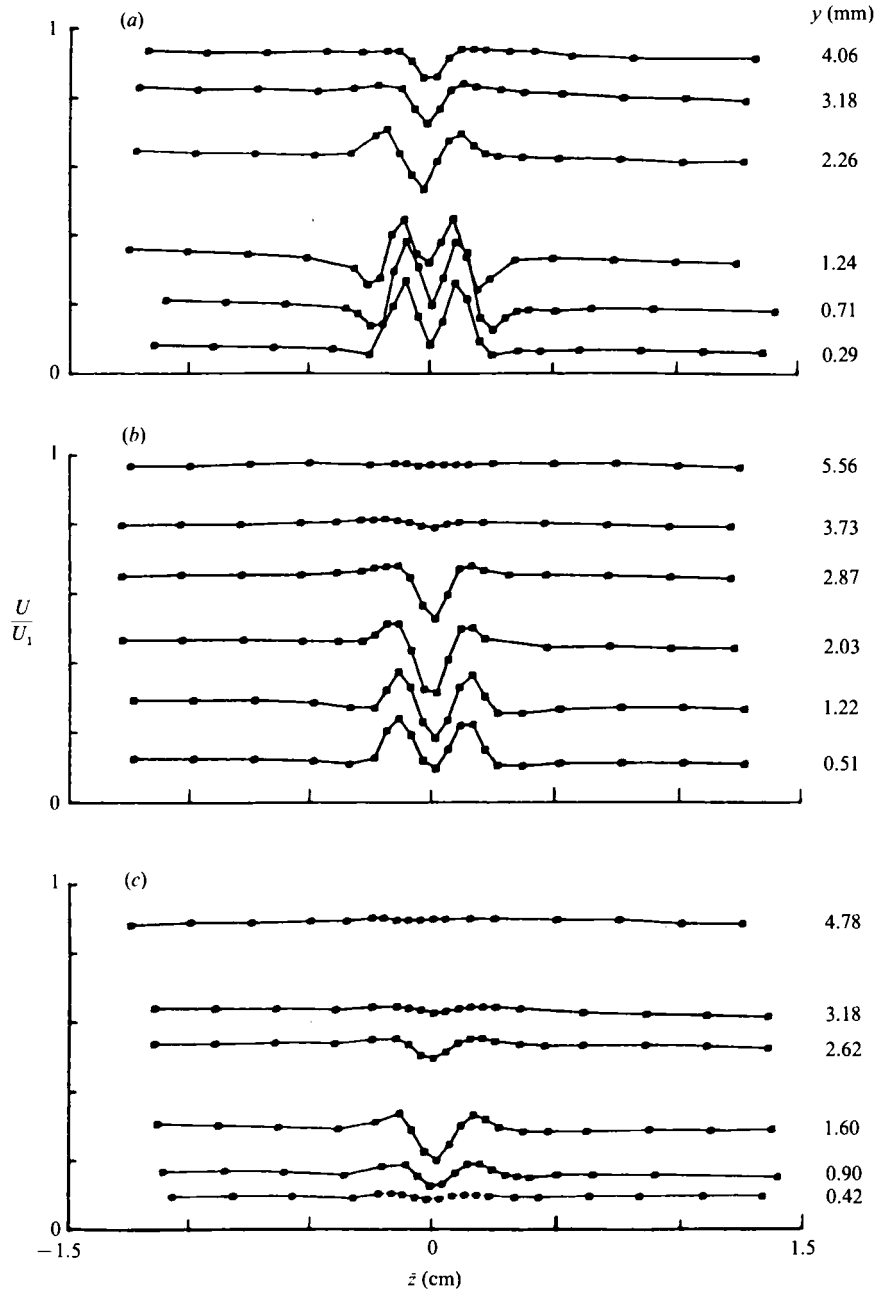

FIGURE 31. Spanwise distributions of mean velocity at various positions from the surface for varying unit Reynolds number. $k = 1.7$ mm, $x_k = 91.4$ cm, $\bar{x} = 2.54$ cm. (*a*) $U_1 \approx 11.8$ m/s, $U_1/\nu = 6.81 \times 10^5$ m^{-1}; (*b*) $U_1 \approx 8.3$ m/s, $U_1/\nu = 4.82 \times 10^5$ m^{-1}; (*c*) $U_1 \approx 6.1$ m/s, $U_1/\nu = 3.54 \times 10^5$ m^{-1}.

facilitate the comparison. It is seen that the degree of correlation increases with $\bar{U}_1$. For example, at $\bar{U}_1 = 8$ m/s the duration of the turbulent spot at $\bar{x} = 30.5$ cm is 0.73 of the duration of eddy shedding. At $\bar{U}_1 = 9$ m/s the duration of the turbulent spot at $\bar{x} = 30.5$ cm is 0.9 of the duration of eddy shedding. This supports the view previously expressed, i.e. that with increasing Re_k the intensity of the eddies may

increase, and a greater number may participate in the development of the spot. At $\bar{x} = 61.0$ cm the duration of the spot at $\bar{U}_1 = 8.0$ and 9.0 m/s is greater than that at $\bar{x} = 30.5$ cm. This is not unexpected since the velocity of the leading edge of the spot is much larger than the velocity of the trailing edge, and a small difference in ΔT can represent a large difference in the size of the spot. The high degree of correlation of the duration of turbulent spots with the duration of eddy shedding, coupled to the fact that when the eddy shedding is periodic with the frequency of the free-stream oscillation, the turbulent spots also become periodic, warrant the conclusion that not only is the eddy shedding essential to the transition process, but also the eddies, although modified in form, are intrinsic to the structure of the turbulence. An interesting inference with practical application is that unsteady flow effects may play a role in the variations, i.e. periodicity, randomness, and duration, of turbulent spots as indicated, for example, by surface gauges in transition tests on free-running vehicles.

7. Instability and transition

In their study of the transition process for a Blasius flow on a flat plate, Klebanoff *et al.* (1962) drew an analogy between the secondary inflexional instability occurring in the later stage of transition and the behaviour of a three-dimensional roughness element. The hairpin eddies described in §§5 and 6 are markedly similar to the eddies described in connection with the secondary instability. However, the eddy-shedding frequency associated with the roughness, as shown in figure 14, varies with U_1^2 rather than with $U_1^{\frac{3}{2}}$ as in Klebanoff *et al.* (1962). The analogy, therefore, may best be regarded as qualitative. However, this does not negate the possibility that the eddy shedding associated with roughness may well be a consequence of inflexional instability. It may be that for a roughness sufficiently larger than studied herein, for which the inflexion is further from the wall, an instability characteristic of a free-shear layer and a variation of eddy-shedding frequency with $U_1^{\frac{3}{2}}$ may occur.

The nature of the flow about a three-dimensional roughness element which results in an inflexional velocity profile in the immediate downstream vicinity of the roughness has been well documented. The essential features disclosed primarily by flow-visualization studies (Gregory & Walker 1950; Mochizuki 1961*a*, *b*; Matsui 1962; Norman 1972) are that two sets of vortices are established at a subcritical Reynolds number. One is a closely spaced pair of vortex filaments which form in the near wake, spiral upward at the rear of the roughness, and at the height of the roughness turn and trail downstream. The other is a horseshoe-shaped vortex close to the surface, which wraps around the front of the roughness forming a pair of streamwise vortices which also extend downstream. This array of vortices which results in an inflexional velocity profile at $\bar{z} = 0$ cm has been observed for a variety of three-dimensional roughness geometries such as spherical, cylindrical, hemispherical, conical, and rectangular. The flow-visualization studies (Mochizuki 1961*a b*) have also yielded the observation that as the free-stream velocity is increased the trailing vortex filaments begin to wave and this waviness increases with increasing velocity with a resulting roll-up into hairpin eddies. However, a differing view for the origin of the hairpin eddies from that observed by Mochizuki is presented herein.

The qualitative behaviour revealed by the flow-visualization studies manifests itself in the spanwise distributions of U and u' as shown in figures 31 and 32, respectively. The measurements were made at a distance of 14.9 roughness heights

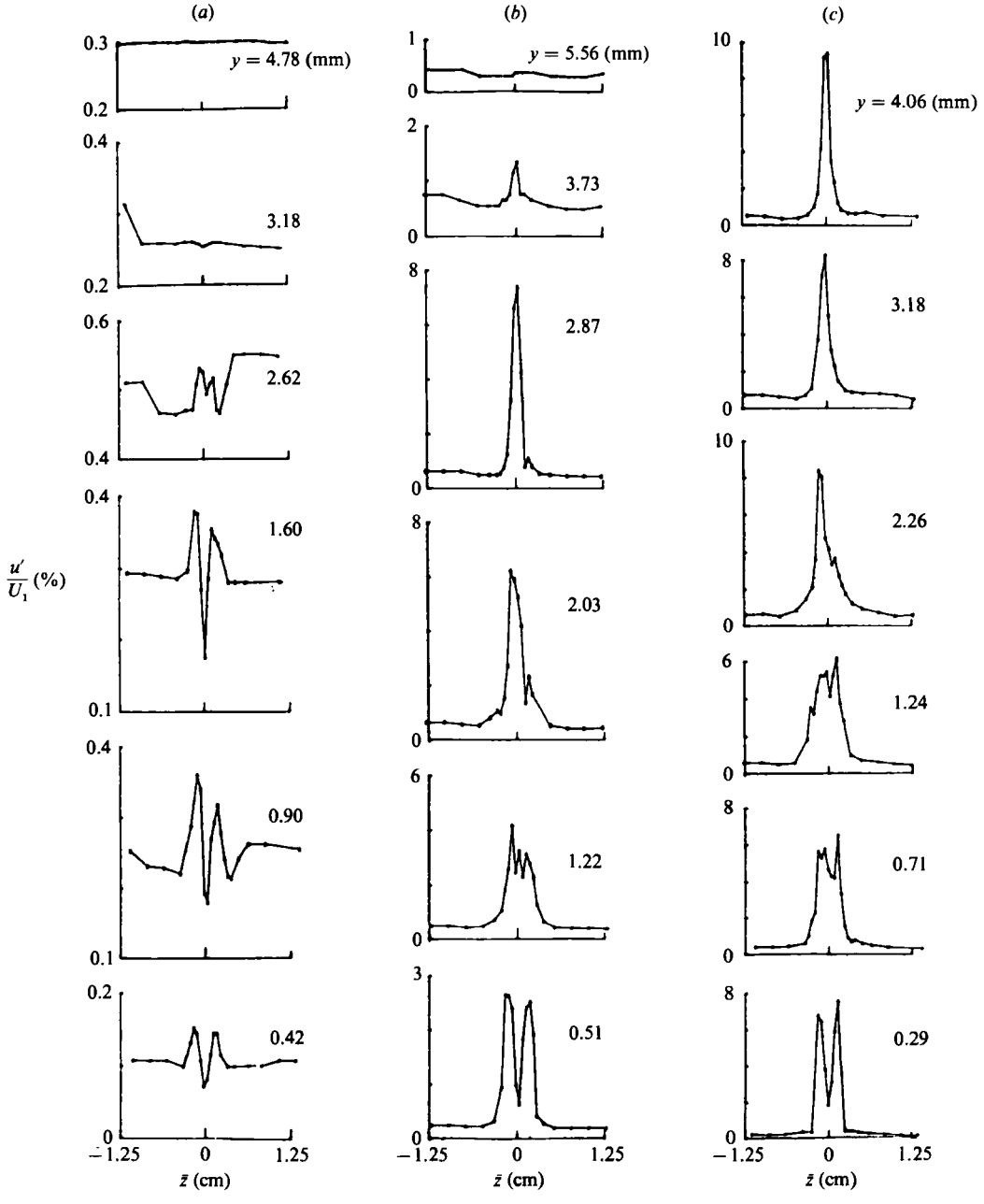

FIGURE 32. Spanwise distributions of the intensity of u-fluctuation at various positions from the surface for varying unit Reynolds number. $k = 1.7$ mm, $x_k = 91.4$ cm, $\bar{x} = 2.54$ cm. (*a*) Column $U_1/\nu = 3.54 \times 10^5$ m^{-1}; (*b*) 4.82×10^5 m^{-1}; (*c*) 6.81×10^5 m^{-1}.

downstream of the roughness elements and for three different unit Reynolds numbers. The frequency of eddy shedding discussed in §5 suggested that it would be more appropriate to carry out the boundary-layer surveys at a given U_1/ν rather than U_1, or more particularly at a constant roughness Reynolds number. Consequently, U_1 was adjusted to compensate for changes in ν, and the value of U_1

noted in figure 31 is the average value for the various distributions. The unit Reynolds numbers selected were such that one was below the critical roughness Reynolds number, one was at or slightly above critical, and one was significantly above critical. In this connection, it should be noted that the value of U_1/ν corresponding to a critical roughness Reynolds number of 325 is 4.76×10^5 (m^{-1}). At the subcritical Reynolds number the spanwise distributions of U clearly demonstrate the presence of the two pairs of streamwise vortices observed in the flow-visualization studies. The pair of trailing vortex filaments rotate in such a direction as to transfer momentum away from the plate at $\bar{z} = 0$ cm, and the horseshoe vortex rotates so as to transfer momentum towards the plate at $\bar{z} = \pm 0.5d$. The spanwise distribution of u' at the subcritical Reynolds number apparently reflects a low-level unsteadiness in the two sets of stationary vortices. At the higher Reynolds numbers the peak in the spanwise distributions of u' in figure 32 clearly indicates the presence of hairpin vortices. With increasing Reynolds number the peak increases in intensity and extends further from the surface consistent with the behaviour of the hairpin eddies as discussed in §§5 and 6.

It can be inferred from the spanwise distributions of figures 31 and 32 that above the critical Reynolds number the disturbed boundary layer may be considered to consist of an outer region dominated by eddy shedding and an inner region still dominated by the two sets of vortices alluded to at the subcritical Reynolds number. Implicit in this formulation is that there is a degree of interaction between the two regions. This interpretation is supported by the double peaks in the spanwise distribution of u' close to the surface at the Reynolds number above critical, which have the same spanwise spacing as the peaks at the subcritical Reynolds number. The intensity of these peaks increases from about 0.15% at the subcritical Reynolds number to about 6% at the highest Reynolds number. However, this increase in intensity is not necessarily inconsistent with the presence of the two sets of vortices. The increase in intensity may reflect an increase in concentration of the vortices with increasing velocity as well as an increase resulting from the interaction with the hairpin vortices. The spanwise distributions of U can also be interpreted as being consistent with the separation of the disturbed boundary layer into inner and outer regions as outlined above. The distributions at and above the critical Reynolds number, although they exhibit a greater spanwise variation in U which extends over a greater region of the boundary layer, are markedly similar in appearance to the distributions at the subcritical Reynolds number. The hairpin eddies, although inclined to the surface, have over much of their configuration the same sense of rotation as the trailing vortex filaments, and their orientation is such that figures 31 and 32 may be regarded as being mutually consistent. The lateral extent of the fluctuations associated with eddy shedding beyond the diameter of the roughness element, as shown in figure 13 and 32, suggests an alternative view for the generation of hairpin eddies from that deduced from flow-visualization studies, i.e. that the hairpin eddies may not result from a rolling-up of the trailing vortex filaments, but rather are an additional eddy system that develops nonlinearly from an unstable inflexional mean flow established by the pre-existing vortices. In order to reconcile the two points of view, one may speculate that the vagaries of flow visualization do not provide an insight into the realities of such distinctions. For example, is the flow tracer, with increasing Reynolds number, captured by the hairpin eddies at the expense of the trailing vortex filaments, thus resulting in an apparent transition from the trailing vortex filaments to the hairpin eddies?

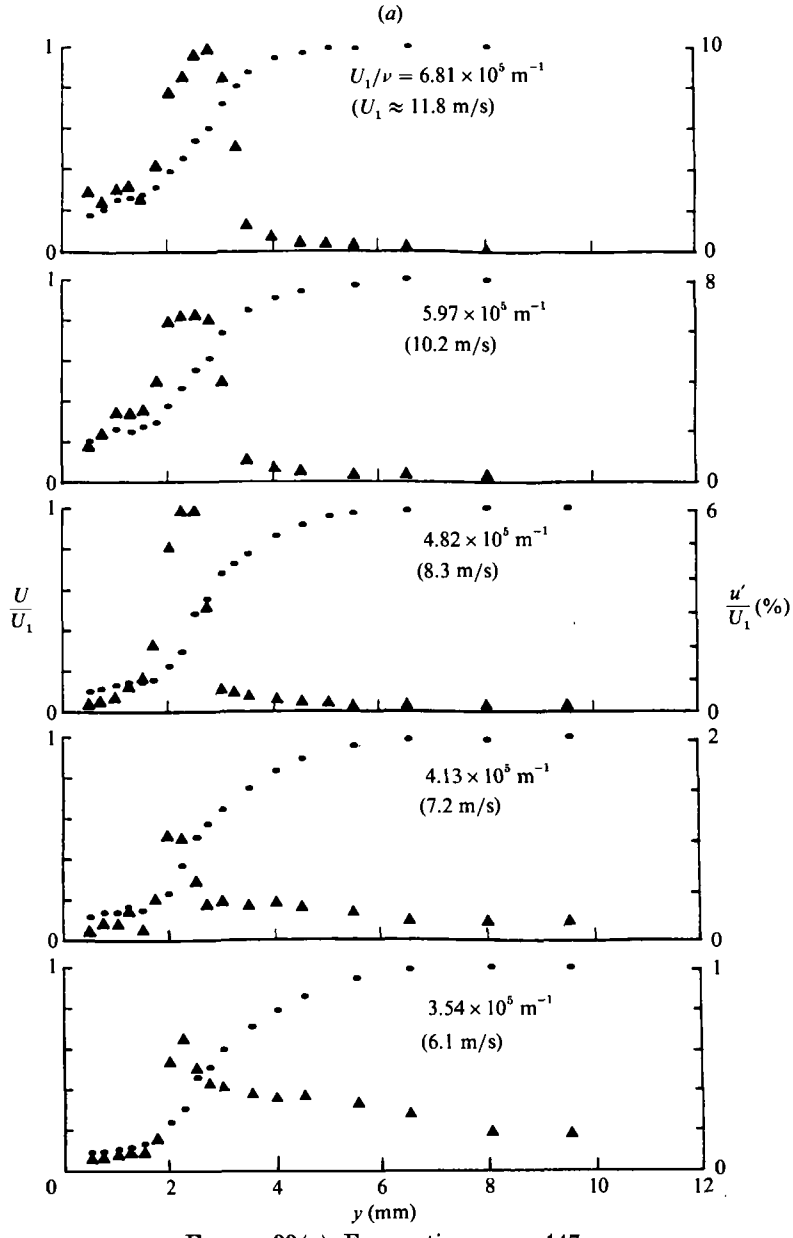

FIGURE 33(*a*). For caption see p. 147.

7.1. *Nature of instability*

In order to examine the instability question further, as well as to examine the transition to a fully developed turbulent boundary, profiles of U and u', across the boundary layer, were measured on the centreline for different downstream positions ranging from $\bar{x} = 1.27$ to 30.5 cm. The resulting distributions for U and u' are shown in figure 33(*a–g*). The distributions at each $\bar{x}$-position, except those at $\bar{x} = 30.5$ cm were measured at five different unit Reynolds numbers, three of which were the same as for the spanwise distributions of figures 31 and 32, the other two being additional unit Reynolds numbers below and above critical.

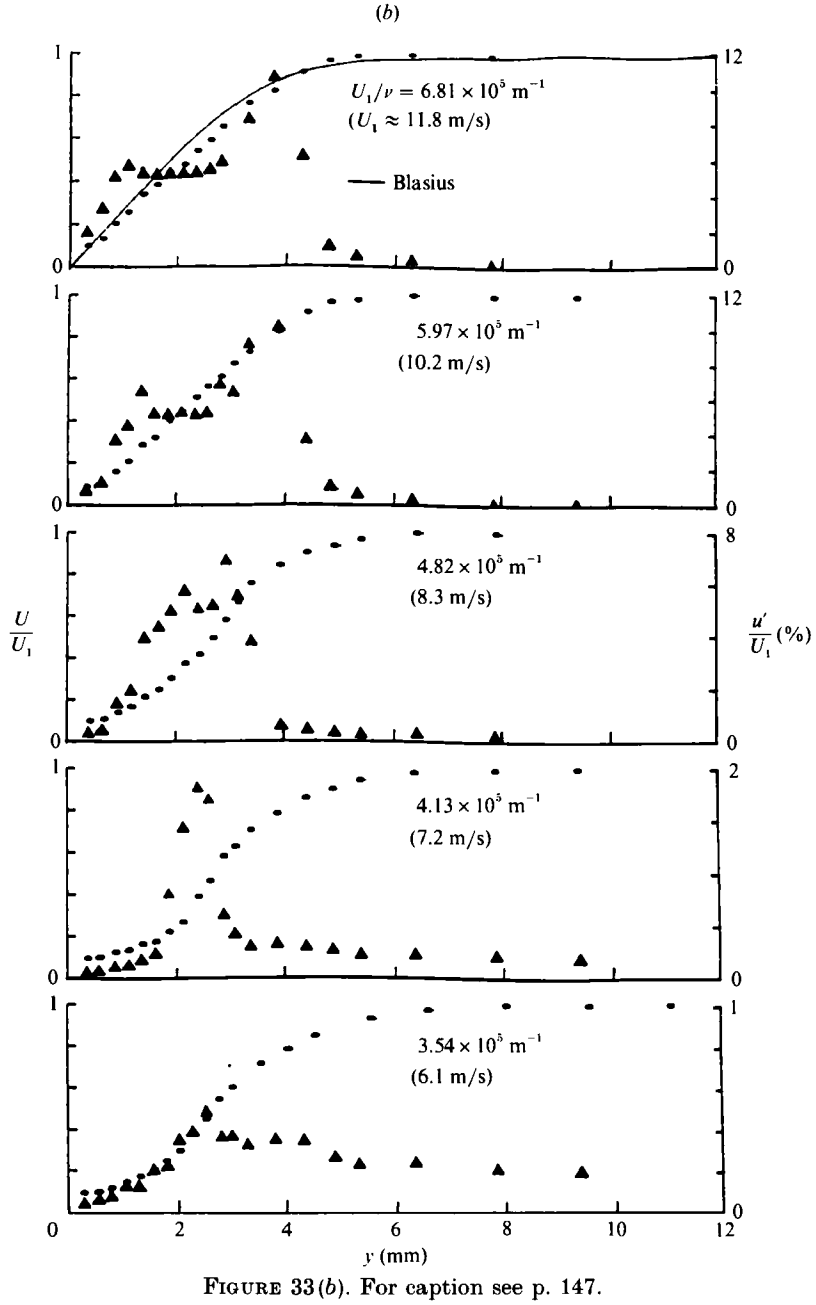

FIGURE 33(*b*). For caption see p. 147.

The mean velocity profiles at $\bar{x} = 1.27$ cm in figure 33(*a*) are sufficiently inflexional to sustain an incipient wave type of instability which develops into a rolled-up vortex, and eddy generation at and above the critical roughness Reynolds number. The inflexional nature of the mean velocity profiles immediately downstream of the roughness at $\bar{x} = 1.27$ cm ($7.5k$), and $\bar{z} = 0$ cm, is illustrated in figures 34(*a*) and 34(*b*) in which they are compared with inflexional profiles for which stability calculations have been carried out. In figure 34(*a*) the mean velocity profiles at unit Reynolds numbers up to and including the unit Reynolds number which is slightly above

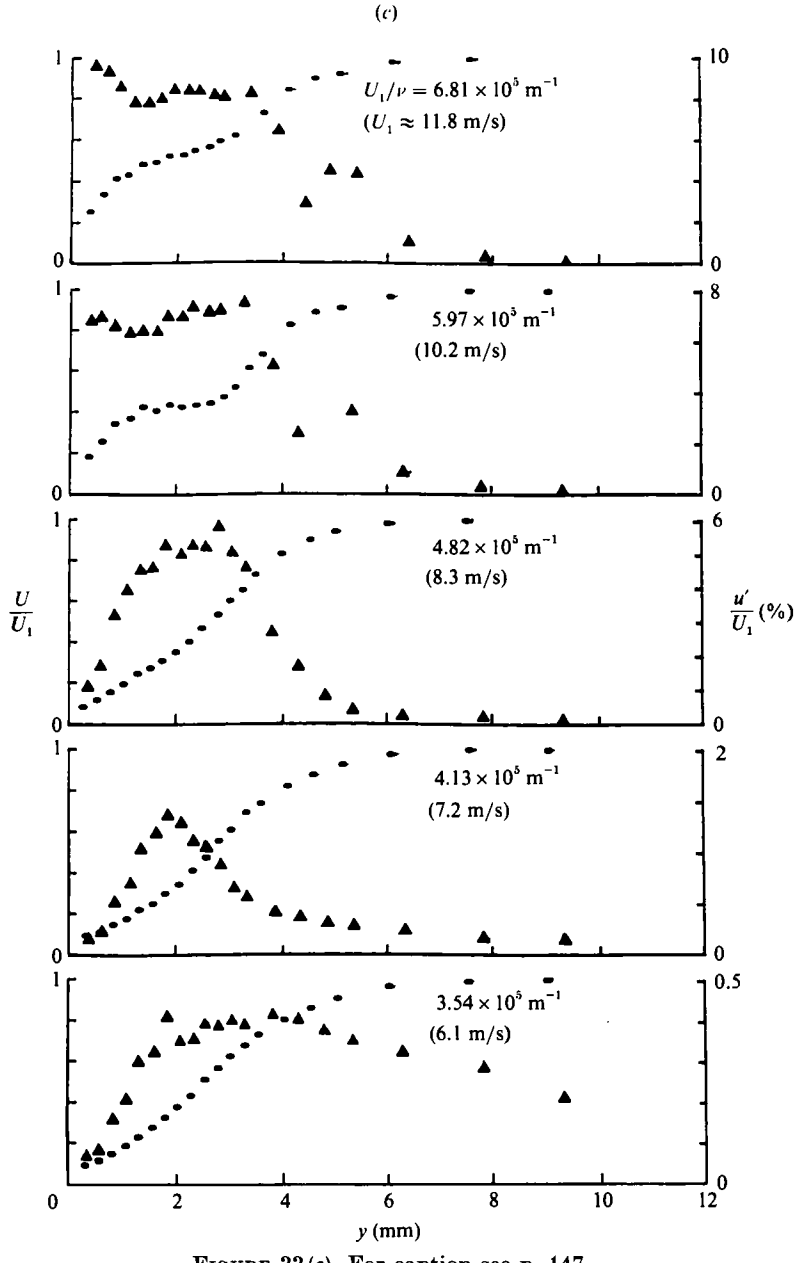

FIGURE 33(*c*). For caption see p. 147.

critical are compared with the Lin profile (Lin 1953) for a two-dimensional mixing layer in which one fluid is at rest. Similarly, in figure 34(*b*) the same profiles are compared with the Hartree profile (Hartree 1937) for a two-dimensional separated layer. The measurements of mean velocity close to the surface, which are nearly constant, reflect the behaviour of a hot wire in a separated region. The momentum thickness, θ, was obtained by extrapolating the distributions smoothly to zero at the surface. The boundary-layer profiles were matched to the mixing-layer distribution at $U/U_1 = 0.5$, and it is seen from the comparison, as well as from the comparison in

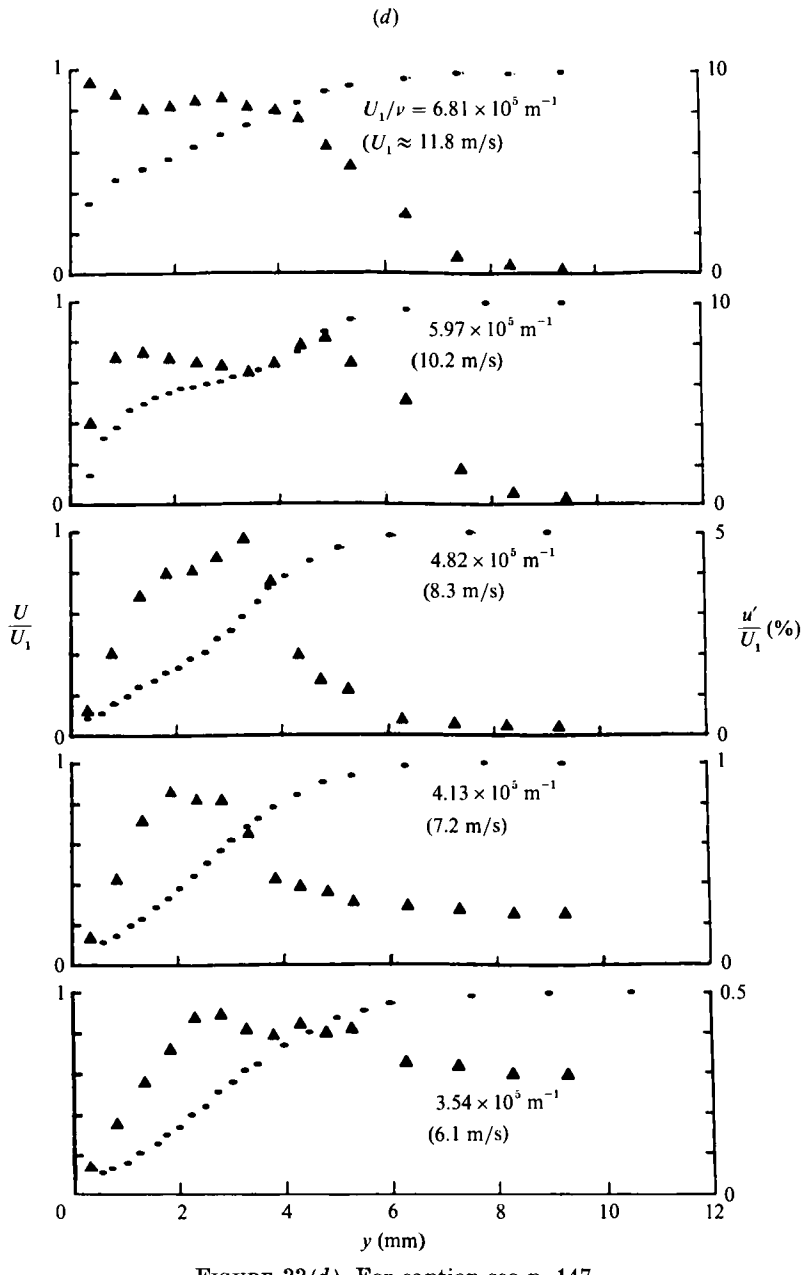

FIGURE 33(*d*). For caption see p. 147.

figure 34(*b*), that the inflexion is sufficiently close to the wall that the instability may be regarded as being more characteristic of a wall-bounded flow rather than a free-shear layer, but one which is specific to the geometry of the roughness and the Reynolds number. This is supported by the variation of frequency with U_1^2, at least for the size of roughness elements herein investigated, whereas a free-shear layer would imply a variation with U_1^3. In addition, the mixing layer and the separated laminar boundary layer have their inflexion at $U/U_1 = 0.5$. The presence of the separated region tends to obscure the inflexion point in the boundary-layer profiles.

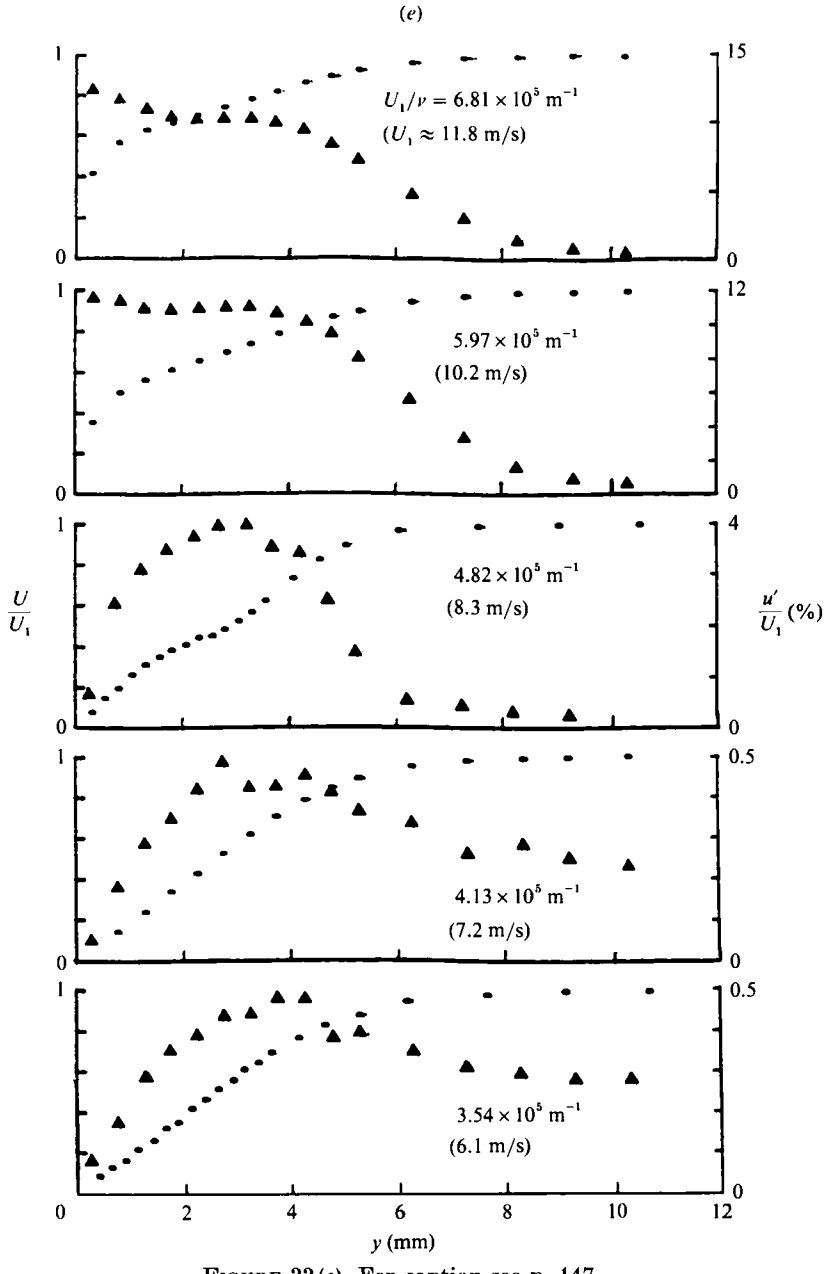

FIGURE 33(*e*). For caption see p. 147.

However, the distributions of u' at $\bar{x} = 1.27$ cm in figure 33(*a*) at the two lower unit Reynolds numbers indicate a maximum in u' at $y/k = 1.31$. It is reasonable to assume that for these Reynolds numbers this position is the point of inflexion. The corresponding average value of U/U_1 is 0.34. Assuming that this value is applicable at the critical Reynolds number yields a wavelength of 6.5 mm for the instability at $U_1 = 8.3$ m/s. From this point of view, the instability at the critical Reynolds number is nonlinear with a u'/U_1 of about 6 %, and the hairpin eddy develops within one or two wavelengths. The rapid onset of nonlinearity implied in the above is not

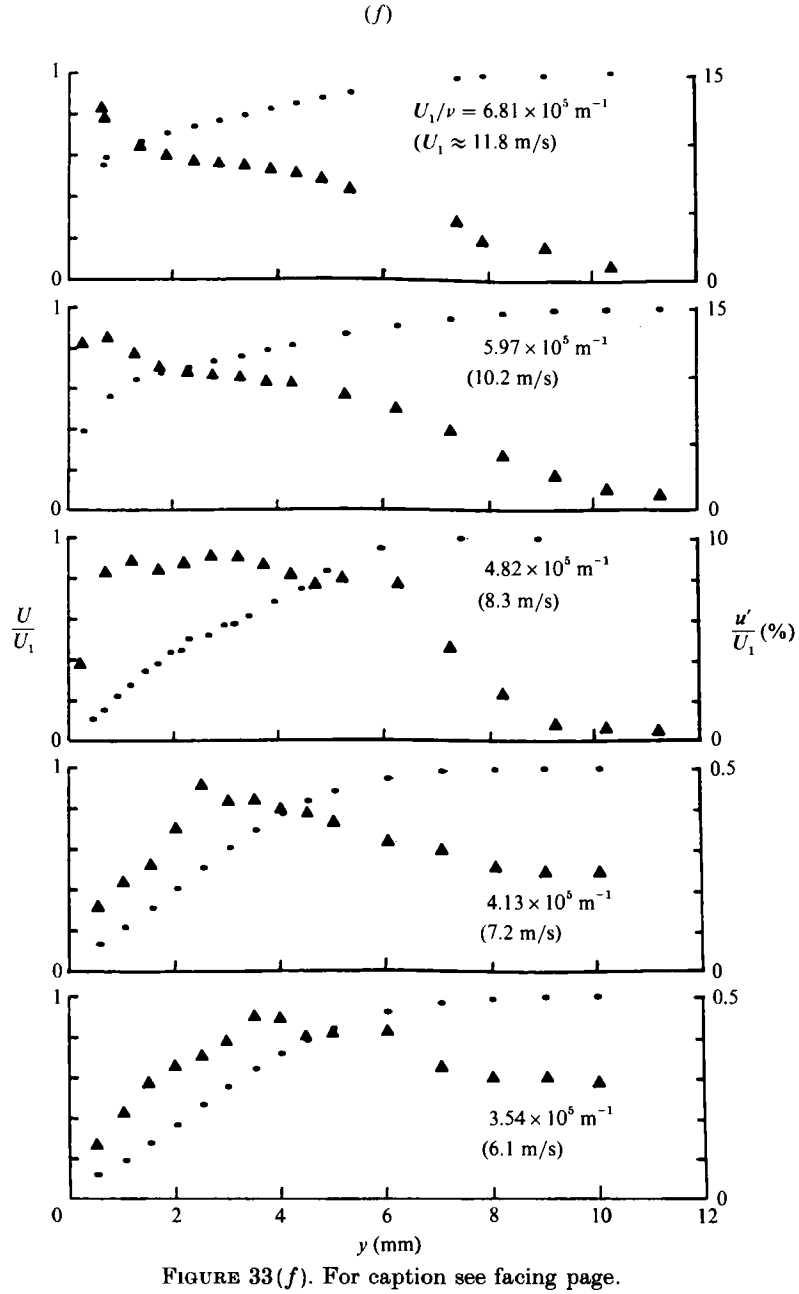

FIGURE 33(*f*). For caption see facing page.

unreasonable in view of the observation by Miksad (1972) that for a free-shear layer the extent of the linear range was less than one wavelength of the unstable disturbance, and the rapid development of the hairpin eddy is consistent with the theory of Greenspan & Benney (1963) for shear-layer instability.

The distributions of u' at the subcritical Reynolds numbers indicate that the observed instability may behave linearly, i.e. governed by linear stability theory. At $U_1/\nu = 4.13 \times 10^5$ m^{-1} the maximum in u'/U_1 increases from 1.0% at $\bar{x} = 1.27$ cm to 1.8% at $\bar{x} = 2.54$ cm, and then damps with increasing distance downstream. At the

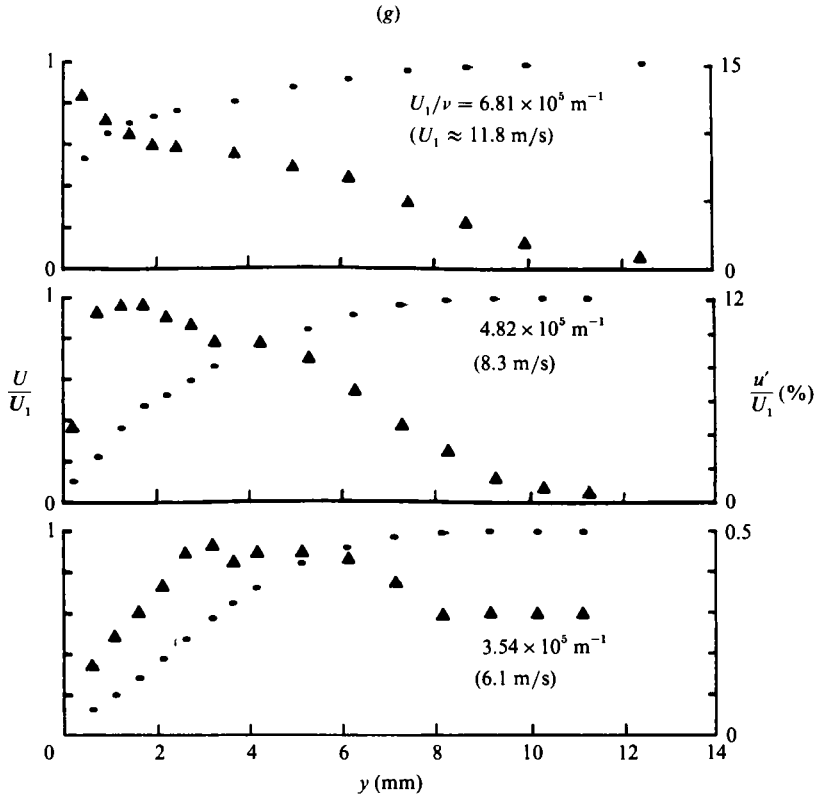

FIGURE 33. Distributions of mean velocity (●) and intensity of u-fluctuations (▲) for varying unit Reynolds number. $k = 1.7$ mm, $x_k = 91.4$ cm, $\bar{z} = 0$ cm. (*a*) $\bar{x} = 1.27$ cm, (*b*) 2.54 cm, (*c*) 5.08 cm, (*d*) 7.62 cm, (*e*) 12.7 cm, (*f*) 20.3 cm, (*g*) 30.5 cm.

lower Reynolds number of 3.54×10^5 (m^{-1}) the maximum in u'/U_1 at $\bar{x} = 1.27$ cm is 0.65%, and the nature of the distribution indicates that this represents a small degree of amplified disturbance above the background disturbances. However, in contrast to the higher Reynolds number, it exhibits no further growth and damps with increasing downstream distance. It was shown in Klebanoff & Tidstrom (1959) that in a laminar boundary layer with zero pressure gradient a relatively weak three-dimensional Tollmien–Schlichting wave with an intensity level of 2% may still behave linearly. Similarly, Miksad (1972) observed that an unstable disturbance in a free-shear layer with an intensity up to 2% behaved linearly. It is therefore reasonable to infer that the instabilities at the subcritical Reynolds numbers are also behaving linearly. In this connection it is of interest, despite the three-dimensionality of the instability, to compare the unstable frequency observed at $U_1/\nu = 4.13 \times 10^5$ m^{-1} with the two-dimensional stability calculations of Wazzan *et al.* (1968), and Lessen (1949) for the separated boundary layer and mixing layer, respectively. The pertinent non-dimensional frequency parameters, $2\pi f\nu/U_1^2$ and $2\pi f\theta/U_1$ are 68×10^{-5} for the separated layer, and 0.20 for the mixing layer. The corresponding Reynolds numbers based on displacement thickness and momentum thickness, R_{δ^*} and R_θ, are 1170 and 300. At $2\pi f\nu/U_1^2 = 68 \times 10^{-5}$, Branch II of the stability diagram for the separated layer is at $R_{\delta^*} = 1000$. At $R_{\delta^*} = 1170$, the unstable frequency, at $U_1/\nu = 4.13 \times 10^5$ m^{-1} is barely outside the unstable region. At

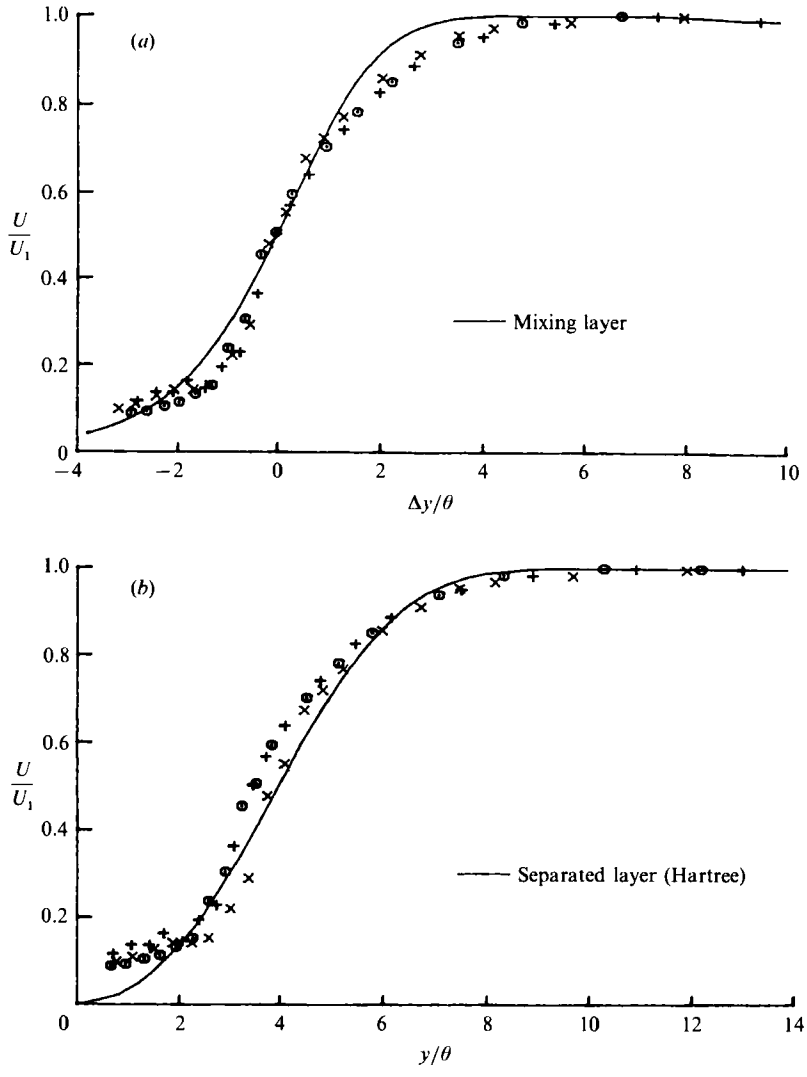

FIGURE 34. Comparison of mean velocity profiles 1.27 cm downstream of a hemispherical roughness element with the mean velocity profiles of (*a*) mixing layer and (*b*) separated boundary layer. $k = 1.7$ mm, $x_k = 91.4$ cm, $\bar{z} = 0$ cm: ⊙, $U_1/\nu \times 10^5 = 3.54$ m^{-1}; +, 4.13 m^{-1}; ×, 4.82 m^{-1}.

$2\pi f\theta/U_1 = 0.20$ and $R_\theta = 300$, the unstable frequency is within the instability region for the mixing layer which has as its outer bound $2\pi f\theta/U_1 = 0.27$. Comparison of the unstable frequencies at the higher Reynolds numbers is moot since they are regarded as behaving nonlinearly. However, it is evident that with increasing Reynolds number the unstable frequencies extend further into the damped region for the separated layer. As for the mixing-layer comparison, the unstable frequency at the Reynolds number slightly above critical is still within the unstable region, but at $U_1/\nu = 5.97 \times 10^5$ and 6.81×10^5 m^{-1} the unstable frequencies are outside the zone of instability.

The purpose of the foregoing comparison with the stability calculations is not to imply any direct correspondence, but is solely for the purpose of evaluating whether the profiles immediately downstream of the roughness may be sufficiently inflexional

to undergo the observed instabilities. The 'strength' of the inflexion and its position relative to the surface are the significant criteria in assessing, at least qualitatively, the instability of an inflexional profile in a wall-bounded flow. In general, increased proximity of the inflexion to the surface tends to have a stabilizing effect, whereas an increase in the strength of the inflexion is destabilizing. Inasmuch as it has been previously assumed that the instability is essentially inviscid, i.e. that the inflexion is at the critical layer, the inflexion should be the governing criterion. It is seen in figures 34 (*a*) and 34 (*b*) that the measured profiles are more inflexional than either the Hartree or mixing-layer profiles, and it can be concluded that the measured profiles are sufficiently inflexional to undergo the observed instabilities. In this connection it would be helpful to have a stability calculation, albeit two-dimensional, of a profile that is representative of the measured profile. There is also an indication from the measured profiles in figures 34 (*a*) and 34 (*b*) that the inflexion may increase with increasing Reynolds number. This may contribute to the very rapid increase in amplification, shown in figure 33 (*a*), for the corresponding range of Reynolds numbers.

The foregoing discussion has attempted to characterize the instability resulting from a three-dimensional roughness element as an inflexional instability. In lieu of any theoretical calculations for evaluating three-dimensional instabilities in three-dimensional flows, the rationalization has taken the liberty of comparison with the theoretical guidelines existing for two-dimensional instabilities in two-dimensional flows, and a reasonable case for inflexional instability has been made. The sensitivity of the eddy-shedding frequencies to background disturbances, and their non-dimensional scaling, as discussed in §5, also provide indirect evidence for an inflexional instability. The consideration of an inflexional instability provides a simple model for the behaviour of a three-dimensional roughness element. The critical roughness Reynolds number reflects the separation into linear and nonlinear instabilities. In the linear range, at subcritical Reynolds numbers, the disturbance, although it may be initially amplified, cannot sustain itself. It can dissipate laterally and damp as it travels downstream into more stable regions, where the mean flow profiles become less and less inflexional, as evidenced by the profiles in figure 33. At some Reynolds number the instability becomes nonlinear. In this range the disturbance can no longer be characterized by linear theory. A frequency which may be stable according to linear theory may well be unstable when it is nonlinear. The amplification in the nonlinear range of Reynolds numbers is extremely rapid, and the instability results in a rolled-up vortex.

The above model, however, does not explicitly account for the observations of Hall (1967), and Morkovin (1984) referred to in §6, i.e. the occurrence of hairpin eddies with an intensity level as high as 4% which develop and decay without the onset of turbulence. This behaviour implies a narrow range of nonlinearity with Reynolds number for which the resulting vortices are not unstable. The distributions of intensity in figure 33 (*a*) are not inconsistent with this possibility. In any event, this aspect merits further investigation, not only to ascertain its role in the context of the present investigation, but also in view of its importance in understanding the vortex dynamics involved in the onset of turbulence. In the same vein, it is not evident that the formation of the hairpin eddies from the trailing vortex filaments can be reconciled with an inflexional instability. If the flow visualization is to be taken literally, then the evolution of the hairpin eddies from the trailing vortex filaments involves a vortical instability. On the other hand, their formation from an inflexional instability would involve nonlinear development of an initial Rayleigh instability,

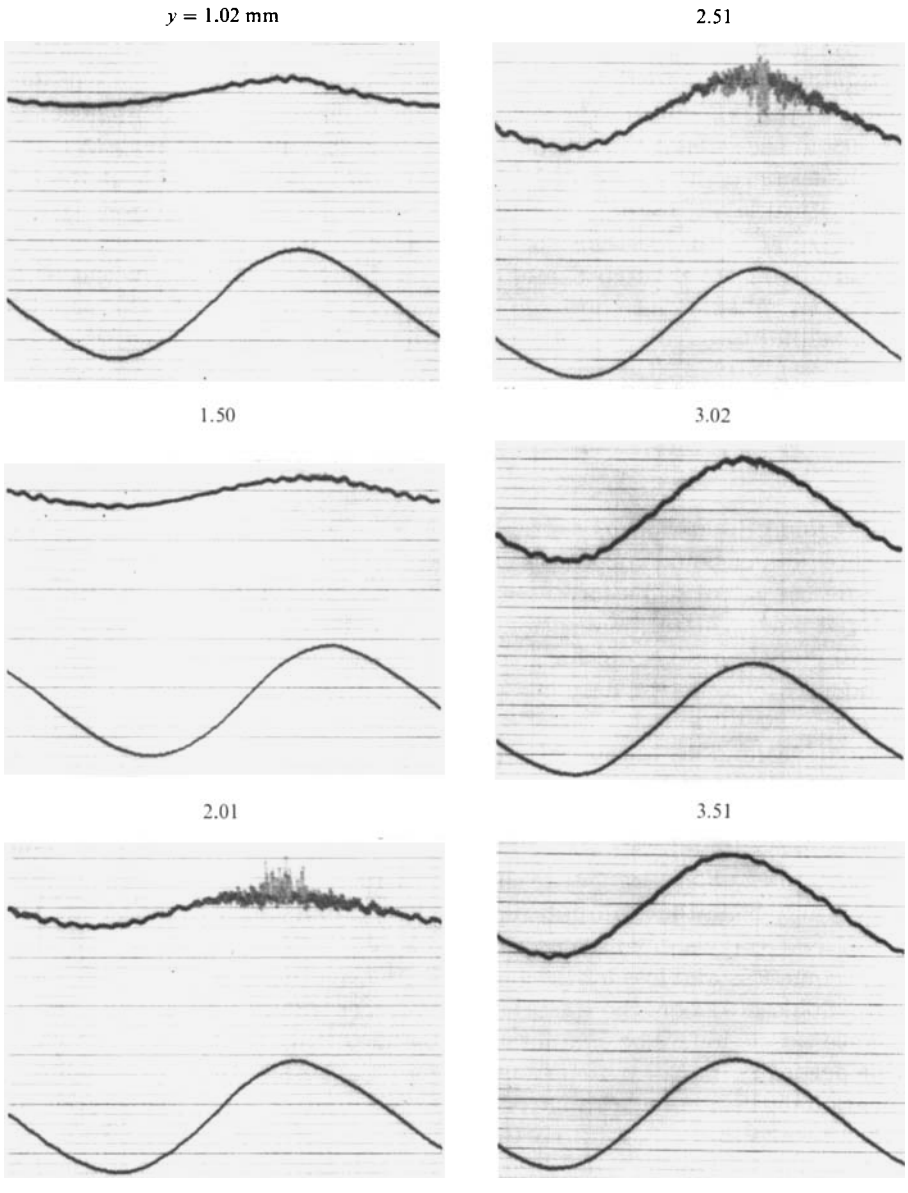

FIGURE 35. Strip-chart recordings of the simultaneous U_1-fluctuation in an oscillatory free stream and the u-fluctuation in the boundary layer downstream of a hemispherical roughness element at various y positions in boundary layer. $k = 1.7$ mm, $x_k = 91.4$ cm, $\bar{x} = 2.54$ cm, $\bar{z} = 0$ cm, $\bar{U}_1 = 6.8$ m/s, $\Delta U_1 = 0.83$ m/s, $n = 1.0$ Hz.

and not an altered state of the trailing vortex filaments. One may speculate that the vagaries of flow visualization do not provide insight into the realities of such distinctions. Involved therein is the degree of amalgamation that may occur between an inflexionally generated eddy system and the trailing vortex filaments.

7.2. *Eddy topology*

The question of an inflexionally generated eddy system *vis à vis* the rolling-up of the trailing vortex filaments was investigated further by examining the 'topology' of

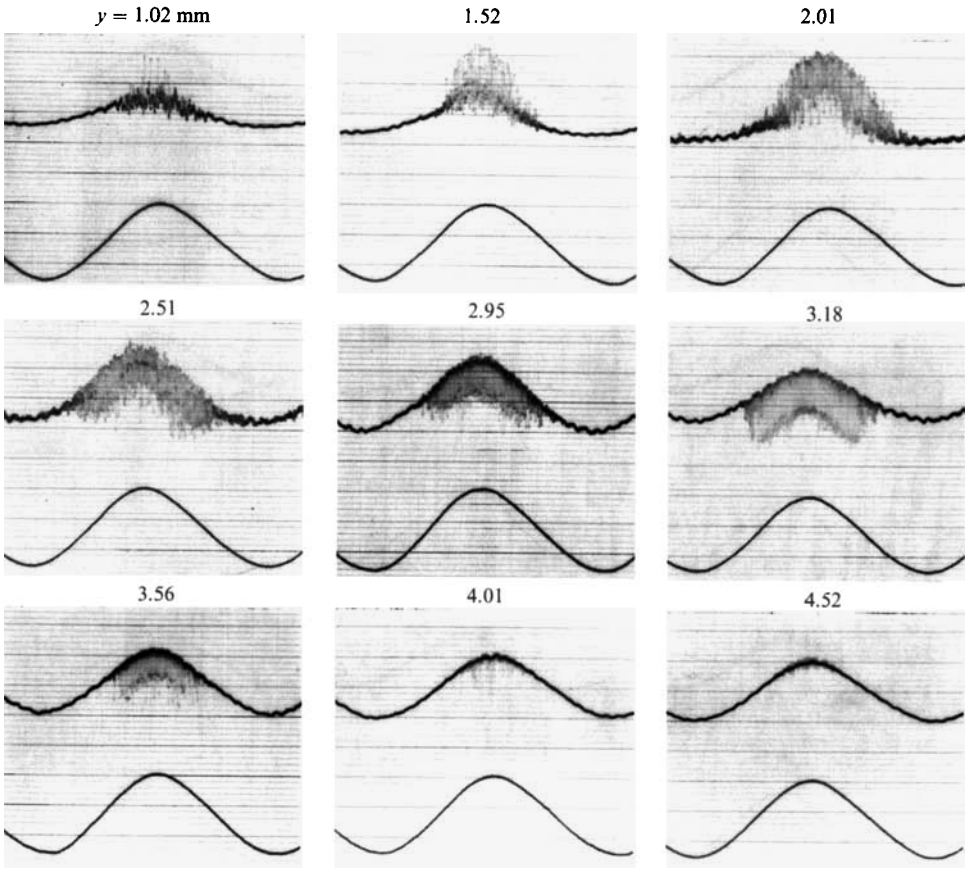

FIGURE 36. As figure 35 but for $\bar{U}_1 = 8.2$ m/s, $\Delta U_1 = 1.08$ m/s.

eddies generated for a duration, ΔT, with an oscillatory free-stream velocity as described in §6. Representative strip-chart recordings of the simultaneous signals of u in the boundary layer and U_1 in the free stream for a free-stream frequency of 1 Hz are shown in figures 35, 36, and 37. The upper trace in each recording is the u-fluctuation in the boundary layer, and the lower trace is the free-stream oscillating velocity. They illustrate the nature of the instability superposed on the primary oscillation in the boundary layer relative to the free-stream oscillation. The recordings shown are for approximately one cycle of the free-stream oscillation, time increases from left to right, and decreasing velocity is in a downward direction. In figures 35, 36, and 37 the beginning and end of the disturbances superposed on the primary oscillation exhibit a considerably greater degree of symmetry with respect to the free-stream oscillation than that displayed in figures 24 and 25. This is because a low-frequency cutoff of 0.1 Hz was substituted for the inadvertent cutoff of 2 Hz discussed in §6. The phase advance relative to the disturbances for an oscillating frequency of 1 Hz with the 0.1 Hz cutoff was 7.9°, in contrast to the 60° phase advance for the 2 Hz cutoff.

The recordings shown in figures 35 and 36 were obtained for varying y-positions at $\bar{x} = 2.54$ cm and $\bar{z} = 0$ cm. The values of $\bar{U}_1$ and ΔU_1 were 6.8 m/s and 0.83 m/s for figure 35, and 8.2 m/s and 1.08 m/s for figure 36. The recordings shown in figure 37 were also obtained at $\bar{x} = 2.54$ cm and the same values of $\bar{U}_1$ and ΔU_1 as for figure 36,

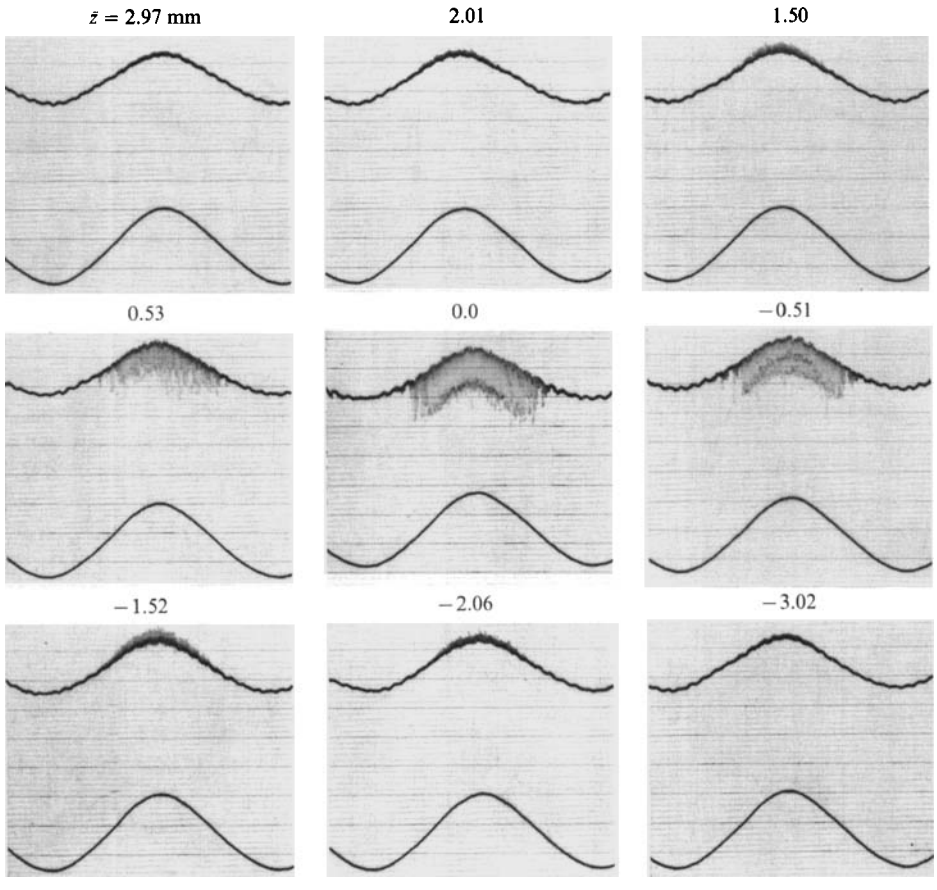

FIGURE 37. As figure 35 but for various $\bar{z}$-positions. $y = 3.18$ mm, $\bar{U}_1 = 8.2$ m/s, $\Delta U_1 = 1.08$ m/s.

but with varying $\bar{z}$ at a fixed $y = 3.18$ mm. The values of $\bar{U}_1$ and ΔU_1 for figure 35 were selected so that $\bar{U}_1 + \Delta U_1$ was slightly below the critical velocity U_c. It is seen that for this condition the instability is restricted to a relatively narrow region of the boundary layer from $y/k = 0.9$ to 1.8. The position of maximum ΔT for the instability appears from the recordings to be between $y = 2.01$ and 2.51 mm which is consistent with the previously drawn conclusion that the inflexion in the mean velocity profile is at $y/k = 1.31$. The instability manifests itself as a periodic disturbance which initially is of amplitude that is small and symmetric about the primary oscillation. It increases in amplitude with increasing velocity, and consistent with the discussion in §6 there is a transition to vortex shedding, albeit of relatively weak intensity. This is inferred from the recording at $y = 2.51$ mm which shows the disturbance in the boundary layer becoming negatively skewed, i.e. in the direction of lower velocity, in the region of the maximum in free-stream velocity. In this regard, it is of interest to note that the disturbance at $y = 2.01$ mm becomes positively skewed with increasing free-stream velocity. The values of $\bar{U}_1$ and ΔU_1 for the recordings in figure 36 were selected so that $\bar{U}_1$ corresponded to the critical velocity U_c and the free-stream velocity would oscillate above and below critical and overlap the free-stream oscillation of figure 35. It is evident that for this condition the instability is much more intense and the resulting disturbance extends over

practically the entire boundary layer. Since $U_1(t)$ for figure 36 overlaps $U_1(t)$ for figure 35 it is not unexpected that the recordings at $y = 2.01$ and 2.51 mm show that a disturbance is present over the entire cycle. The recording at $y = 2.51$ mm also illustrates the rapid transition from a wave-type disturbance to eddy shedding with increasing velocity. This is deduced from the observation that the velocity fluctuations change with increasing $U_1(t)$ from being symmetric about the trace of the 1 Hz unsteady flow oscillation to being negatively skewed. This is perhaps masked somewhat in figure 36 owing to the reduction in scale of the figure but it is clearly evident in the original strip-chart recording. It is also seen that there is a change in skewness from a negatively skewed to a positively skewed disturbance in the near-wall region of the boundary layer. It appears, at least qualitatively, that the change in skewness occurs on either side of the inflexion in the mean velocity profile. In addition, on close examination of the recordings at $y = 1.02$ and 1.52 mm in figure 36 the disturbances generated near the wall, in addition to being positively skewed, appear to have a lower frequency content than the eddy-shedding frequency. The spanwise extent of the hairpin eddies at $y = 3.18$ mm is indicated in figure 37. The phase changes in $\bar{z}$ associated with the eddy structure previously discussed for the steady-flow condition in §5 are evident in the recordings for $\bar{z} \geqslant 1.5$ mm. However, it should be noted in this connection that the phase reversal was observed to occur initially at $\bar{z} = \pm 1.0$ mm. It is seen in figure 37 that the duration of the disturbance decreases with increasing $\bar{z}$. This, particularly in view of the relative uniform amplitude of the skewed disturbance at $\bar{z} = 0$ cm, supports the view previously expressed in §5 that the phase reversal reflects the presence of vortical structures rather than a continuity condition associated with a wave-type disturbance.

The topology of the eddies inferred from figures 36 and 37 is shown by the open-circle symbols in figure 38. The closed-circle symbols and the associated dashed curve represent the disturbances in the near-wall region which was previously discussed as having a different character than that characterizing the periodic shedding of the hairpin eddies. T_L and T_T indicate respectively the time of the beginning and end of the disturbance relative to the minimum in $U_1(t)$ which served as a fixed reference. Their values were obtained by averaging over 7 cycles of the free-stream oscillation, and were corrected for the phase advance of 7.9° for $U_1(t)$. Although the recordings at $y = 2.01$ and 2.51 mm in figure 36 show that a disturbance was present in some form over the entire cycle, the symbols in figure 38(*b*) for these positions denote T_L and T_T when the disturbance is skewed. The behaviour illustrated by the open-circle symbols in figure 38(*b*) with increasing y-position can be readily attributed to the increasing extent of the hairpin eddies across the boundary layer with increasing free-stream velocity. As a result of the increasing extent of the hairpin eddy with increasing free-stream velocity, and concomitant mutual induction effects, the eddy geometry is not only changing but the position relative to the eddy geometry is changing when traversing in $\bar{z}$ at a fixed y-position. Consequently figure 38(*a*) should be viewed with some qualification. Nevertheless, figure 38(*a*) does illustrate that the spanwise extent of the hairpin eddies increases with increasing U_1, and that their duration decreases with increasing $\bar{z}$. At the cross-section at which the measurements were made, i.e. $\bar{x} = 14.9k$ and $y/k = 1.87$, the hairpin eddies, consistent with the observations from figures 13 and 32, have a lateral extent which is about twice the diameter of the roughness element. One interpretation of the behaviour illustrated by figure 38(*a*) is that the hairpin eddies are generated by concentration of spanwise vorticity, and that the spanwise extent of concentrated vorticity increases with U_1. On the other hand, the possibility of an increase in the lateral separation of the sides

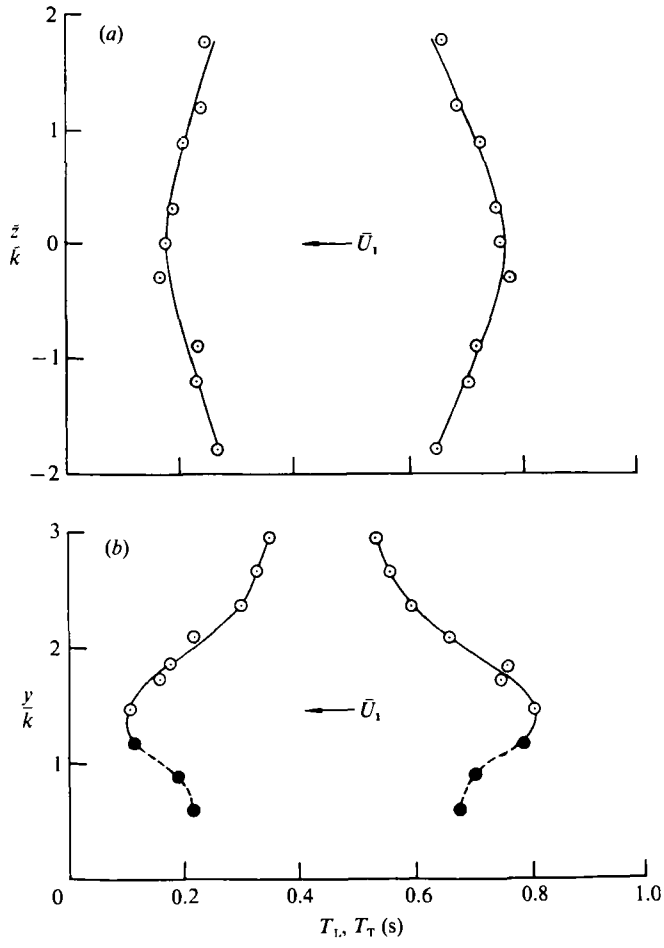

FIGURE 38. Duration of eddy shedding by a hemispherical roughness element relative to one cycle of the oscillating free stream. $k = 1.7$ mm, $x_k = 91.4$ cm, $\bar{x} = 2.54$ cm, $n = 1$ Hz, $\bar{U}_1 = 8.2$ m/s, $\Delta U_1 = 1.08$ m/s. (*a*) varying $\bar{z}$-positions in boundary layer, $y = 3.18$ mm, (*b*) varying y-positions in boundary layer, $\bar{z} = 0$ cm.

of the hairpin eddy with increasing U_1 associated with the development of a bottleneck or Ω-shape near the tip region of the eddy, as in the analyses of Hama (1962*b*), Moin & Kim (1985) and Moin, Leonard & Kim (1986), also has to be considered.

The lateral extent of the hairpin eddy beyond the diameter of the roughness element would support the view that it does not result from a rolling-up of the pre-existing trailing vortex filaments, if it were not for the possibility of the hairpin eddy developing a lateral bulge (Ω-shape) in its outer region. The trailing vortex filaments at subcritical Reynolds numbers, for example, are not only positioned within the diameter of the roughness element but the mutual induction effect is such that the filaments would move closer together and away from the surface. It is to be expected that the legs of the hairpin eddy would undergo a similar mutual inductance effect over part of their configuration and that this would be enhanced by the hairpin eddy being subjected to a degree of stretching as evident from its increasing extent in y

with $\bar{x}$ and U_1. Although the spanwise distributions of u' in figure 32 do show an increase in lateral extent of the hairpin eddy with increasing unit Reynolds number, they show no evidence of an Ω-shape. The lateral extent of the hairpin eddy decreases with increasing y-position for the range of y-positions and unit Reynolds numbers shown in figure 32. In addition, at $y = 3.73$ and 4.06 mm at unit Reynolds numbers of 4.82×10^5 and 6.81×10^5 m^{-1} the lateral extent of the hairpin eddy is 4.5 and 6 mm, respectively, and it is not likely that a characteristic dimension of the Ω-shape to be so large relative to the boundary-layer thickness. It would have been of interest to have attempted a more detailed evaluation by obtaining data of the type shown in figure 38(*a*) at different $\bar{x}$- and y-positions for selected values of $\bar{U}_1$ and ΔU_1. Nevertheless it is concluded, inasmuch as the measurements shown were made at $y = 3.18$ mm, that the more appropriate interpretation of figure 38(*a*) is that it reflects the hairpin eddy having been generated by a concentration of spanwise vorticity, and that its legs at their upstream extrema are in the spanwise direction and merge with the spanwise vorticity. This conclusion is consistent with the view, previously discussed herein, that the essential instability is inflexional. In this context, the initial inflexional mean velocity profile is a precursor for the generation of hairpin eddies and not a consequence of their presence. The development of an Ω-shape in the tip region of the hairpin eddy, perhaps at a $y > 4.06$ mm or an $\bar{x} > 2.54$ cm, is not necessarily precluded since it is one of its properties, i.e. the mutual induction effect associated with its curved geometry, irrespective of how it is initially formed. In this connection, it should be remarked that the possible existence of an Ω-shaped tip region of the hairpin eddy is considered in subsequent discussion of spectral data.

Considerable emphasis has been given for several decades to the origin and nature of large-scale structures in a turbulent boundary layer. Reviews of the various investigations and their essential features can be found in Cantwell (1981), Hussain (1983), and Moin & Kim (1985). Although a variety of views exist in the literature as to the nature of the large-scale structures in a turbulent boundary layer, a consensus has gradually developed that the large-scale structures are hairpin vortices or horseshoe vortices as initially proposed by Theodorsen (1952). However, two different points of view as to their origin have emerged. One is that the hairpin eddies in the turbulent boundary layer have their origin in longitudinal vortex motions near the wall, and their topology is such that their legs extend longitudinally upstream. The other is that the hairpin eddy originates from the 'warping' of spanwise vorticity. These two views may be regarded as having been inherent in the evaluation in the present investigation of the origin of the hairpin eddies formed in the near-wake of a three-dimensional roughness element, and it is interesting that the conclusion drawn that the hairpin eddy is formed by a concentration of spanwise vorticity in the presence of pre-existing longitudinal vortices may contribute to a resolution of these differing views.

7.3. *Spectral behaviour*

In order to gain insight into the nature and relative significance of the near-wall region and outer region indicated in figure 38(*b*), spectral measurements were made on the centreline for various y-positions at $\bar{x} = 2.54$, 5.08, and 12.7 cm for a hemispherical roughness element at $x_k = 91.4$ cm with $k = 1.7$ mm. The results are shown in figures 39, 40, and 41. The measurements were made under steady flow conditions at a free-stream unit Reynolds number of 6.81×10^5 m^{-1} and $Re_k = 550$, corresponding to the maximum unit Reynolds numbers at which distributions of U

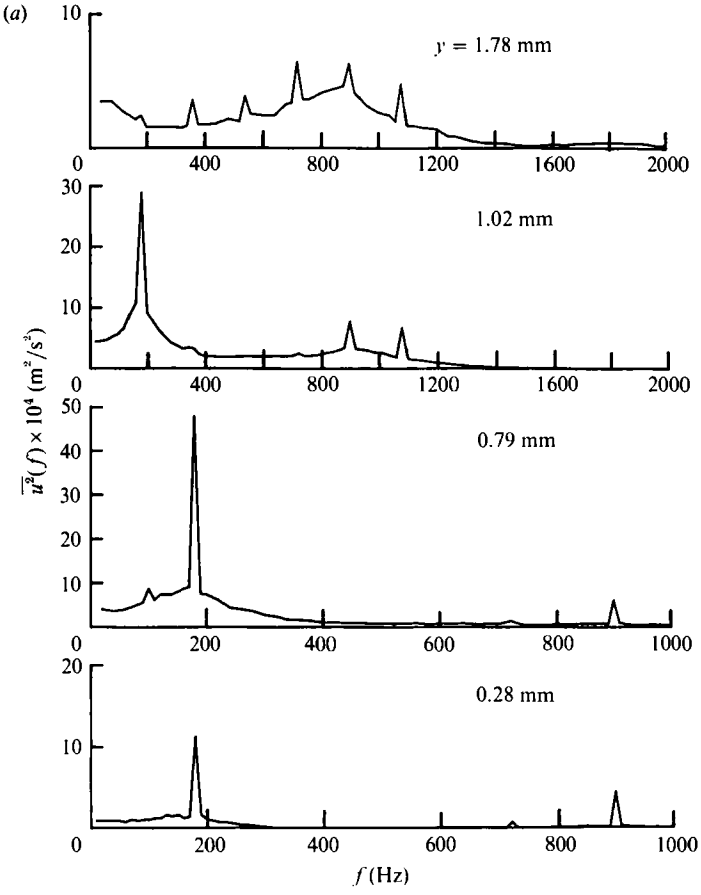

FIGURE 39(a). For caption see facing page.

and u' shown in figure 33 were made. The spectral data are not normalized and $u^2(f)$ is defined such that

$$\overline{u^2} = \int_0^\infty \overline{u^2}(f)\,\mathrm{d}f.$$

The mean-square values of the u-fluctuation between frequencies f and $f+\mathrm{d}f$ were obtained using a real-time spectral analyser. The distributions shown were obtained by smoothing the distributions from the x-y plotter used in conjunction with the spectral analyser and were corrected for the bandwidth. As mentioned previously, the bandwidth scaled linearly with the bandpass and the effective bandwidth was 8 Hz at a bandpass of 2 KHz.

The various spectra at $\bar{x} = 2.54$ cm $(14.9k)$ in figure 39 exhibit multiple peaks which, when considering all the spectra irrespective of y-position, range in frequency from 180 to 1260 Hz and include all the intervening harmonics. However, their relative intensity and whether or not a particular peak frequency is observed are strongly dependent on the y-position. Although the various spectra were obtained at a much higher Reynolds number than figure 38(*b*), and despite the complication that the peak frequencies have their counterpart in the free-stream disturbances as shown in figure 7, they display certain features which clarify the difference between the near-wall region and the outer region alluded to in connection with figure 38(*b*).

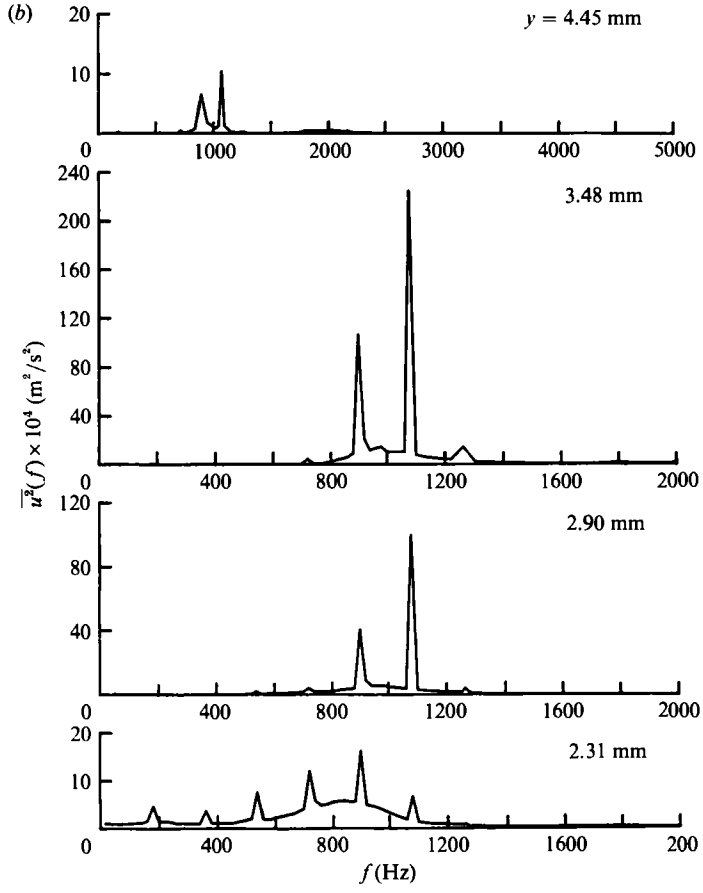

FIGURE 39. Spectra of u-fluctuation at various y-positions in the boundary layer downstream of a hemispherical roughness element. $k = 1.7$ mm, $x_k = 91.4$ cm, $\bar{x} = 2.54$ cm, $\bar{z} = 0$ cm, $U_1/\nu = 6.81 \times 10^5$ m^{-1}.

Figure 42 shows a cross-plot of the data in figure 39 and illustrates the distribution of intensity of each peak frequency across the boundary layer. It is seen that there are three frequencies that are very dominant in spectral intensity. In an outer region, $y/k > 1.36$, the eddy-shedding frequencies, f_1 and f_2, of 900 and 1080 Hz dominate the spectral content. It is interesting to note in this connection that it was previously inferred, albeit at a lower Reynolds number, that the position of the inflexion in the mean velocity profile was at $y/k = 1.31$. It is not surprising, as discussed in §5 in connection with figure 13, that for the experimental conditions at which figure 39 was obtained f_1 and f_2 are frequencies which reflect the influence of the free-stream disturbances on the initial inflexional instability. On the other hand, the spectral content of the inner region, $y/k < 1.0$, is radically different and is dominated by the difference frequency, $f_2 - f_1$, of 180 Hz. There are also spectral peaks at the eddy-shedding frequencies, f_1 and f_2, in this region, but they are considerably reduced in intensity relative to the difference frequency and their intensity in the outer region. It should be noted that at $y = 0.28$ and 0.79 mm the spectral bandpass was 1000 Hz. Nevertheless, it is reasonable to assume that a relatively low-intensity peak at f_2, in addition to that shown for f_1, also exists at these positions. The reason for the presence of the difference frequency with its relatively large intensity in the inner

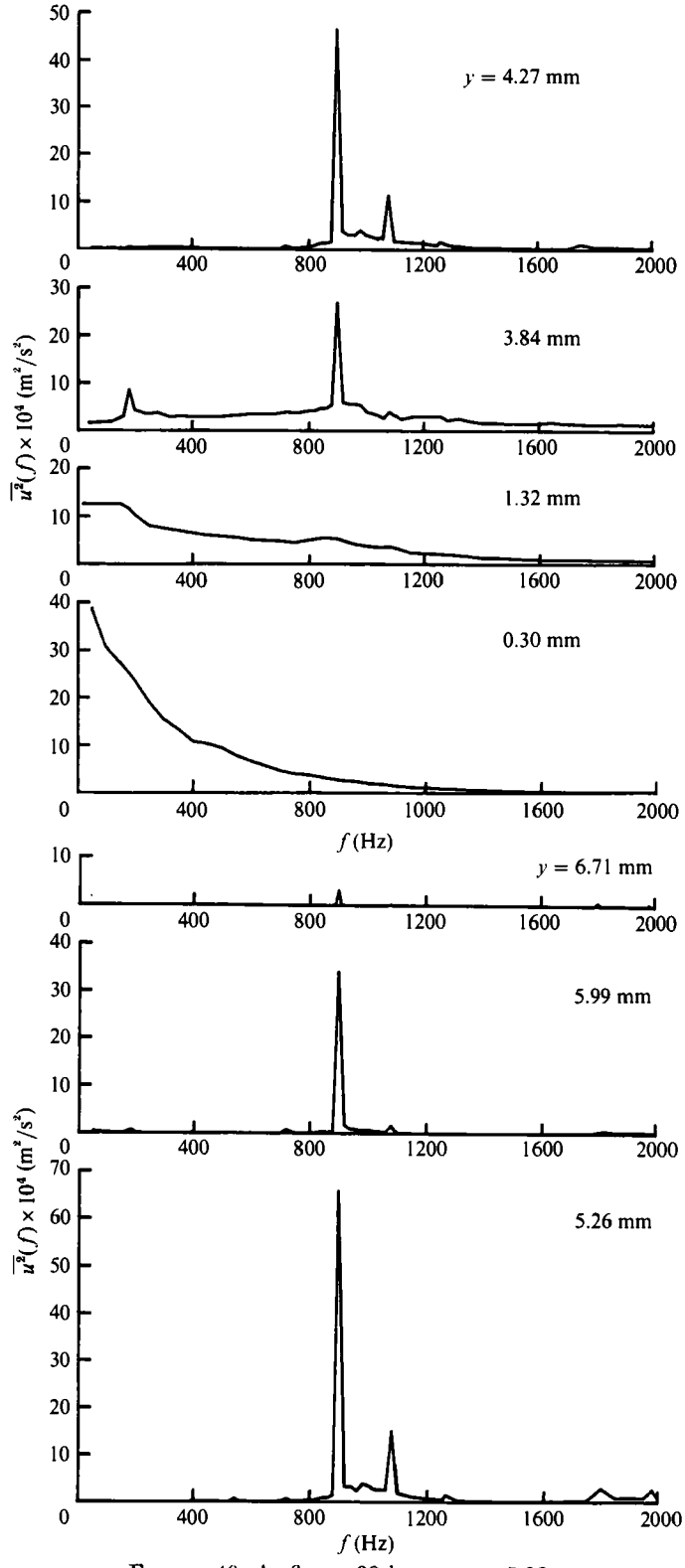

FIGURE 40. As figure 39 but at $\bar{x} = 5.08$ cm.

region posed an interesting question. It cannot be attributed to the aforementioned initial inflexional instability since, as shown in figures 35 and 36, the disturbances in the inner region exist only in the presence of eddy shedding. In addition, the distributions of intensity at the different frequencies shown in figure 42 cannot be rationalized as being solely a consequence of the initial inflexional instability and it is apparent that they reflect some other behavioural characteristic.

The behaviour outlined above is markedly similar to that observed by Norman (1972) in the flow downstream of a three-dimensional rectangular trip which was excited under controlled conditions by the sound from two speakers with different frequencies. Norman (1972) offered the explanation that the difference frequency arose from nonlinear modulation of the two acoustic frequencies and, as in the present experiment, is not observed in the outer region, which he termed the 'top shear layer', because it lies outside the range of frequencies for which the top shear layer is unstable and is damped. In order to account for the difference frequency in the inner region Norman (1972) proposed a mechanism similar to that proposed by Klebanoff & Tidstrom (1972) for the amplification of disturbances downstream of a two-dimensional roughness element, i.e. that the change in instability associated with the change in the mean velocity profile during reattachment is such that the lower frequencies, seeded by nonlinear modulation of the frequencies in the top shear layer, have become unstable and consequently the difference frequency can undergo a Tollmien–Schlichting amplification. Norman (1972) concluded that it is this process of amplification of low-frequency disturbances in the reattached flow which in due course leads to turbulence. The data of the present investigation shown in figures 33(*a*), 39, and 40, however, do not support a Tollmien–Schlichting instability as an explanation for the relatively large intensity at the difference frequency, nor the subsequent onset of turbulence.

7.4. *Lateral instability*

It is seen in figure 33(*b*) that the mean velocity distribution at a unit Reynolds number of 6.81×10^5 m^{-1} is fairly well approximated by a Blasius distribution. The dimensionless frequency parameter, $2\pi f\nu/U_1^2$, for the difference frequency of 180 Hz is 1.4×10^{-4} which at the boundary-layer Reynolds number, R_{δ^*}, of 1530 is well within the stable region for such a profile. In addition, comparison of the spectra at $\bar{x} = 2.54$ and 5.08 cm in figures 39 and 40, respectively, shows that the difference frequency does not amplify at all y-positions with increasing distance downstream. Its maximum intensity did not increase with distance downstream from its value at $\bar{x} = 2.54$ cm, and at the y-position where it has a maximum in intensity at $\bar{x} = 2.54$ cm it has actually damped. It is not consistent with stability theory that the disturbance amplify and damp at different y-positions within the boundary layer. A more appropriate explanation for the presence of the difference frequency is suggested by figure 43, in which oscillograms illustrate the nature of the fluctuations associated with the spectral measurements shown in figures 39, 40, and 41. No particular significance should be attached to the relative amplitudes since the gain settings were arbitrary. The oscillogram at $\bar{x} = 2.54$ cm and $y = 0.79$ mm is of particular interest inasmuch as it clearly shows the difference frequency of 180 Hz on which is superposed a manifestation of the eddy-shedding frequency. It is seen, as has previously been noted in connection with figure 36, that the u-fluctuation is skewed in the direction of positive velocity. This behaviour lends itself to the interpretation that it is a lateral instability in the near wake that manifests itself in the inner region and, more particularly involves a periodic spanwise oscillation at the

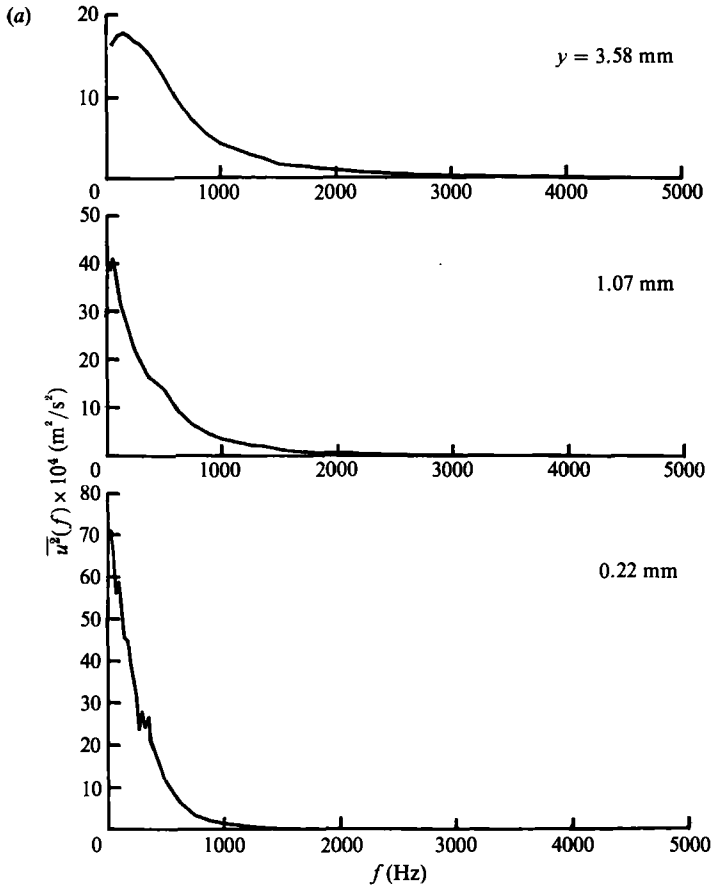

FIGURE 41 (a). For caption see facing page.

difference frequency of the pre-existing 'horseshoe' vortex. The intensity of the difference frequency is therefore not indicative of a frequency undergoing Tollmien–Schlichting amplification but may reflect the lateral oscillation of the velocity defect in the wake and the associated spanwise gradient in U. This is supported, notwithstanding the presence of a surface, by the stability analyses (Crow 1970) for a pair of trailing vortices in which the lateral instability of 180 Hz, herein inferred, is an admissible unstable symmetric mode. In making this evaluation it is assumed that the perturbation velocity is the inflexional velocity, $0.34U_1$, and from figure 31 it is inferred that the diameter, c, of the downstream legs of the 'horseshoe' vortex is 0.14 cm, and their separation, b, is 0.35 cm which for Crow's stability parameters β and δ/β yield 0.99 and 0.13, respectively.

According to Crow's analyses the plane of lateral instability will incline at an angle of about 45° to the horizontal. On the other hand, it would be expected from the mutual induction effect with their mirror image that the legs of the horseshoe vortex would 'hug' the surface and separate laterally. However, there is support for the view that the instability is the governing behaviour from the flow-visualization experiments of Mochizuki (1961 *a*) in which it is observed that the 'horseshoe vortex detaches itself upward from the surface as the velocity is increased,' and in Mochizuki (1961 *b*), 'the horseshoe vortex filament waves three-dimensionally and

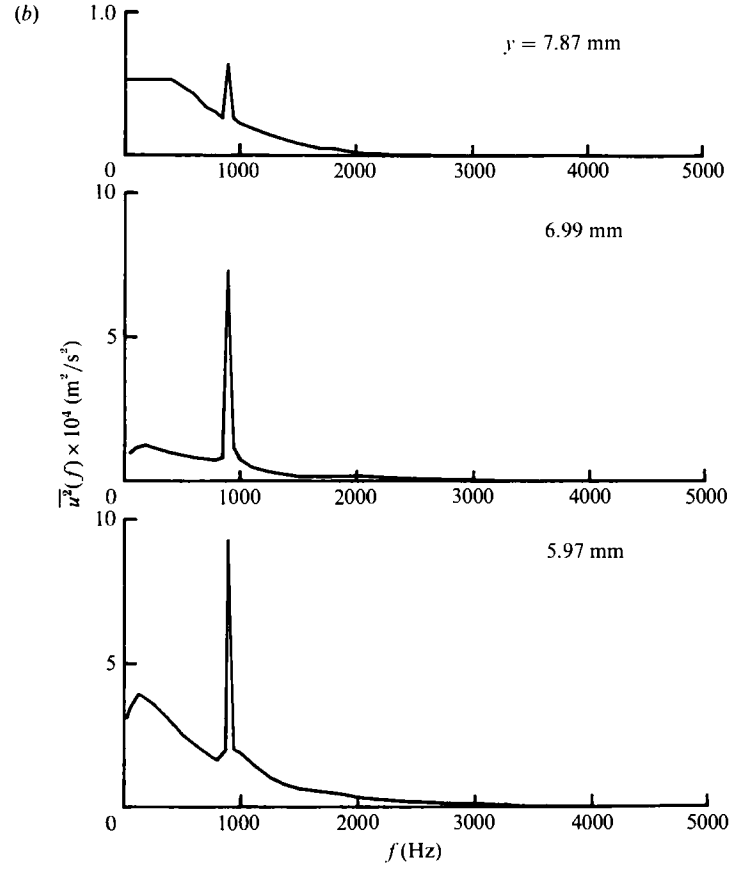

FIGURE 41. As figure 39 but at $\bar{x} = 12.7$ cm.

seems to rotate about x-axis'. The lateral instability of the horseshoe vortex also provides a more appropriate explanation than nonlinear modulation of f_1, f_2, for the spectral content illustrated in figures 39 and 42 for the intermediate region between the inner and outer regions. In this intermediate region the spectral peaks are more appropriately considered to be integral harmonics of $f_2 - f_1$, rather than subharmonics of f_1, f_2. The spectral peaks in the intermediate region are of relatively low intensity compared to $f_2 - f_1$, and f_1, f_2, and apparently reflect an overlapping and resulting interaction of the inner and outer regions. The process of nonlinear modulation as examined by Norman (1972) does not yield all of the harmonics in the intermediate region that are illustrated in figures 39 and 42. In addition to $f_2 - f_1$, nonlinear modulation provides only for the presence of $2f_1 - f_2$ and $2f_2 - f_1$, or more specifically in the present case for frequencies of 720 and 1260 Hz. However, their presence cannot be construed as necessarily being a consequence of nonlinear modulation since their amplitudes cannot be related in a meaningful way to the amplitudes of f_1, f_2. However, in the presence of a lateral instability the behaviour in the intermediate region can be explained simply by the eddy-shedding frequencies being frequency modulated by the frequency of the lateral instability, i.e. 180 Hz and the harmonics of 180 Hz observed in the intermediate region are a permissible consequence.

It is evident that the lateral instability is induced by the eddy shedding, and it can be inferred from the discussion of figure 36 that a lateral instability was also present

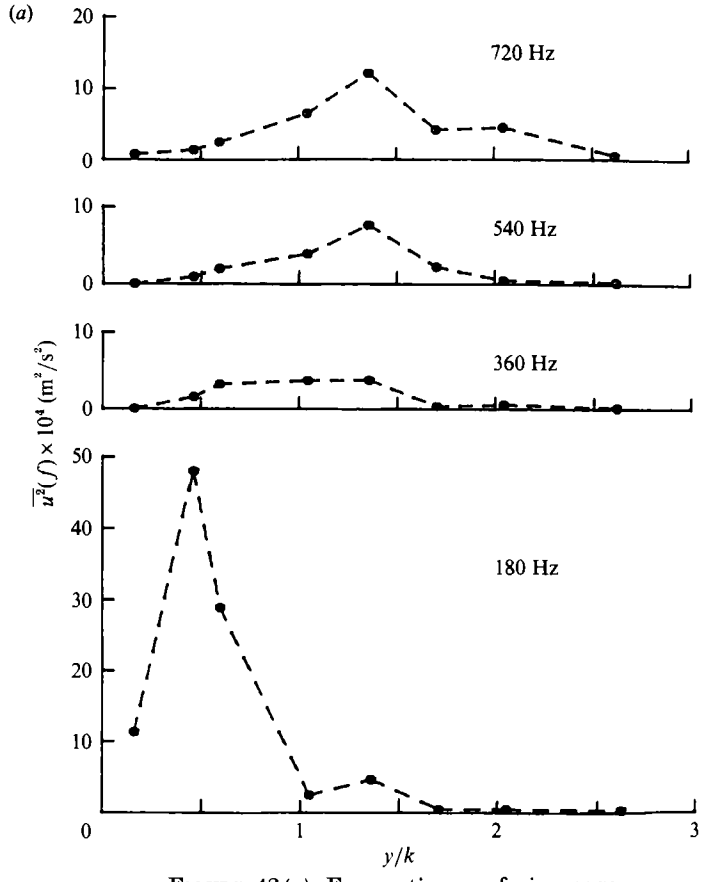

FIGURE 42(a). For caption see facing page.

in the unsteady flow and at a lower free-stream velocity. Nevertheless, it is open to question as to whether this lateral instability is intrinsic to transition induced by a three-dimensional roughness element or a special situation arising from the nature and disturbing influence of the free-stream disturbances. In this connection, it should be noted that Norman (1972) also induced transition downstream of a three-dimensional roughness element with a single acoustic frequency. However, this by itself does not provide assurance that a lateral instability was not present. Be that as it may, further hot-wire studies of the near-wake behaviour, incorporating measurements with probes sufficiently small to make meaningful measurements of the transverse fluctuations, appear warranted not only because of their intrinsic importance but also because the near-wake behaviour appears to be a fruitful avenue of experimentation for important questions related to the turbulent boundary layer.

7.5. *Inner- and outer-region behaviour*

Comparison of the spectra in figures 39, 40, and 41, as well as the oscillograms in figure 43, illustrates that turbulence is initially generated in the near-wall region, and with increasing distance downstream the turbulence extends further from the wall. In this context turbulence is defined solely by the spectrum being continuous, i.e. a broadening of the spectral band, and by the fluctuations having lost their discrete character. This change, depending on the Reynolds number, can occur rapidly, and

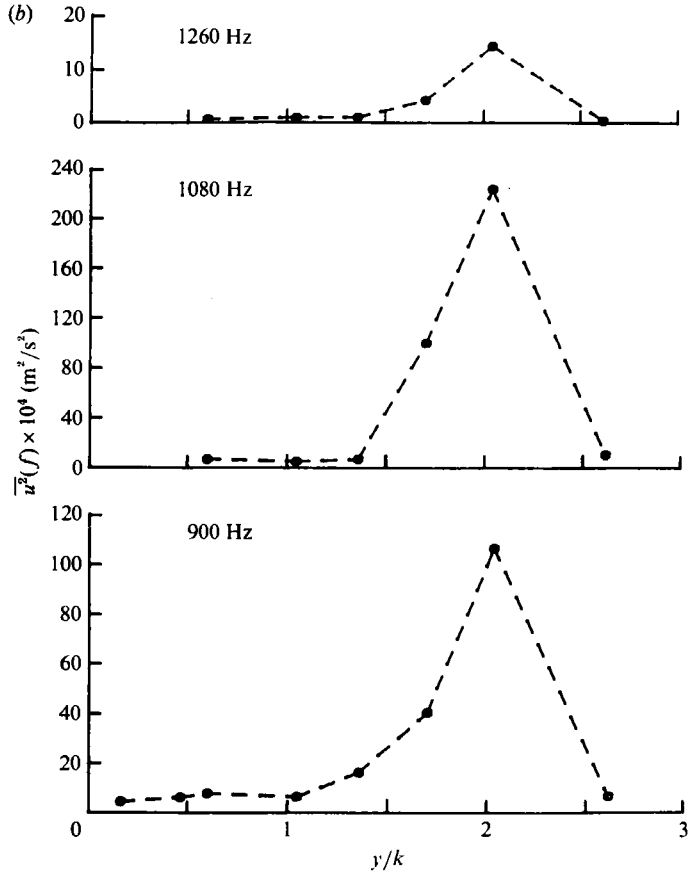

FIGURE 42. Distributions across the boundary layer of the intensity of peak frequencies in the spectra of the u-fluctuation downstream of a hemispherical roughness element. $k = 1.7$ mm, $x_k = 91.4$ cm, $\bar{x} = 2.54$ cm, $\bar{z} = 0$ cm, $U_1/\nu = 6.81 \times 10^5$ m^{-1}.

near the surface at $U_1/\nu = 6.81 \times 10^5$ m^{-1} it occurs within a downstream distance of $14.7k$. The spatial extent in y of the spectral broadening increases with increasing $\bar{x}$, and at $\bar{x} = 12.7$ cm, $44.8k$ further downstream, the spectral broadening is evident at all y-positions across the boundary layer with a small peak in the intensity of the eddy-shedding frequency still present in the outer region.

The change in y-position of the maximum in the intensity of the eddy-shedding frequencies with $\bar{x}$ shown in the spectral data reflects the tendency, previously noted, of the apex of the hairpin eddies to move outward from the surface with increasing $\bar{x}$, and it can be inferred from the oscillograms shown in figure 43 at $\bar{x} = 5.08$ cm that the tip of the hairpin eddy is located near the edge of the boundary layer. The spectral data illustrate that the intensity of the eddy-shedding frequencies damps rapidly with increasing $\bar{x}$. In this connection, it should be noted that the spectra at $\bar{x} = 20.3$ cm, and $U_1/\nu = 6.81 \times 10^5$ m^{-1} showed no evidence of spectral peaks at the eddy-shedding frequencies. Oscillograms that illustrate the nature of the u-fluctuation in the outer region of the boundary layer at $\bar{x} = 20.5$ cm and $U_1/\nu = 6.81 \times 10^5$ m^{-1} are shown in figure 44, where no particular significance should be attached to the relative amplitudes. The various y-positions are shown relative to the boundary-layer thickness, δ, which was estimated from the velocity distribution to be 9.5 mm,

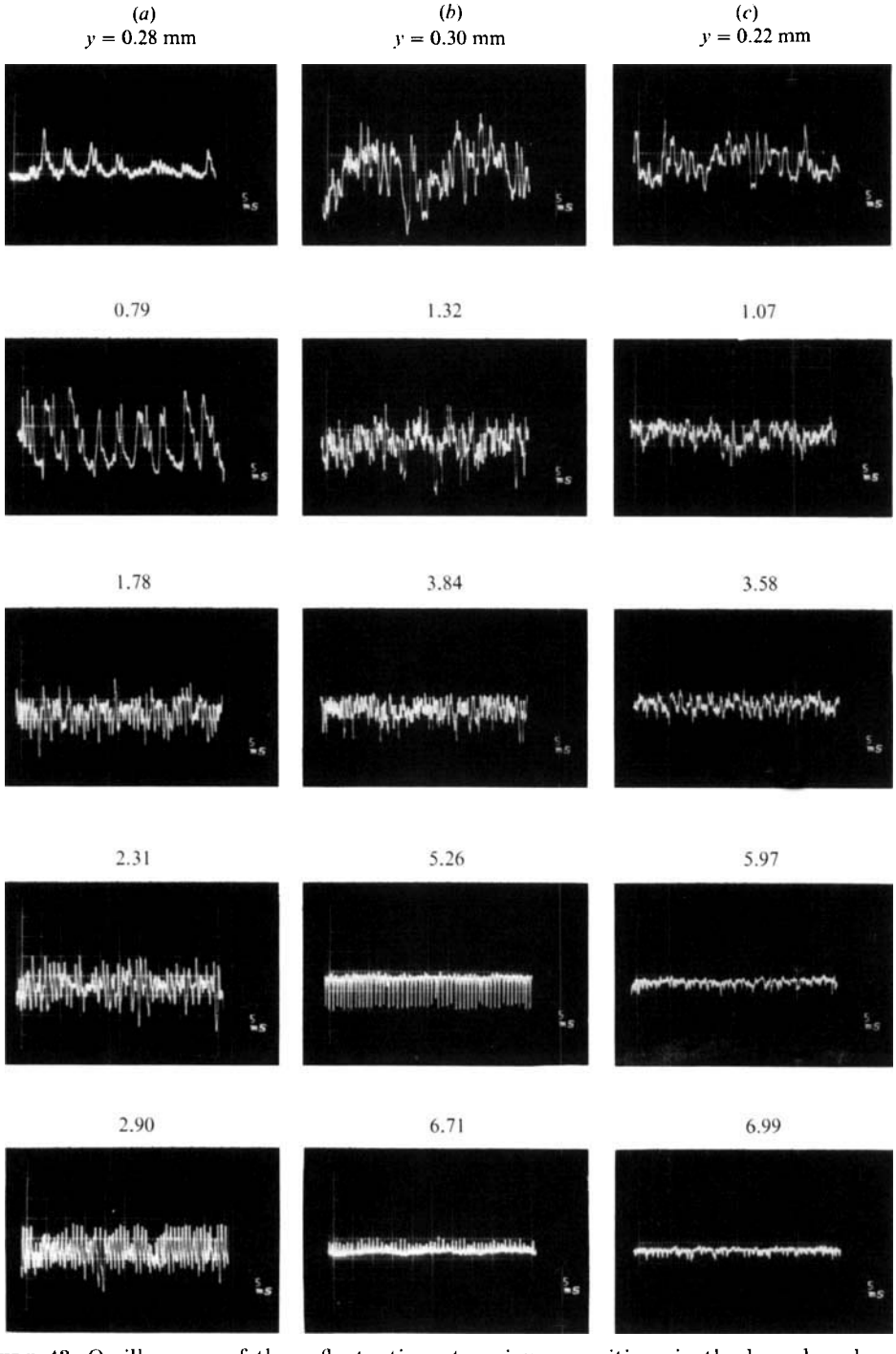

FIGURE 43. Oscillograms of the u-fluctuation at various y-positions in the boundary layer for different distances downstream of a hemispherical roughness element. $k = 1.7$ mm, $x_k = 91.4$ cm, $\bar{z} = 0$ cm, $U_1/\nu = 6.81 \times 10^5$ m^{-1}. Time increasing from left to right, decreasing velocity in downward direction, sweep speed = 5 ms/cm. Column (*a*) $\bar{x} = 2.54$ cm, (*b*) 5.08 cm, (*c*) 12.7 cm.

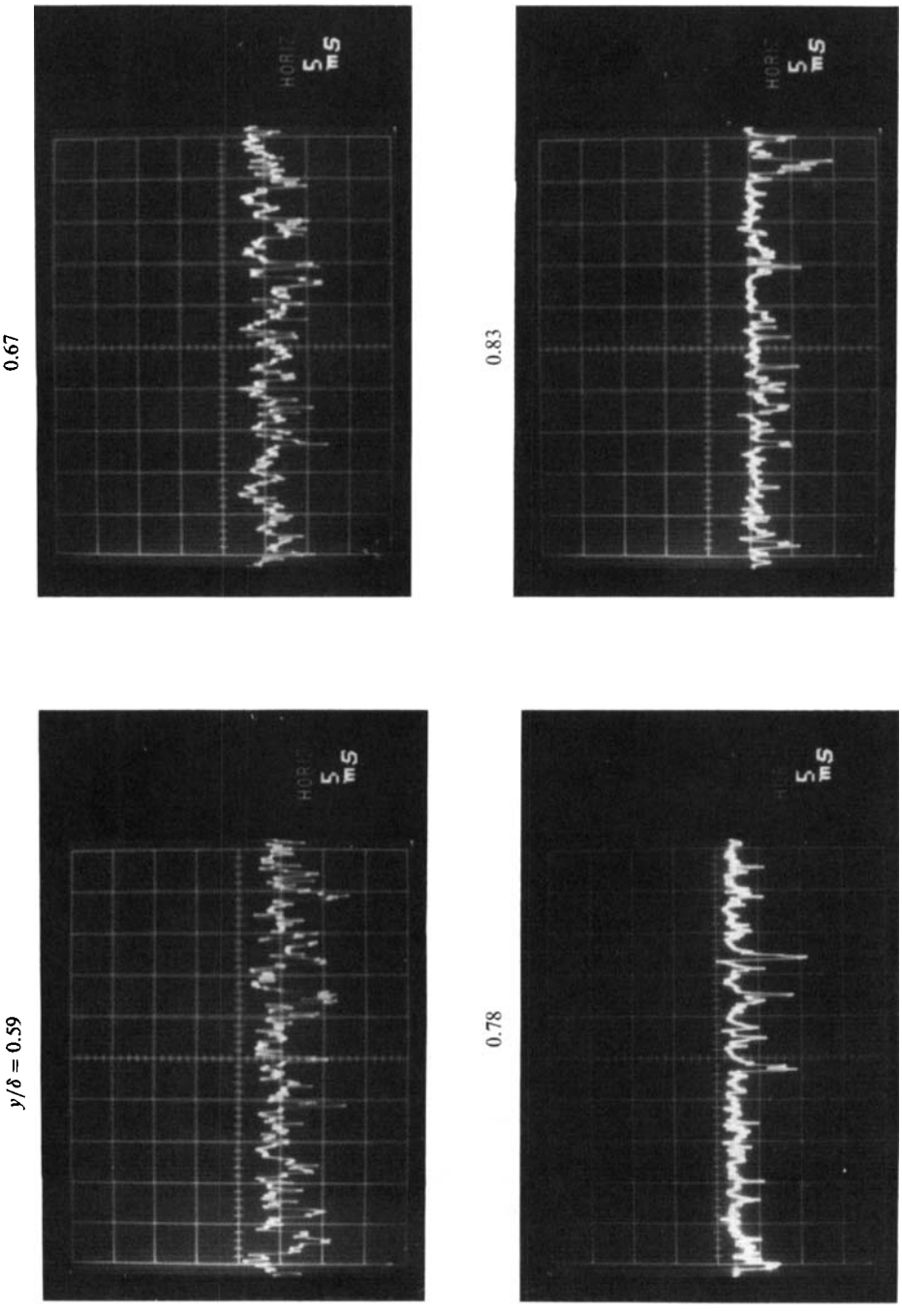

FIGURE 44. Oscillograms of the u-fluctuation in the outer region of the boundary layer at $\bar{x} = 20.3$ cm. $k = 1.7$ mm, $x_k = 91.4$ cm, $\bar{z} = 0$ cm, $U_1/\nu = 6.81 \times 10^5$ m^{-1}. Time increasing from left to right, decreasing velocity in downward direction, sweep speed = 5 ms/cm.

i.e. y at $U/U_1 = 1.0$. This position for δ was chosen to be consistent with Klebanoff (1954) and Corrsin & Kistler (1954). It is seen from the oscillograms that there are pulses in the direction of decreasing velocity which may be indicative of the presence of distinct eddy structures, but they occur randomly. Apart from the absence of a definitive eddy-shedding frequency, an interesting feature illustrated by the oscillograms in figure 44 is the lack of an intermittent outer region, as observed for a turbulent boundary layer by Klebanoff & Diehl (1951), Townsend (1951), Klebanoff (1954), Corrsin & Kistler (1954), and Kovasznay, Kibens & Blackwelder (1970), despite the fact that at this $\bar{x}$-position and unit Reynolds number the mean velocity distribution has evolved as shown in figure 47 below to where it is fairly close to being representative of a fully developed turbulent boundary layer. The values of the intermittency factor, γ, i.e. the percentage of the time the flow is turbulent as observed by Klebanoff (1954) for a fully developed turbulent boundary layer at the y/δ-positions of figure 44, are 0.90, 0.78, 0.48, and 0.35, respectively, and the oscillograms in figure 44 do not reflect this. Thus, the development of the intermittent outer-region characteristic of a fully developed turbulent boundary layer cannot by attributed to the evolution of a boundary layer to its initial fully developed turbulent condition when induced by a three-dimensional roughness element. As a corollary, it may also be inferred that the intermittent state of the outer region is not a determining factor in establishing the nature of the y-distributions of U and u' for a fully developed turbulent boundary layer.

The spectral distributions coupled to the behaviour illustrated in figure 38 reflect a difference in vortical behaviour in the inner and outer regions of the evolving boundary layer, with the structural element common to both regions being the hairpin eddy. It is the damping of the intensity of the eddy-shedding frequencies in the outer region of the boundary layer that is consistent with the view, cited in §6, that such eddies are not involved or at best only indirectly related to the induced transition. However, it has also been shown in §6 that the hairpin eddies are intrinsic to the induced transition and the developing turbulence. In order to reconcile these points of view, an attempt should be made to clarify the contrasting behaviour between the inner and outer regions of the evolving boundary layer.

The onset of turbulence which originates near the surface and is characterized by a continuous spectrum may be rationalized as resulting from a randomizing process involving vortical instabilities and associated deformation of vortical structures, inherent phase jitter, and a randomized amplitude modulation coupled to a degree of frequency modulation. This complicated interaction extends further and further from the surface with $\bar{x}$. Involved in this process is the interaction of the shedding vortices with the pre-existing longitudinal vortices and the lateral instability of the horseshoe vortex. The interaction is exceedingly complex and strongly conditioned by the geometry, intensity, stretching, and mutual induction aspects of the various structures. In view of the variance in vortical alignments it is difficult to assess the degree of amalgamation that may occur. It may well be that under appropriate conditions, for example a relatively large difference in intensity, vortical structures may intertwine. It is evident from the spectral data that the degree of vortical stretching over the spatial configuration of the hairpin eddy as it moves outward from the surface is not uniform and the increase in intensity resulting from stretching occurs primarily in the inner region.

Figure 45 compares the y-distributions of U and u' at $\bar{z} = 0$ cm for the same $\bar{x}$-position at which the spectral measurements were made. The distributions are consistent with the conceptual model of inner and outer regions outlined above and

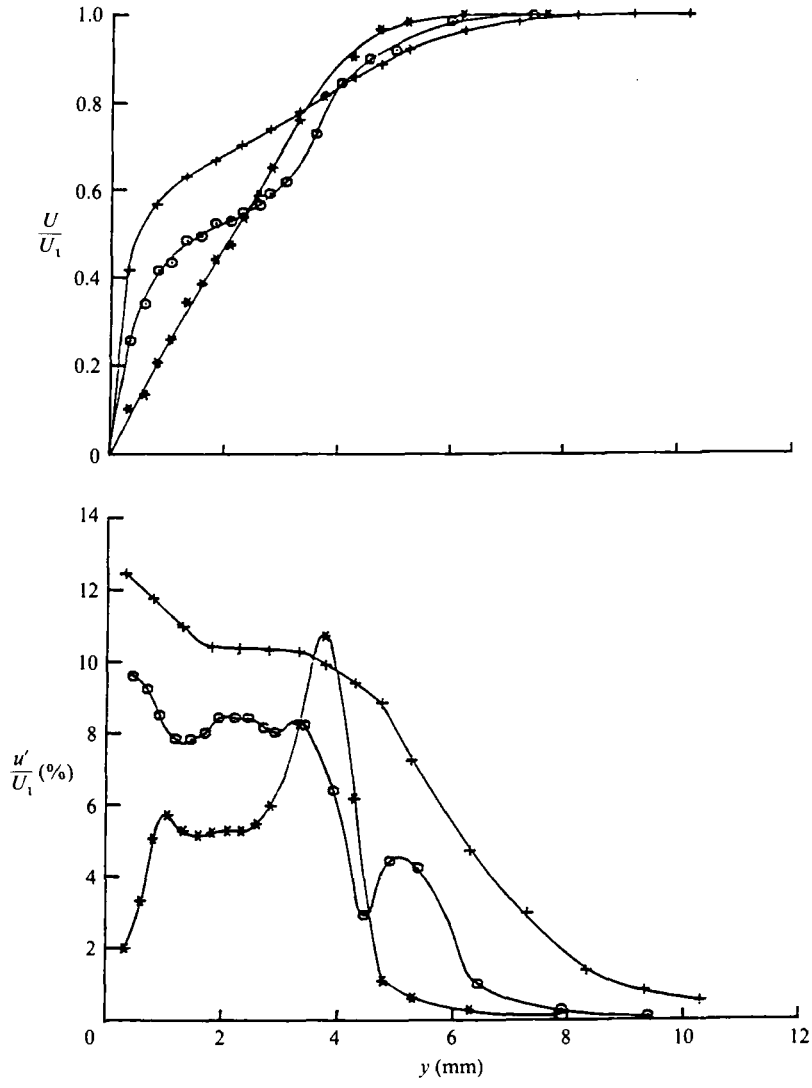

FIGURE 45. Comparison of boundary-layer distributions of U and u' at $\bar{x} = 2.54$ (*), 5.08 ($\odot$) and 12.7 cm (+). $k = 1.7$ mm, $x_k = 91.4$ cm, $\bar{z} = 0$ cm, $U_1/\nu = 6.81 \times 10^5$ m^{-1}.

suggest that the development of turbulence in each region involves a different mechanism. The increase in u' with $\bar{x}$ in the inner region may be rationalized by the complex vortex–vortex interactions and vortex instabilities described above coupled to the increase in the intensity of the various vortices resulting from the stretching associated with their outward movement from the surface into regions of increasing velocity. In order to account for the steepening of the velocity gradient at the surface with $\bar{x}$, a transfer of higher velocity fluid inward toward the surface and inner region is required. The increase in the velocity gradient occurs not only at $\bar{z} = 0$ cm but also over a lateral extent which increases in accordance with the spread of the turbulent wedge. This suggests that vortices close to the surface, which develop at the boundary of the wedge as it spreads downstream, provide the required transfer of high-velocity fluid.

The peaks in the distribution of u' in figure 45 at $\bar{x} = 2.54$ and 5.08 cm reflect the presence of the hairpin eddies in the outer region of the boundary layer and the damping accompanying the outward movement of their apex with increasing $\bar{x}$. As the intensity of the outer region of the hairpin eddy is damping rapidly with increasing $\bar{x}$, the intensity of u' in the outer region of the boundary layer at $\bar{x} = 12.7$ cm has increased significantly. It is tempting to arbitrarily draw the conclusion that turbulence diffuses across the boundary layer from the inner region to the outer region as the hairpin eddy damps. However, it does not seem reasonable that the vortical behaviour described above for the generation of turbulence in the inner region can be expected to increase in spatial extent to encompass the entire boundary layer, since the only vortical elements present in the outer region of the boundary layer in the early stage of development are the regions contiguous to and encompassing the tip of the hairpin eddies, and these regions are damping.

The behaviour in the outer region suggests that the decay of the concentrated vorticity associated with the hairpin eddies occurs in the presence of a developing turbulent field. Thus, it is of interest to examine whether the inflexional mean velocity distribution at $\bar{x} = 5.08$ cm in figure 45 may provide an appropriate mechanism. As previously mentioned, this profile is regarded as being distinct from that referred to in connection with the initial instability. The latter arose essentially from the stationary vortices induced by the roughness element while the former is associated with the presence of the hairpin eddies. The inflexional nature of the mean velocity profile varies with Reynolds number as can be seen from the mean velocity distributions at the various $\bar{x}$-positions and unit Reynolds numbers of 4.82×10^5, 5.97×10^5 and 6.81×10^5 m^{-1} in figure 33. The downstream extent of the inflexional profile is greatest at the unit Reynolds number of 4.82×10^5 m^{-1}. This is not surprising since at this Reynolds number, which is slightly above the critical Reynolds number, the hairpin eddy maintains its original configuration for a greater distance downstream. At a unit Reynolds number of 5.97×10^5 m^{-1} the downstream extent of the inflexional mean velocity profile is less than that at the lower unit Reynolds number but greater than that at the higher unit Reynolds number of 6.81×10^5 m^{-1}. However, the strength of the inflexion, for example at $\bar{x} = 5.08$ cm, is greater for the unit Reynolds number of 5.97×10^5 m^{-1} than either of the other two Reynolds numbers. It is apparent, therefore, that the inflexional nature of the mean velocity profile is not solely a consequence of the presence of the hairpin eddy. This is also readily seen in figure 45 from the mean velocity distributions at the same unit Reynolds number at $\bar{x} = 2.54$ cm, where the hairpin eddy is more intense as evidenced by the larger value of u', but there is little evidence of an inflexion in the profile. The inflexional nature of the mean velocity profile, consequently, is also dependent on the background flow in which it is embedded and on the influx of the higher momentum fluid near the surface. The inflexional mean velocity profiles at the two higher unit Reynolds number bear a marked similarity to the instantaneous velocity profiles observed by Klebanoff *et al.* (1962), Kovasznay, Komoda & Vasudeva (1962), Hama Nutant (1963), and Van Muiswinkel (see Hinze 1975, p. 608) over one cycle of the hairpin eddies occurring during the transition process on a flat plate. Thus, the possibility arises of a self-induced secondary free-shear-layer type of instability which from a quasi-steady approximation may involve the generation of a secondary hairpin eddy system at $\bar{z} = 0$ cm as observed in the flow-visualization experiments of Acarlar & Smith (1987). Acarlar & Smith conclude from their flow-visualization studies combined with hot-film measurements that the interaction of the secondary hairpin with the primary hairpins, involving their pairing, is

responsible for the observed fully developed turbulent boundary layer. The observations and conclusions of Acarlar & Smith are not clearly shown by the present measurements except perhaps for the presence of a very weak second harmonic of 1800 Hz of limited y-extent in the outer region of the boundary layer. However, this second harmonic can be equally well rationalized by an appropriate deformation of the primary hairpin eddy. Nor can the interactions of the secondary hairpin with the primary one involving pairing be reconciled with the damping of the hairpin eddies observed in the outer region of the boundary layer when it is expected that such pairing may result in an increase in energy. Nor is it evident that the pairing, *per se*, results in spectral broadening. In addition, the required instability accompanying the more rapid onset of turbulence with increasing Reynolds number is not consistent with the variation of the inflexional nature of the profile with Reynolds number. Although the present measurements do not necessarily negate the secondary structures observed by Acarlar & Smith (1987), the conclusion, nevertheless, is that a more appropriate rationalization than the onset of a secondary inflexional instability is required for the observed behaviour of the outer region.

Apart from the question as to whether the mean velocity gradient is actually representative of the instantaneous strain rate, it can be reasonably inferred that the tip region of the hairpin eddy is subject to little external strain. Under such a condition, the damping of the intensity of the eddy-shedding frequencies in the outer region may be thought of as being due to the development of an Ω-shaped tip region as previously discussed and that the associated vortex core increases in diameter by viscous diffusion resulting in a decrease in circulation. However, this does not explain the increase in u' and spectral broadening. It is therefore further proposed, as demonstrated by the numerical experiments of Moin *et al.* (1986), that the Ω-shaped tip region of the hairpin eddy pinches off and separates to form a vortex ring. It is also speculated that not only do the diameters of the vortex rings and their cores increase, but also the vortex rings are unstable and break down into turbulent vortex rings. As a result there is the accompanying process of fluid entrainment, and an enhanced cancellation of the intensity of the eddy-shedding frequency by turbulent diffusion. Assuming the validity of the model, the formation of the Ω-shaped tip region and the development therefrom of unstable rings and their breakdown into turbulence apparently accelerates in $\bar{x}$ with increasing unit Reynolds number. Although it is difficult to correlate the various aspects of the model with $\bar{x}$ from the limited measurements that were made, it is conjectured that at $U_1/\nu = 6.81 \times 10^5$ m^{-1} the separation of the vortex rings occurs at an $\bar{x} > 5.08$ cm. It should be noted that the foregoing postulate for the behaviour observed in the outer region is based to a large extent on the instability of vortex rings in an ambient fluid at rest (Maxworthy 1972, 1974; Widnall, Bliss & Tsai, 1974; Widnall & Tsai 1977; Saffman 1978) and hence inherently assumes that an ambient fluid with velocity U_1 does not materially change the unstable behaviour nor the Reynolds-number criterion for the onset of instability. Assuming that the propagation velocity of the vortex rings may be regarded as being approximated by U_1, the vortex ring Reynolds number, $U_1 D/\nu$, where D is the diameter of the ring, would have to be greater than 600 (Maxworthy 1972) for the onset of instability. At $U_1/\nu = 6.81 \times 10^5$ m^{-1} this would require that the ring diameter be greater than 0.9 mm, which is a requirement compatible with the boundary-layer thickness and the characteristics of the outer region.

Flow-visualization studies of the transition process are at best ambiguous as to the merit of the behavioural model proposed for the outer region. Flow-visualization studies of transition on a flat plate by Hama & Nutant (1963) and on an ogive-nose

cylinder with an adverse pressure gradient by Knapp & Roache (1968) show the occurrence of the bottleneck or Ω-shaped outer region of the hairpin eddy and the separation of the Ω-shaped outer region to form a vortex ring. However, a different interpretation of the physical significance of the vortex rings is given by Hama & Nutant, and neither of the studies indicate that the vortex rings became unstable and break down into turbulence. In addition, the flow-visualization studies by Mochizuki (1961*a*, *b*) and Acarlar & Smith (1987) make no reference to the presence of bottleneck hairpin eddies or vortex rings in the outer region, although the Reynolds numbers of their experiments were sufficient to produce a turbulent wedge. There is, however, some indirect support for the model from the observation by Falco (1977) of ring vortices in the outer region of the turbulent boundary layer. Be that as it may, it is felt that the vagaries of the flow-visualization studies are such as to preclude any definite conclusion as to the merit of the behavioural model proposed. The explanations proposed for the behaviour of the inner and outer regions, albeit speculative and requiring further evaluation, are believed to be appropriate for the observations of the present study and reconcile this behaviour with the intrinsic importance of eddy shedding. The foregoing discussion describes the inner and outer regions of the boundary layer as having different behavioural characteristics involving different mechanisms. Consequently the conclusion may be drawn that it is the merging of these two regions with $\bar{x}$ toward a quasi-equilibrium condition that constitutes the evolutionary process toward establishing a fully developed turbulent boundary layer.

8. Turbulent boundary layer

The critical behaviour of a three-dimensional roughness element in inducing a turbulent boundary layer is demonstrated by the distributions of U and u' at the various unit Reynolds numbers. At subcritical Reynolds numbers the distributions return to that which would exist without the roughness present. This is shown in figure 46 in which the mean velocity distributions at the various $\bar{x}$ for the subcritical Reynolds numbers and a Reynolds number which is slightly above critical are compared non-dimensionally with the mean velocity profile measured without the roughness. The distance $\bar{x}$ required to return to the condition without roughness decreases with decreasing Reynolds number. At the Reynolds number which is just above critical, the mean velocity distributions are indicative of transitional flow consisting of intermittent turbulent spots. The changes in profile shape with $\bar{x}$ reflect an increase in the percentage of time that the flow is turbulent with increasing $\bar{x}$, consistent with the downstream growth of turbulent spots. However, at this Reynolds number the flow condition is extremely sensitive to Reynolds number. The distributions of u' at this Reynolds number in figure 33 reflect this sensitivity in their variation with $\bar{x}$.

As discussed in §6 turbulent spots are initiated closer to the roughness with increasing Reynolds number until at some Reynolds number the wedge of turbulence may be regarded as being attached to the roughness. Since a finite distance is required for the instability, the wedge of turbulence, albeit close to the roughness, is not actually attached. At a unit Reynolds number of 6.81×10^5 m^{-1}, which is the highest for which distributions of U and u' were measured, the corresponding Re_k is 550, and the wedge of turbulence has its origin at $\bar{x} = 5.08$ cm. The turbulence at or near the origin of the wedge, as defined by the spectral measurements, is initiated near the surface and is not characteristic of that for a fully developed turbulent

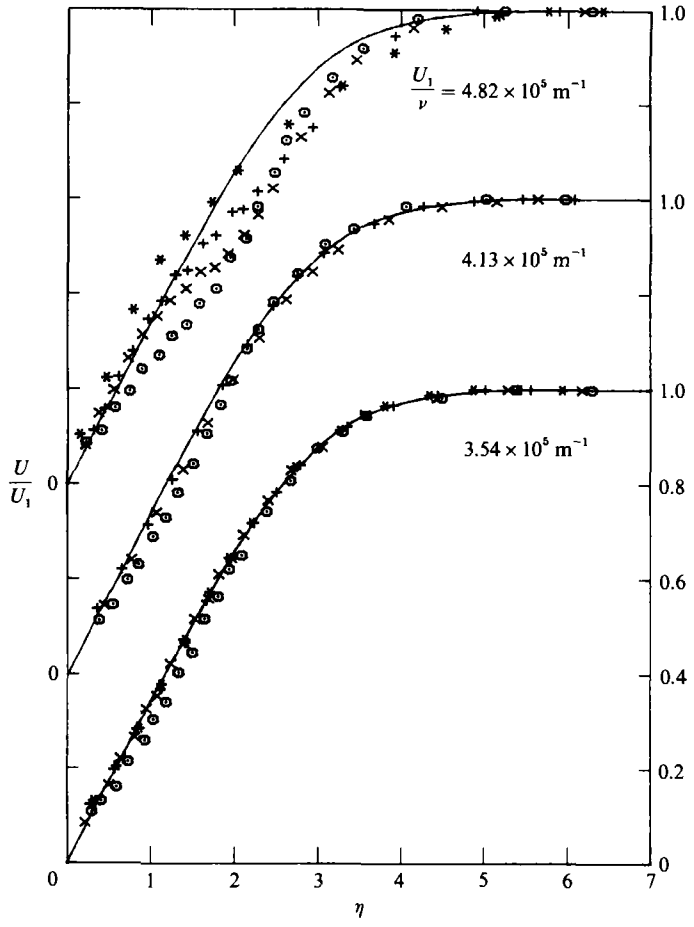

FIGURE 46. Comparison of mean velocity profiles downstream of a hemispherical roughness element for varying $\bar{x}$ and unit Reynolds number with the mean velocity profile without roughness (——). $k = 1.7$ mm, $x_k = 91.4$ cm, $\bar{z} = 0$ cm. ⊙, $\bar{x} = 7.62$ cm; ×, 12.7 cm; +, 20.3 cm; *, 30.5 cm.

boundary layer until some distance further downstream from the origin. This is shown in figure 47 in which the mean velocity distributions along the centreline of the wedge at various $\bar{x}$, for unit Reynolds numbers of 5.97×10^5 and 6.81×10^5 m^{-1}, are plotted non-dimensionally with δ^*, the boundary-layer displacement thickness, and compared with a turbulent boundary-layer profile measured by Purtell, Klebanoff & Buckley (1981) at about the same Reynolds number, $R_\theta = U_1\theta/\nu$. The values of R_θ at $\bar{x} = 23.7$ and 30.5 cm are 715 and 745, respectively, for $U_1/\nu = 6.81 \times 10^5$ m^{-1}, and 720 at $\bar{x} = 20.3$ cm for $U_1/\nu = 5.97 \times 10^5$ m^{-1}. The mean velocity profile at $\bar{x} = 30.5$ cm and $U_1/\nu = 6.81 \times 10^5$ m^{-1} is in good agreement with that of Purtell *et al.* (1981) for a fully developed turbulent boundary layer on a flat plate with zero pressure gradient. In figures 48 and 49 the distributions of u' and U_1 along the centreline for $\bar{x} \geqslant 30.5$ cm are compared at $U_1/\nu = 6.81 \times 10^5$ m^{-1}. In figure 48 the distributions of u' are compared with the distributions of Purtell *et al.* (1981) for a comparable range of Reynolds numbers and show the same trend with Reynolds number. Although the differences are small, the values of u'/U_1 are higher than those of Purtell *et al.* at comparable Reynolds numbers. The measurements of Purtell *et al.*

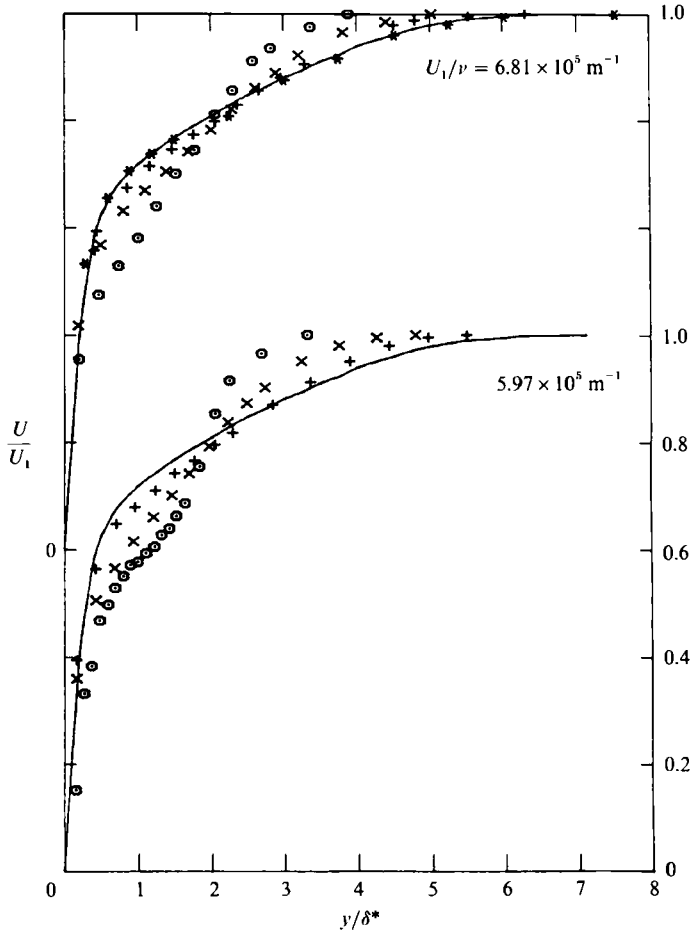

FIGURE 47. Comparison of mean velocity profiles downstream of a hemispherical roughness element for varying $\bar{x}$ and unit Reynolds number with the mean velocity profile for a fully developed turbulent boundary layer. $k = 1.7$ mm, $x_k = 91.4$ cm, $\bar{z} = 0$ cm. ⊙, $\bar{x} = 7.62$ cm; ×, 12.7 cm; +, 20.3 cm; *, 30.5 cm; ——, turbulent boundary layer (Purtell *et al.*). $R_\theta = 700$.

were made with a linearized hot-wire response whereas the present ones were not. However, the difference between the distributions at $R_\theta \approx 700$ is such that attributing the difference to the method of measurement is questionable. Although there is the possibility of experimental uncertainties, it is also possible that the difference is real and may reflect a small distortion in the turbulence structure, i.e. that it still retains a memory of how it was induced, to which, as can be seen from the data presented in figures 47 and 49, the mean velocity distribution is insensitive. However, there are questions pertaining to the dependence of the distributions of mean velocity and turbulence intensity on Reynolds number, and the behaviour of 'new' versus 'aged' turbulence to be answered before the disparity in the u' distributions at $R_\theta \approx 700$ can be properly assessed. In this regard, it is of interest to note that Klebanoff & Diehl (1951) observed that the mean velocity distribution afforded an adequate means for identifying a fully developed turbulent boundary layer. Complete similarity of the mean velocity distribution over the whole of the boundary layer is not to be expected because of the difference in behaviour of the inner and outer regions. However, the similarity of the mean velocity distributions shown in figure

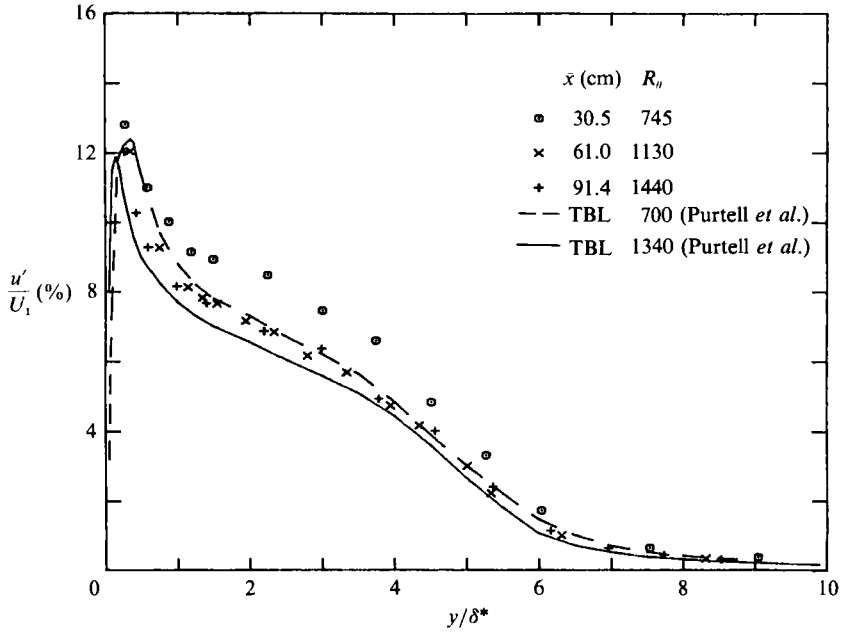

FIGURE 48. Comparison of the boundary-layer distributions of u' for $\bar{x} \geqslant 30.5$ cm with the distributions for a fully developed turbulent boundary layer. $k = 1.77$ mm, $x_k = 91.4$ cm, $\bar{z} = 0$ cm, $U_1/\nu = 6.81 \times 10^5$ m^{-1}.

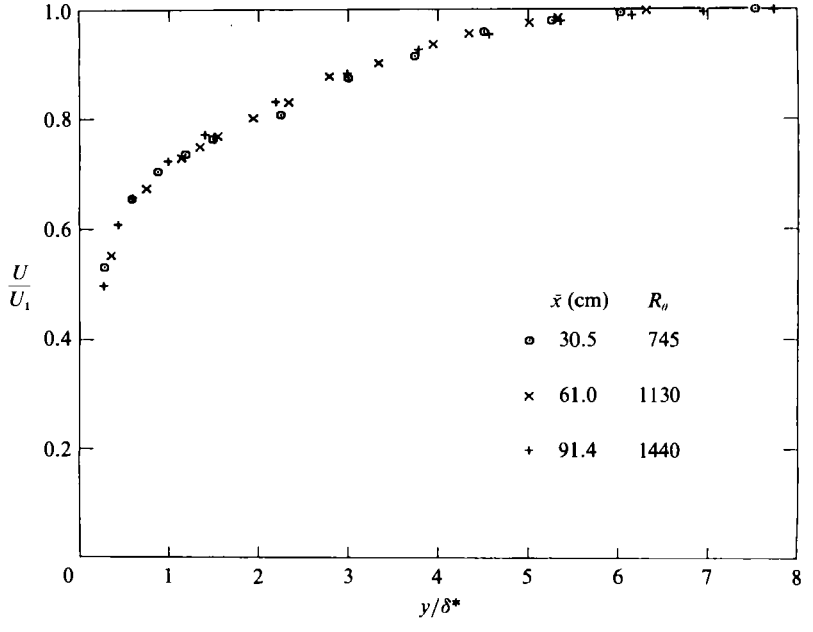

FIGURE 49. Comparison of the boundary-layer distributions of U for $\bar{x} \geqslant 30.5$ cm. $k = 1.7$ mm, $x_k = 91.4$ cm, $\bar{z} = 0$ cm, $U_1/\nu = 6.81 \times 10^5$ m^{-1}.

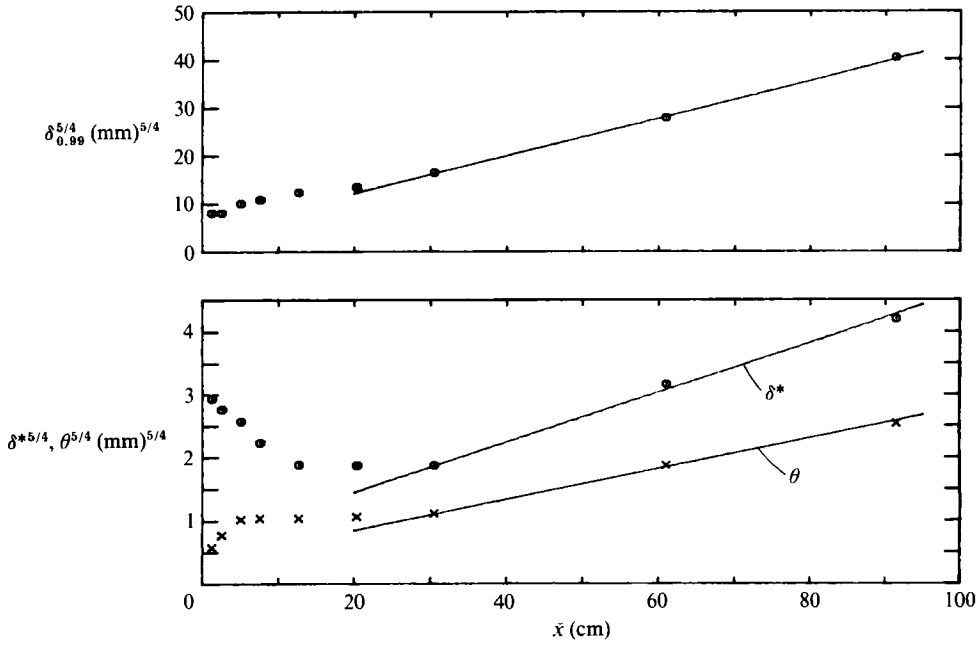

FIGURE 50. Variation of boundary-layer parameters with $\bar{x}$. $k = 1.7$ mm, $x_k = 91.4$ cm, $\bar{z} = 0$ cm, $U_1/\nu = 6.81 \times 10^5$ m^{-1}.

49 is consistent with that which would be expected for a fully developed turbulent boundary layer scaled with U_1 and δ^*.

The state of the induced boundary layer is further evaluated in figures 50 and 51. The variation of the boundary-layer parameters, $\delta_{0.99}$, δ^*, and θ with $\bar{x}$ are shown in figure 50 in a form to facilitate comparison with a fully developed two-dimensional turbulent boundary layer with zero pressure gradient. In this comparison, $\delta_{0.99}$ is the boundary-layer thickness at which $U/U_1 = 0.99$. It is seen that for $\bar{x} \geqslant 30.5$ cm the parameters behave as for the fully developed turbulent boundary layer, i.e. the linear variation with $\bar{x}^{\frac{4}{5}}$. It was also of interest to deduce the local skin-friction coefficient, c_f, using the two-dimensional momentum equation, that is

$$c_f = \frac{2\mathrm{d}\theta}{\mathrm{d}x} = \frac{2\tau_0}{\rho U_1^2}, \tag{6}$$

where τ_0 is the shear stress at the surface and ρ is the air density. The values of c_f were 0.0038, 0.0035, and 0.0033 at $\bar{x} = 30.5$, 61.0, and 91.4 cm, respectively. These values of c_f are significantly lower than those for a fully developed two-dimensional turbulent boundary layer with zero pressure gradient at corresponding values of R_θ, which from Coles (1962) are 0.0049, 0.0043, and 0.0040. The discrepancy and its direction is not surprising in view of the three-dimensional nature of the flow associated with the turbulent wedge as previously described, and the spanwise flow required to explain the discrepancy in the momentum equation is small. Assuming that the values of c_f given by Coles (1962) are a more accurate estimate, the velocity distributions at $\bar{x} = 30.5$, 61.0, and 91.4 cm are compared in figure 51 with the logarithmic law suggested by the Stanford Conference on the computation of turbulent boundary layers (Coles & Hirst 1968):

$$U^+ = 5.0 + 5.6 \log y^+, \tag{7}$$

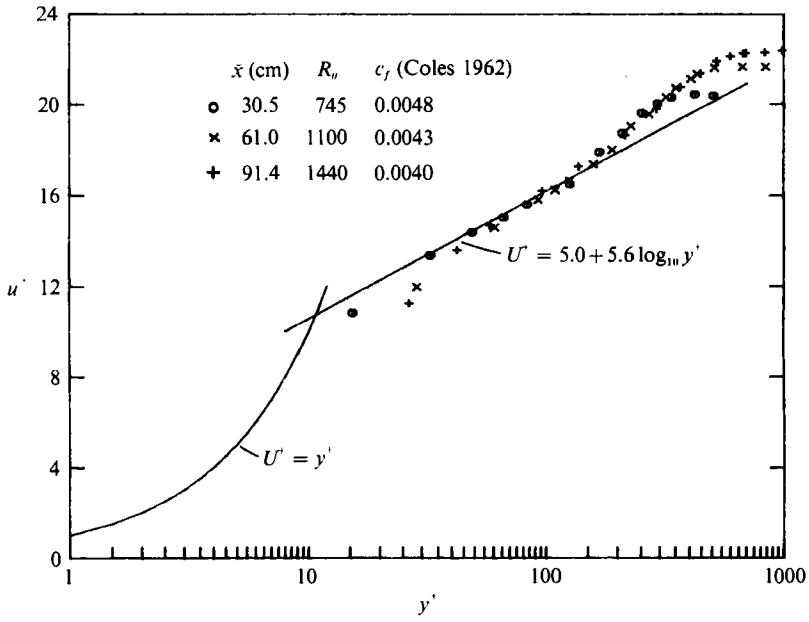

FIGURE 51. Comparison of the boundary-layer distributions of U at $x \geqslant 30.5$ with the logarithmic law. $k = 1.7$ mm, $x_k = 91.4$ cm, $\bar{z} = 0$ cm, $U_1/\nu = 6.81 \times 10^5$ m^{-1}.

where $U^+ = U/U_\tau$, $y^+ = yU_\tau/\nu$, and U_τ is the friction velocity $(\tau_0/\rho)^{\frac{1}{2}}$. Although the logarithmic range is limited due to the limited range of Reynolds number, the agreement is reasonably satisfactory. The conclusion is therefore drawn that the evolutionary process downstream of a three-dimensional roughness element in a zero-pressure-gradient laminar boundary layer at an appropriate Reynolds number and roughness size leads to a turbulent wedge in which the fully developed turbulent region is representative of a fully developed two-dimensional turbulent boundary layer with zero pressure gradient. A reasonable inference from this is that the converse is true, i.e. the detailed structure of the fully developed two-dimensional turbulent boundary layer is similar to that which has evolved in establishing the fully developed turbulent wedge. Consequently, the instantaneous local flow in the two-dimensional turbulent boundary layer with or without pressure gradient is three-dimensional, varying randomly in space and time, and the two-dimensional momentum equation is an adequate representation of the skin friction only in that on the average there is no lateral mean flow unless induced by a bias in the experimental configuration.

In the comparison of the turbulent wedge and turbulent boundary layer there is the question of intermittency of the outer region of the boundary layer inasmuch as, as in the discussion of figure 43, it was not observed to occur in the evolutionary process that established the fully developed turbulent wedge. To the authors' knowledge the outer region of the fully developed turbulent wedge along its centreline, for example, has yet not been studied in any detail. It would have been of interest to have investigated this aspect further to determine if and how the intermittency develops, and its coupling to the nature of the mean velocity distribution. Regrettably, circumstances prevented doing so. Nevertheless, it is assumed that the fully developed turbulent region of the wedge exhibits an intermittency in the outer region similar to that for the turbulent boundary layer.

Consequently, the intermittency is an inherent property of an interface between turbulent fluid and an irrotational free stream (Corrsin & Kistler 1954; Townsend 1970; Phillips 1972) in which the interface is distorted by the large-scale eddies in the outer region of the turbulent boundary layer. Vorticity diffuses into the irrotational fluid owing to the action of viscosity, and there is entrainment of free-stream fluid by the unsteady irregular outline of the interface (Maxworthy 1972; Laufer 1975; Blackwelder 1980). According to the evolutionary process postulated in §7.3, the turbulent vortex rings would be the large-scale structures in the outer region of the layer controlling the entrainment process. Since the intermittency factor, γ, scales as y/δ (Klebanoff 1954; Corrsin & Kistler 1954) the amplitude of the irregular outline of the boundary layer as it moves downstream should increase at the same rate as does the change in momentum associated with the shear flow.

The distributions of U and u' presented at various $\bar{x}$ which characterize the evolution of a turbulent boundary layer induced by a three-dimensional roughness element have not been scaled with k since there is not adequate evidence to indicate that such scaling is appropriate. Furthermore, the measurements were made for the same roughness element and such scaling is readily obtained. As shown in figure 47, the position, $\bar{x}$, at which the turbulence in the wedge becomes characteristic of a fully developed turbulent boundary layer moves upstream with increasing unit Reynolds number, but this should not be interpreted that an asymptotic $\bar{x}/k$ will necessarily be reached. It may well be that with an increasing unit Reynolds number, which may be critical, the $\bar{x}$-position at which the fully developed turbulent state is reached may actually reverse and move further downstream from the roughness. This possibility is suggested by the observation by Klebanoff & Diehl (1951) that the boundary layer retains a long memory of disturbances introduced by obstacles extending into the outer region of the layer. The distortion they introduce, in contrast to much smaller obstacles in the inner region, may persist for a considerable distance downstream before the boundary layer returns to the fully developed state. The observations by Klebanoff & Diehl were made using two-dimensional roughness elements, and it was of interest to determine whether a three-dimensional roughness element would exhibit similar behaviour. In this regard, the only data available for such an evaluation with a roughness of appropriate shape, i.e. hemispherical, with which the present results could be compared are those obtained by Acarlar & Smith (1984, 1987) on a flat plate in a free-surface water channel.

Acarlar & Smith made measurements of the y-distributions of U and u' along the centreline at two values of Re_k for $k = 8.4$ mm: $Re_k = 750$ (Acarlar & Smith 1984, 1987), and $Re_k = 1500$ (Acarlar & Smith 1984). In the present investigation k and Re_k were 1.7 mm and 550, respectively. Acarlar & Smith (1987) present distributions of U and u' for $Re_k = 750$ at $\bar{x}/k = 4$, 10, 40, and 80, and state that the distributions of U and u' at $\bar{x}/k = 80$ 'display a shape characteristic of a turbulent boundary layer. It has been shown (see Acarlar & Smith 1984) that increasing the free-stream velocity causes the profiles to become fuller much earlier, i.e. closer to the hemisphere. Development of the turbulence intensity profiles follows the same trend as lower-velocity cases, with the value of turbulence intensity attaining a slightly higher maximum value.' The behaviour described in the foregoing quotation coupled to that of the present study in which for $Re_k = 550$ the boundary layer becomes fully developed at $\bar{x}/k = 179$, or possibly within the precision of the experiment at $\bar{x}/k = 150$, suggests that there may be an appropriate k-scaling irrespective of the much larger roughness size. It was therefore of interest to make a more detailed comparison of the available data.

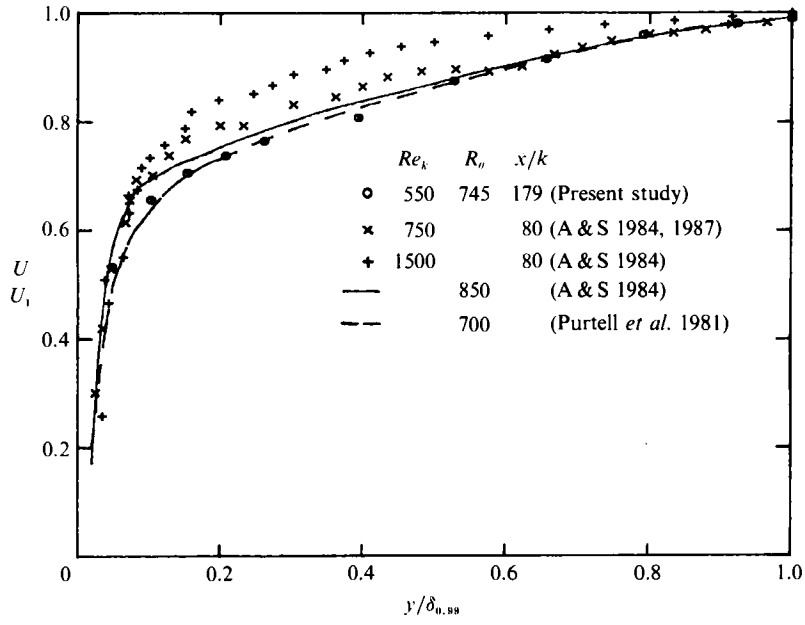

FIGURE 52. Comparison of the boundary-layer distributions of U with the data of Acarlar & Smith (1984, 1987) and Purtell *et al.* (1981).

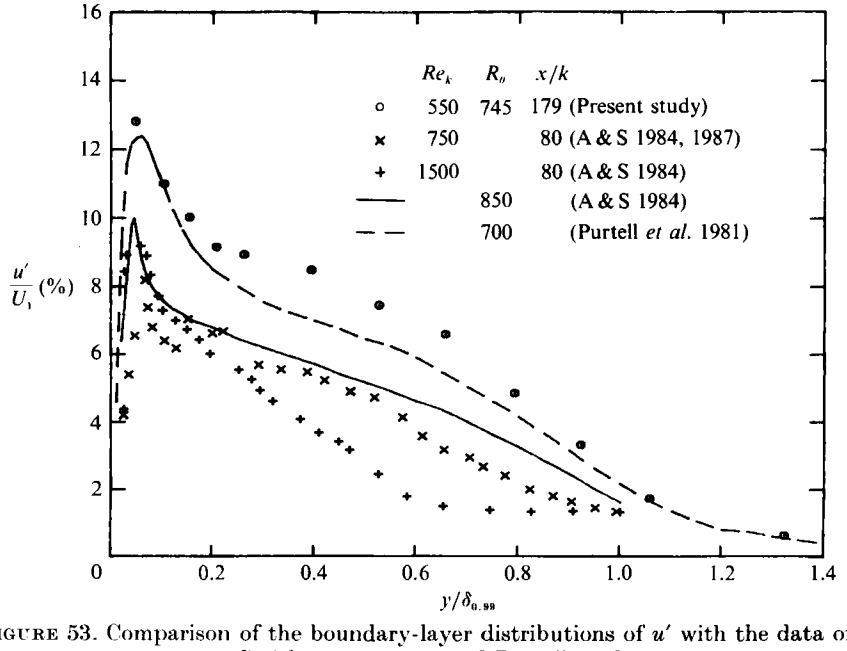

FIGURE 53. Comparison of the boundary-layer distributions of u' with the data of Acarlar & Smith (1984, 1987) and Purtell *et al.* (1981).

In Acarlar & Smith (1984) distributions of U and u' for $Re_k = 1500$ are presented at the same $\bar{x}/k$ as for $Re_k = 750$. Acarlar & Smith do not provide sufficient data to explicitly obtain the ratio of k to the boundary-layer thickness, δ_k, at the roughness position. However, they state (Acarlar & Smith 1984) that the change in Re_k from 750 to 1500 was obtained by doubling the free-stream velocity. This imposes the

condition that $k/\delta_k \geqslant 1.0$ for both values of Re_k with k/δ_k for $Re_k = 1500$ being 40% greater than that for $Re_k = 750$. This is in contrast to the present study in which $k/\delta_k = 0.29$. It is reasonable to expect that at $k/\delta_k \geqslant 1.0$ the initial inflexional instability may be characteristic of that for a free-shear layer. Their distributions of U and u' at $\bar{x}/k = 4.0$ support this view, and it is speculated that this may account for the difference in gradient of Strouhal behaviour discussed in §5 and in particular that at the larger values of k and Re_k.

A comparison of the distributions of U and u' obtained by Acarlar & Smith for $Re_k = 750$ and 1500 at $\bar{x}/k = 80$ are compared with the data of the present investigation obtained for $Re_k = 550$, and $\bar{x}/k = 179$ in figures 52 and 53. The currently obtained data and that of Purtell *et al.* (1981) were made non-dimensional with $\delta_{0.99}$ since this definition for δ appeared to be consistent with the graphical representation by Acarlar & Smith of their data. Although Acarlar & Smith explicitly state that the change in Re_k was obtained by doubling U_1, there is a slight ambiguity in that the values they cite for U_1 are 8 and 15 cm/s. Also shown in the figures are distributions of U and u' for a turbulent boundary layer in the water channel without roughness (Acarlar & Smith 1984) and for a turbulent boundary layer in a wind tunnel (Purtell *et al.* 1981) at values of $R_\theta = 850$ and 700, respectively. The distributions of U and u' for the turbulent boundary layer in the water channel are qualitatively similar to those by Purtell *et al.*; however, they do show differences in magnitude. Although the differences in the distributions of U and u' are in the direction of a Reynolds effect, they cannot be attributed to such an effect since the variation in Reynolds number is too small for the differences observed. The reason for the disparity in the distributions for the turbulent boundary layers shown in figures 52 and 53 is not apparent, and in this connection it would have been of interest to have had information as to the conditions under which the turbulent boundary layer in the water channel was established.

It is evident that the distributions of both U and u' at $\bar{x}/k = 80$ for $Re_k = 1500$ in the water channel are far from being fully developed whether compared with the turbulent boundary layer in its own flow system or with that in the wind tunnel. The inference that at this Re_k the fully developed turbulent state moved closer to the roughness appears incorrect. The deviations of the distributions of U and u' are so large as to make it doubtful that they would return to the characteristic turbulent state within the length of the 2.5 m test plate. In any event, it is evident that an $\bar{x}/k$ much larger than 80 is required before the distribution can be expected to exhibit similarity with a fully developed turbulent boundary layer. The distributions for $Re_k = 750$ also exhibit departure from such a similarity, and although the difference is masked to some extent by the difference in Reynolds number, the departure is of much lesser degree than at $Re_k = 1500$. It is therefore possible that for $Re_k = 750$ similarity with the turbulent boundary layer may be reached at $80 < \bar{x}/k < 179$. However, it should be noted that for $\bar{x}/k = 80$, $\bar{x}$ is 37 cm further downstream from the roughness than for $\bar{x}/k$ in the present study. The behaviour observed by Acarlar & Smith at large k/δ_k and that for a relatively small k/δ_k in the present study supports the view, at least qualitatively, that a three-dimensional roughness element in inducing transition to a fully developed turbulent boundary layer behaves in a manner observed by Klebanoff & Diehl (1951) for two-dimensional roughness elements.

The trends of the distributions of U and u' toward a fully developed turbulent state shown by Acarlar & Smith and those of the present investigation are in opposite directions, i.e. with decreasing k/δ_k and Re_k in the former, and with increasing k/δ_k

and Re_k in the latter. This suggests the possibility of an appropriate k-scaling, and a critical combination of k/δ_k and Re_k for which there may exist a minimum $\bar{x}/k$ at which a fully developed turbulent boundary layer is induced. The measurements of Acarlar & Smith and of the present investigation were each made for only one, albeit different, size and shape of the roughness element, and the question of scaling, including the effect of roughness size, shape, and position on such scaling, merits further investigation. It is important to wind-tunnel testing procedures, particularly at transonic and supersonic speed, and it is apparent that considerable care should be given to the state of a tripped boundary layer in order to ascertain the degree to which it is free of distortion.

9. Concluding remarks

The onset of the fully developed state as illustrated by the growth of the boundary-layer parameters in figure 50 indicates that the onset of a quasi-equilibrium in the vortical nature of the boundary layer has been reached for $\bar{x} \geqslant 30.5$ cm involving the effect of shear, entrainment, the exchange of outer and inner fluid, and the decay and regeneration of appropriate large-scale vortical structures, i.e. the hairpin-like structures that govern the flow in the inner region, and the turbulent vortex rings that characterize the outer region, and the entrainment process. An inherent consequence of the process of decay and regeneration of vortical structures is a randomization of the structures in space and time. The lateral extent of this fully developed state, i.e. the extent over which U and u' are fairly constant, was examined at $\bar{x} = 30.5$ cm and is approximately 2.5 cm. This increase in lateral extent over that shown in figure 38 for the hairpin eddy at $\bar{x} = 2.54$ cm, even though the latter is at a somewhat lower Reynolds number, indicates, apart from the lateral spreading of the turbulence wedge, the occurrence of hairpin-like vortical structures within the spanwise region of fully developed turbulent flow in addition to those initially generated at $\bar{z} = 0$ cm. This interpretation is supported by the observations of Perry, Lim & Teh (1981) and Acarlar & Smith (1987) that secondary hairpins are generated in the spanwise direction and is consistent with the average wavelength or distance between vortical structures, λ_z, which is estimated to be 3 mm from the low-speed streak observations of Kline *et al.* (1967), i.e. $\lambda_z U_\tau/\nu = 100$. The vortical structures in the lateral direction within the turbulent wedge are not necessarily phase locked and the question of spreading of the turbulent wedge and its relation to the lateral development of hairpin vortices, together with detailed spanwise measurements of U and u' at various y and $\bar{x}$ positions, will be discussed in a subsequent paper.

In any event, having appropriate turbulent and mean velocity distributions within such a narrow region as 2.5 cm implies that the nature of the profiles is determined by the vortical elements contained therein, which have been shown to be of relatively large scale in the evolutionary process. Thus it is the passage of the large-scale structures with their attendant flow dynamics which on average constitute the mean velocity profile. In this connection, it is of interest to note that Schubauer & Klebanoff (1950) showed that for a zero and adverse pressure gradient, the turbulent shear-stress correlation coefficient arises from components of the turbulence that extend over much of the boundary-layer thickness, and near the surface could be represented more appropriately by an overall mean velocity gradient, i.e. U_1/δ, rather than the local gradient at any one point. From this point of view, the behaviour cannot be characterized, at least physically, by a mean velocity with superposed velocity fluctuations, and raises a serious question as to

whether the instantaneous strain rate can be adequately represented by the mean velocity profile and whether Reynolds averaging adequately characterizes the physical behaviour. Consequently, it does not appear feasible that gradient diffusion-type models can lead to universal modelling of turbulent flows. Since it is reasonable to expect that the nature of the large-scale structures are dependent on the flow geometry, it is not evident that such modelling can lead to a universality from geometry to geometry, nor is it evident that it can cover a wide range of Reynolds numbers and pressure gradients for a given flow geometry without adjustment of the appropriate empirically determined constants. It may be that the best that can be hoped for with these types of models is an engineering usefulness that lies in what is so aptly described by Kline (1982) as zonal modelling.

A more appropriate perspective might be that the evolving turbulent boundary layer and its associated distributions of U_1, u', etc., are the result of an integrating effect of the dynamical behaviour and characteristics of the vortical structures, and the accommodation of the free-stream velocity thereto which serves as a source of flow for the generation of vorticity, particularly near the surface. It is proposed that the logarithmic law of the wall is intrinsic to the large-scale structures and is a property of their shape, convective velocity, vorticity, and mutual interaction. The similarity condition also implies that on average they preserve their shape and scale with the boundary-layer thickness. The hairpin-type structures may be expected to increase in scale across the boundary layer as long as they have the necessary supply of vorticity. These structures can grow sufficiently in y to yield the vortex rings in the outer region, which become unstable, as the evolutionary process described in §7.3. It is conceivable that this process is repeated as the structures travel downstream, provided that there is an adequate supply of vorticity and the plane strain is relatively small. It may be expected, however, that at some stage the plane strain will dominate and the hairpin-like structures will decay. As a result the hairpin structures, although they on occasion may extend to the turbulent–non-turbulent interface, are in general confined to the inner region of the boundary layer and may increase in y^+ with increasing Reynolds number. Assuming that the turbulent vortex rings in the outer region behave in a manner similar to that for an ambient fluid at rest, they are encompassed by a relatively large mass of turbulent fluid entrained from the outer ambient flow (Maxworthy 1974, 1977). In addition, vortex rings with approximately the same velocity travelling a similar path may become entrained with one another to form a large single vortex (Maxworthy 1972). It may be conjectured that those characteristics of turbulent vortex rings are revealed in the large-scale structures characterizing the intermittent interface and give rise to the large-scale bulges in the intermittency contours for the turbulent boundary layer. The turbulent vortex rings also increase in scale as they travel downstream in that their radius increases with $\bar{x}$, but once they deposit their vorticity by turbulent mixing into the surrounding entrained fluid, the ring motion will cease (Maxworthy 1974, 1977).

Heuristically, the question may be raised as to whether the model postulated above is adequate for boundary layers of very large thickness. It appears that it can be justified as long as there is an adequate supply of vorticity compatible with the circulation requirements of the vortical structures. In this connection, it is of interest that Perry & Chong (1982) proposed a model of hairpin-type vortical structures which, when coupled to a hierarchy of similar structures that increased in scale with y^+ and increasing Reynolds number, was able to reproduce the logarithmic law of the wall and its increasing range in y^+ with increasing Reynolds number. The model of

Perry & Chong also yielded the k^{-1} spectral range ($k = 2\pi f/U$) for the spectral function of the u-fluctuation which had been experimentally observed in the near-wall region by Laufer (1953) in pipe flow, Klebanoff (1954) in a turbulent boundary layer, and Perry & Abell (1977) in pipe flow. However, Perry & Chong conclude that the $k^{-\frac{5}{3}}$ spectral range of Kolmogorov (1941 *a*, *b*, 1962) is not of material significance in boundary-layer turbulence, and that it is but an incidental consequence of the falling-off of the k^{-1} spectrum with wavenumber. This latter conclusion is at variance with the spectral measurements of Klebanoff & Diehl (1951), Laufer (1953) and Klebanoff (1954) which showed in an outer region not too close to the wall an extensive spectral range of $k^{-\frac{5}{3}}$ without any significant evidence of a k^{-1} range. In addition, an alternative explanation for the k^{-1} spectral range near the wall, without negating the significance of the $k^{-\frac{5}{3}}$ spectral range in the outer region, has been provided by Tchen (1953) by considering the influence of the mean velocity gradient on the spectrum. It should also be noted that the hierarchy of scales, as proposed by Perry & Chong (1982) is not observed in the present study. Apart from these caveats, the interesting feature is that they were able to reproduce some of the general characteristics of the turbulent boundary layer from a vortical structure perspective. The model postulated herein to conform to the experimental measurements, although similar to that of Perry & Chong (1982) in that it considers the hairpin-type of vortical structure as fundamental to the turbulent boundary layer is, conceptually different in proposing a two-region model for the turbulent boundary layer as described in §7.3. However, both models emphasize the importance of a vortical structure perspective toward understanding the behaviour of the turbulent boundary layer.

For several decades the perspective in the study of the turbulent boundary layer has been approached from two points of view stemming probably from the dual structure of turbulence proposed by Townsend (1956) in which a large coherent type of eddy structure exists within a background of relatively unstructured small-scale turbulence. Most research during this period has emphasized the large-scale coherent structures with the approach that an appropriate understanding could only be reached by flow-visualization methods, supplemented by conditional sampling techniques, and a de-emphasis on the statistical approach to turbulence since the statistical averaging would tend to mask the presence of coherent structures in the flow. A review of much of this work and appropriate bibliographies can be found in Smith & Abbott (1978), Cantwell (1981), and Hussain (1983). On the other hand, the work on small-scale turbulence has been statistical in nature, consisting primarily of measurements of probability density distributions and moments of velocity fluctuations and their derivatives. Much of the emphasis has been on the latter since they are considered to be representative of the small-scale turbulence. Examples of this approach and associated bibliographies can be found in Kuo & Corrsin (1971), Frenkiel & Klebanoff (1975), and Antonia, Satyaprakash & Hussain (1982). Hussain (1981) attempted to incorporate both views by proposing that the large-scale structures become increasingly disorganized in the downstream direction, i.e. as they 'age', and at this stage they play a no more important role than the background turbulence.

It is felt that the results of the present investigation indicate that views of large-scale structure *vis-à-vis* small-scale structure are too extreme. They are not mutually exclusive but complement one another, and the double structure of turbulence is not adequate for furthering the understanding of turbulence behaviour. The tendency to view the turbulent boundary layer from either the large-scale or small-scale point of

view is rather arbitrary. It may be regarded as a matter of perception in that one is pertinent to an overall spatial view, and the other to a local and point-like view. The measurement of the small-scale turbulence is a local measurement and as such may not be physically independent of the large-scale structure as it passes by; however, it may still be statistically independent from flow to flow in the sense that, being a local measurement, it is not particularly sensitive to the nature of the large-scale structure which reflects the flow geometry, i.e. wake, jet, boundary layer, etc. Measurements of the third- and fourth-order moments of the temporal gradient of the longitudinal velocity fluctuation, which may be regarded in some measure as being reflective of the vorticity, provide support for this point of view inasmuch as they exhibit universality irrespective of the flow geometry (Frenkiel & Klebanoff 1975; Tavoularis, Bennett & Corrsin 1978).

Assuming the validity of the foregoing, coupled to the model of a turbulent boundary layer consisting of vortical structures as evidenced by the evolutionary process described in §7.3, permits a new perspective on the significance of the turbulence spectrum. Owing to the randomness in space and time of the vortical structures, the hot-wire signal at a given position may be regarded as being characterized by the general features of having velocity fluctuations and associated frequencies dependent on periods between occurrences, i.e. the passage of a vortical structure, as well as the passage of structures having a wide range of vorticity resulting from various stages of the 'aging' process, and those that have been newly generated. It thus may be inferred, for example, that the low wavenumbers of the spectrum reflect the passage of vortices of relatively large diameter with low energy and low vorticity, coupled to velocity fluctuations associated with periods between occurrences which are generally of longer duration. On the other hand, the vortices with high velocity fluctuations and vorticity are associated with the higher wavenumbers of the spectrum. This interpretation leads to the postulate that the characteristic eddy timescales decrease with decreasing probability. This is consistent with the fine-scale structure of turbulence being intermittent (Batchelor & Townsend 1949) and the amplification of vorticity and vorticity gradients by the rate of vorticity production concentrating the vorticity into intermittent fine-scale vortical structures (Corrsin & Kistler 1954; Saffman 1968; Kraichnan 1974).

There is no requirement in the preceding discussion for the existence of local isotropy and an energy cascade as hypothesized in the inertial range theories of Kolmogorov (1941*a*, *b*, 1962). It is to be expected that owing to the stretching of vortical structures by self-induced strain and by the strain field associated with mutual interacting vortices, energy transfer to smaller scales would occur, but this process does not necessarily provide a justification for the energy cascade as envisaged by Kolmogorov. Although reference has been made in the previous discussion to the presence of a $k^{-\frac{5}{3}}$ spectral range in the boundary layer, local isotropy as a realizable physical condition in the Kolmogorov inertial subrange, which is characterized by $k^{-\frac{5}{3}}$ has not been as yet adequately established. Measurements by Laufer (1953) for pipe flow, Klebanoff (1954) for boundary-layer flow, and Kistler & Vrebalovich (1966) for high-Reynolds-number grid turbulence have shown that the $\frac{5}{3}$ law is an insensitive indicator of the existence of a locally isotropic inertial subrange, i.e. that although a $\frac{5}{3}$ spectral range was observed in the spectrum for the longitudinal fluctuation, a corresponding $\frac{5}{3}$ range did not exist in the spectra for the lateral fluctuations. In this connection, it is of interest that Lundgren (1982), using a vortex model, obtained the $\frac{5}{3}$ law from the Navier–Stokes equations without the

assumptions of isotropy or homogeneity, and that Moffatt (1984) also obtained the $\frac{5}{3}$ law from vortical dynamics.

In the present study of the evolution of a turbulent boundary layer induced by a three-dimensional roughness element serious questions have been raised about certain basic tenets in our perception of the nature of the turbulent boundary layer which merit further consideration. In large measure these questions can best be resolved by giving as much attention to what has been termed the small-scale structure as that given to the large-scale structure. In the context of the present paper it means that local measurements of pertinent statistical quantities under appropriate conditions, which in the past have been somewhat denigrated by the emphasis on flow visualization and large-scale structures, may provide much needed insight into the physics and universality of turbulent processes as well as the mathematical modelling of turbulent flows.

This research was supported in part by the Arnold Engineering Development Center and the authors wish to express their appreciation to Mr E. Thompson and Dr K. Kushman for their support and encouragement. The authors also wish to thank Professor M. Morkovin for his encouragement and interest. P.S.K. and K.D.T. are guest researchers at the National Institute of Standards and Technology. This paper is dedicated to the memory of Professor Itiro Tani, who was a pioneer in the study of roughness elements and the boundary layer.

REFERENCES

ACARLAR, M. S. & SMITH, C. R. 1984 An experimental study of hairpin-type vortices as a potential flow structure of turbulent boundary layers. *AFOSR Rep.* FM-5. Dept of Mech. Engng and Mech., Lehigh University.

ACARLAR, M. S. & SMITH, C. R. 1987 A study of hairpin vortices in a laminar boundary layer. Part 1. *J. Fluid Mech.* **175**, 1–41.

ANTONIA, R. A., SATYAPRAKASH, B. R. & HUSSAIN, A. K. M. F. 1982 Statistics of fine-scale velocity in turbulent plane and circular jets. *J. Fluid Mech.* **119**, 55–89.

BATCHELOR, G. B. & TOWNSEND, A. A. 1949 The nature of turbulent motion at large wave numbers. *Proc. R. Soc. Lond.* A **199**, 238–255.

BETCHOV, R. & CRIMINALE, W. O. 1967 *Stability of Parallel Flows.* Academic.

BLACKWELDER, R. F. 1980 Coherent structures in turbulent boundary layers. In *Turbulent Boundary Layers, Experiments, Theory and Modelling, The Hague, September 1979: AGARD Conf. Proc.* 271, pp. 24-1–24-7.

CANTWELL, B. J. 1981 Organized motion in turbulent flow. *Ann. Rev. Fluid Mech.* **13**, 457–515.

CANTWELL, B., COLES, D. E. & DIMOTAKIS, P. 1978 Structure and entrainment in the plane of symmetry of a turbulent spot. *J. Fluid Mech.* **87**, 641–672.

COLES, D. E. 1962 The turbulent boundary layer in a compressible fluid. *Rand Rep.* R-403-PR.

COLES, D. E. & HIRST, E. A. 1968 (eds) *Proc. AFOSR-IFP Stanford Conf. on Computation of Turbulent Boundary Layers.* Dept. Mech. Engng, Stanford University.

CORRSIN, S. & KISTLER, A. L. 1954 The free-stream boundaries of turbulent flows. *NACA TN* 3133 (also *NACA Rep.* 1244, 1955).

CROW, S. C. 1979 Stability theory for a pair of trailing vortices. *AIAA J.* **8**, 2172–2179.

FALCO, R. E. 1977 Coherent motions in the outer region of turbulent boundary layers. *Phys. Fluids Suppl.* **20**, 5124–5132.

FRENKIEL, F. N. & KLEBANOFF, P. S. 1973 Probability distributions and correlations in a turbulent boundary layer. *Phys. Fluids* **16**, 725–737.

FRENKIEL, F. N. & KLEBANOFF, P. S. 1975 On the lognormality of the small-scale structure of turbulence. *Boundary-Layer Met.* **8**, 173–200.

FURUYA, Y. & MIYATA, M. 1972 Visual studies on the wake of a roughness element proximate to a wall. *Mem. Faculty Engng Nagoya Univ.* **24**, 278–293

GREENSPAN, H. P. & BENNEY, D. J. 1963 On shear-layer instability, breakdown and transition. *J. Fluid Mech.* **15**, 133–153.

GREGORY, N. & WALKER, W. S. 1950 The effect on transition of isolated surface excrescences in the boundary layer. *Aero. Res. Counc. Tech. Rep.* 13436 (also *Aero. Res. Counc. R. & M.* 2799, 1956).

GUPTA, A. K. 1980 Some observations in the wake of a small vertical cylinder attached to a flat plate. *Phys. Fluids* **23**, 221–223.

HALL, G. R. 1967 Interaction of the wake from bluff bodies with an initially laminar boundary layer. *AIAA J.* **5**, 1386–1392.

HAMA, F. R. 1957 An efficient tripping device. *J. Aero. Sci.* **24**, 236–237.

HAMA, F. R. 1962*a* Streaklines in a perturbed shear flow. *Phys. Fluids* **5**, 644–650.

HAMA, F. R. 1962*b* Progressive deformation of a curved vortex filament by its own induction. *Phys. Fluids* **5**, 1156–1162.

HAMA, F. R. & NUTANT, J. 1963 Detailed flow-field observations in the transition process in a thick boundary layer. *Proc. Heat Transfer Fluid Mech. Inst.*, pp. 77–93.

HARTREE, D. R. 1937 On an equation occurring in Falkner and Skan's approximate treatment of the equations of the boundary layer. *Proc. Camb. Phil. Soc.* **33**, 223.

HEAD, M. R. & BANDYOPADHYAY, P. 1981 New aspects of turbulent boundary layer structure. *J. Fluid Mech.* **107**, 297–338.

HILL, P. G. & STENNING, A. H. 1960 Laminar boundary layers in oscillating flow. *Trans. ASME D: J. Basic Engng* **82**, 593–610.

HINZE, J. O. 1975 Turbulence, 2nd edn. McGraw-Hill.

HUSSAIN, A. K. M. F. 1981 Coherent structures and studies of perturbed and unperturbed jets. In *Intl Conf. on Role of Coherent Structures in Modelling Turbulence and Mixing*, Lecture Notes in Physics, vol. 136, pp. 252–291. Springer.

HUSSAIN, A. K. M. F. 1983 Coherent structures – reality and myth. *Phys. Fluids* **26**, 2816–2850.

KISTLER, A. L. & VREBALOVICH, T. 1966 Grid turbulence at large Reynolds numbers. *J. Fluid Mech.* **26**, 37–47.

KLANFER, L. & OWEN, T. R. 1953 The effect of isolated roughness on boundary layer transition. *R.A.E. Tech. Memo. No. Aero.* 355.

KLEBANOFF, P. S. 1954 Characteristics of turbulence in a boundary layer with zero-pressure gradient. *NACA TN* 3178 (also *NACA Rep.* 1247, 1955).

KLEBANOFF, P. S. 1971 Effect of free-stream turbulence on a laminar boundary layer. *Bull. Am. Phys. Soc.* **10**, 1323.

KLEBANOFF, P. S., CLEVELAND, W. G. & TIDSTROM, K. D. 1987 Interaction of a three-dimensional roughness element with a laminar boundary layer. *AEDC-TR*-87-7.

KLEBANOFF, P. S. & DIEHL, Z. W. 1951 Some features of artificially thickened turbulent boundary layers. *NACA TN* 2475 (also *NACA Rep.* 1110, 1952).

KLEBANOFF, P. S., SCHUBAUER, G. B. & TIDSTROM, K. D. 1955 Measurements of the effect of two-dimensional and three-dimensional roughness elements on boundary-layer transition. *J. Aero. Sci.* **22**, 803–804.

KLEBANOFF, P. S. & TIDSTROM, K. D. 1959 Evolution of amplified waves leading to transition in a boundary layer with zero pressure gradient. *NASA TN* D-195.

KLEBANOFF, P. S. & TIDSTROM, K. D. 1972 Mechanism by which a two-dimensional roughness element induces boundary layer transition. *Phys. Fluids* **15**, 1173–1188.

KLEBANOFF, P. S., TIDSTROM, K. D. & SARGENT, L. M. 1962 The three-dimensional nature of boundary-layer stability. *J. Fluid Mech.* **12**, 1–34.

KLINE, S. J. 1982 Universal or zonal modeling – the road ahead. In Proc. 1980–1981 AFOSR-HTTM Stanford Conference on Complex Turbulent Flows (ed. S. J. Kline, B. J. Cantwell & G. M. Lilley), vol. 2, p. 991. Mech. Engng Dept, Stanford University.

KLINE, S. J., REYNOLDS, W. C., SCHRAUB, F. A. & RUNSTADLER, P. W. 1967 The structure of turbulent boundary layers. *J. Fluid Mech.* **30**, 741–773.

KNAPP, C. F. & ROACHE, P. J. 1968 A combined visual and hot-wire anemometer investigation of boundary-layer transition. *AIAA J.* **6**, 29–36.

KOLMOGOROV, A. N. 1941*a* The local structure of turbulence in incompressible viscous fluid for very large Reynolds numbers. *C.R. Acad. Sci. URSS* **30**, 301–305.

KOLMOGOROV, A. N. 1941*b* Dissipation of energy in locally isotropic turbulence. *C.R. Acad. Sci. URSS* **32**, 16–18.

KOLMOGOROV, A. N. 1962 A refinement of previous hypotheses concerning the local structure of turbulence in a viscous incompressible fluid at high Reynolds number. *J. Fluid Mech.* **13**, 82–85.

KOVASZNAY, L. S. G. 1960 A new look at transition. In *Aeronautics and Astronautics*, pp. 161–172. Pergamon.

KOVASZNAY, L. S. G., KIBENS, V. & BLACKWELDER, R. F. 1970 Large-scale motion in the intermittent region of a turbulent boundary layer. *J. Fluid Mech.* **41**, 283–325.

KOVASZNAY, L. S. G., KOMODA, H. & VASUDEVA, B. R. 1962 Detailed flow field in transition. *Proc. Heat Transfer Fluid Mech. Inst.*, pp. 1–26.

KRAICHNAN, R. H. 1974 On Kolmogorov's inertial-range theories. *J. Fluid Mech.* **62**, 305–330.

KUO, A. Y. & CORRSIN, S. 1971 Experiment on the geometry of the fine-structure regions in fully turbulent fluid. *J. Fluid Mech.* **56**, 447–479.

LAUFER, J. 1953 The structure of turbulence in fully developed pipe flow. *NACA TN* 2954 (also *NACA Rep.* 1174, 1955).

LAUFER, J. 1975 Trends in experimental turbulence research. *Ann. Rev. Fluid Mech.* **7**, 307–326.

LESSEN, M. 1949 On stability of free laminar boundary layer between parallel streams. *NACA TN* 1929 (also *NACA Rep.* 979, 1950).

LIN, C. C. 1953 On the stability of the laminar mixing region between two parallel streams in a gas. *NACA TN* 2887.

LOFTIN, L. K. 1946 Effects of specific types of surface roughness in boundary layer transition. *NACA ACR* L5J28a.

LUNDGREN, T. 1982 Strained spiral vortex model for turbulent fine structure. *Phys. Fluids* **25**, 2193–2203.

MATSUI, T. 1962 Transition in a laminar boundary layer due to an isolated roughness element. *Faculty of Engineering, Res. Rep.* 12. Gifu University, Japan.

MAXWORTHY, T. 1972 The structure and stability of vortex rings. *J. Fluid Mech.* **51**, 15–32.

MAXWORTHY, T. 1974 Turbulent vortex rings. *J. Fluid Mech.* **64**, 227–239.

MAXWORTHY, T. 1977 Some experimental studies of vortex rings. *J. Fluid Mech.* **81**, 465–495.

MIKSAD, R. W. 1972 Experiments on the nonlinear stages of free-shear layer transition. *J. Fluid Mech.* **56**, 695–719.

MOCHIZUKI, M. 1961*a* Smoke observation on boundary layer transition caused by a spherical roughness element. *J. Phys. Soc. Japan* **16**, 995–1008.

MOCHIZUKI, M. 1961*b* Hot-wire investigations of smoke patterns caused by a spherical roughness element. *Natural Sci. Rep. Ochanomizu Univ., Tokyo*, vol. 12, no. 2, 87–101.

MOFFATT, H. K. 1984 Simple topological aspects of turbulent vorticity dynamics. In *Turbulence and Chaotic Motion in Fluids, IUTAM* (ed. T. Tatsumi), pp. 223–230. Elsevier.

MOIN, P. & KIM, J. 1985 The structure of the vorticity field in turbulent channel flow. Part 1. Analysis of instantaneous fields and statistical correlations. *J. Fluid Mech.* **155**, 441–464.

MOIN, P., LEONARD, A. & KIM, J. 1986 Evolution of a curved vortex filament into a vortex ring. *Phys. Fluids* **29**, 955–963.

MORKOVIN, M. V. 1969 Critical evaluation of transition from laminar to turbulent shear layers with emphasis on hypersonically traveling bodies. *Air Force Flight Dyn. Lab. Tech. Rep.* AFOL-TR-68-149.

MORKOVIN, M. V. 1984 Bypass transition to turbulence and research desiderata. CP-2386, *Transition in Turbines Symp.* NASA Lewis Research Center.

NORMAN, R. S. 1972 On obstacle generated secondary flows in laminar boundary layers and transition to turbulence. Ph.D. thesis, Illinois Institute of Technology.

NORMAN, R. S. & MORKOVIN, M. V. 1972 A mechanism of transition downstream of an isolated 3-D roughness. *Bull. Am. Phys. Soc.* **17**, 1081.

PERRY, A. E. & ABELL, C. J. 1977 Asymptotic similarity of turbulence structures in smooth and rough-wall pipes. *J. Fluid Mech.* **79**, 785–799.

PERRY, A. E. & CHONG, M. S. 1982 On the mechanism of wall turbulence. *J. Fluid. Mech.* **119**, 173–217.

PERRY, A. E., LIM, T. T & TEH, E. W. 1981 A visual study of turbulent spots. *J. Fluid Mech.* **104**, 285–403.

PHILLIPS, O. M. 1972 The entrainment interface. *J. Fluid Mech.* **51**, 97–118.

PRETSCH, J. 1941 Die Stabilitat einer ebenen Laminarstromung bei Druckgefalle und Druckansteig. *Jahrbuch der Deutschen Luftfahrtforschung*, vol. I, pp. 58–75.

PRETSCH, J. 1942 Die Anfachung instabiler Storungen in einer laminaren Reibungsschicht. *Jahrbuch der Deutschen Luftfahrtforschung*, vol. I, pp. 54–71 (translated as *NASA TM* 1343, 1942.

PURTELL, L. P., KLEBANOFF, P. S. & BUCKLEY, F. T. 1981 Turbulent boundary layer at low Reynolds number. *Phys. Fluids* **24**, 802–811.

RESHOTKO, E. 1976 Boundary-layer stability and transition. *Ann. Rev. Fluid Mech.* **8**, 311–349.

SAFFMAN, P. G. 1968 Lectures on homogeneous physics. In *Topics in Nonlinear Physics* (ed. N. Zabusky), pp. 485–614. Springer.

SAFFMAN, P. G. 1978 The number of waves on unstable vortex rings. *J. Fluid Mech.* **84**, 625–639.

SCHILLER, L. 1932 Stromung in Rohren. *Handbuch der Experimentalphysik*, vol. 4, Pt. 4, p. 189. Leipzig.

SCHLICHTING, H. & ULRICH, A. 1942 Zur Berechnung des Umschlages laminar-turbulent. *Jahrbuch der Deutschen Luftfahrtforschung*, vol. I, pp. 8–35.

SCHUBAUER, G. B. & KLEBANOFF, P. S. 1950 Investigation of separation of the turbulent boundary layer. *NACA TN* 2133 (also *Rep.* 1030, 1951).

SCHUBAUER, G. B. & KLEBANOFF, P. S. 1955 Contributions on the mechanics of boundary-layer transition. *NACA TN* 3489 (also *NACA Rep.* 1289, 1956).

SMITH, A. M. O. & CLUTTER, D. W. 1959 The smallest height of roughness capable of affecting boundary layer transition. *J. Aerospace Sci.* **26**, 229–245.

SMITH, C. R. & ABBOTT, D. E. (eds) 1978 *AFOSR/Lehigh University Workshop on Coherent Structure in Turbulent Boundary Layers.* Dept. of Mech. Engng and Mech., Lehigh University.

STUART, J. T. 1971 Nonlinear stability theory. *Ann. Rev. Fluid Mech.* **3**, 347–368.

TANI, I. 1961 Effect of a two-dimensional and isolated roughness on laminar flow. In *Boundary Layer and Flow Control*, vol. 2, pp. 637–656. Pergamon.

TANI, I. 1969 Boundary-layer transition. *Ann. Rev. Fluid Mech.* **1**, 169–196.

TANI, I. 1981 Three-dimensional aspects of boundary-layer transition. *Proc. Indian Acad. Sci.* **4**, 219–238.

TANI, I., KOMODA, A., KOMATSU, Y. & IUCHI, M. 1962 Boundary layer transition by isolated roughness. *Aero. Res. Inst. Rep.* 375. Tokyo University.

TAVOULARIS, S., BENNETT, J. C. & CORRSIN, S. 1978 Velocity-derivative skewness in small Reynolds number, nearly isotropic turbulence. *J. Fluid Mech.* **88**, 63–69.

TCHEN, C. M. 1953 On the spectrum of energy in turbulent shear flow. *J. Res. Natl Bur. Standards* **50**, 51–62.

THEODORSEN, T. 1952 Mechanism of turbulence. In *Proc. 2nd Midwestern Conf. of Fluid Mech.* Ohio State University (ed. R. W. Powell, S. M. Marco & A. N. Tifford), pp. 1–18.

TOWNSEND, A. A. 1951 The structure of the turbulent boundary layer. *Proc. Camb. Phil. Soc.* **47**, 375–395.

TOWNSEND, A. A. 1956 *The Structure of Turbulent Shear Flow*, 1st edn. Cambridge University Press.

TOWNSEND, A. A. 1970 Entrainment and the structure of turbulent flow. *J. Fluid Mech.* **41**, 13–46.

WAZZAN, A. R., OKAMURA, T. T. & SMITH, A. M. O. 1968 Spatial and temporal stability charts for the Falkner-Skan boundary-layer profiles. *Douglas Aircraft Co. Rep.* DAC 67086.

WESKE, J. 1957 Experimental study of detail phenomena of transition in boundary layers. *Inst. Fluid Dyn. and Appl. Maths*, TN BN91. University of Maryland.

WIDNALL, S. E., BLISS, D. B. & TSAI, C. Y. 1974 The instability of short waves on a vortex ring. *J. Fluid Mech.* **66**, 35–47.

WIDNALL, S. E. & TSAI, C. Y. 1977 The instability of the thin vortex ring of constant vorticity. *Phil. Trans. R. Soc. Lond.* **287**, 273–305.

WYGNANSKI, I. & PETERSEN, R. A. 1985 Coherent motion in excited free-shear flows. *AIAA*-85-0359, *AIAA Shear Flow Control Conf., March 12–14.*

WYGNANSKI, I., SOKOLOV, M. & FRIEDMAN, D. 1976 On a turbulent spot in a laminar boundary layer. *J. Fluid Mech.* **78**, 785–819.